UNIVERSIDADE FEDERAL DO RIO GRANDE DO SUL
INSTITUTO DE CIÊNCIAS BÁSICAS DA SAÚDE
PROGRAMA DE PÓS-GRADUAÇÃO EM CIÊNCIAS BIOLÓGICAS:
BIOQUÍMICA

Guilherme Povala

APLICAÇÃO DE ESTRATÉGIAS NEUROCOMPUTACIONAIS PARA A IDENTIFICAÇÃO DE ALTERAÇÕES FUNCIONAIS NA DOENÇA DE ALZHEIMER

Porto Alegre
2022

Guilherme Povala

APLICAÇÃO DE ESTRATÉGIAS NEUROCOMPUTACIONAIS PARA A IDENTIFICAÇÃO DE ALTERAÇÕES FUNCIONAIS NA DOENÇA DE ALZHEIMER

Tese apresentada ao Programa de Pós-Graduação em Ciências Biológicas: Bioquímica do Instituto de Ciências Básicas da Saúde da Universidade Federal do Rio Grande do Sul como requisito parcial para a obtenção do título de doutor em Bioquímica.

Orientador: Prof. Dr. Eduardo Rigon Zimmer
Coorientador: Prof. Dr. Bruno Zatt

Porto Alegre
2022

CIP - Catalogação na Publicação

Povala, Guilherme
Aplicação de estratégias neurocomputacionais para a identificação de alterações funcionais na doença de alzheimer / Guilherme Povala. -- 2022.
110 f.
Orientador: Eduardo Rigon Zimmer.

Coorientador: Bruno Zatt.

Tese (Doutorado) -- Universidade Federal do Rio Grande do Sul, Instituto de Ciências Básicas da Saúde, Programa de Pós-Graduação em Ciências Biológicas: Bioquímica, Porto Alegre, BR-RS, 2022.

1. Doença de Alzheimer. 2. Biomarcadores. 3. Aprendizado de Máquina. I. Rigon Zimmer, Eduardo, orient. II. Zatt, Bruno, coorient. III. Título.

Elaborada pelo Sistema de Geração Automática de Ficha Catalográfica da UFRGS com os dados fornecidos pelo(a) autor(a).

SUMÁRIO

PARTE I

Na Parte I, são descritos o resumo, a lista de abreviaturas, a introdução e os objetivos desta tese de doutorado.

RESUMO

A deposição cerebral de placas de beta-amiloide (Aβ) e emaranhados neurofibrilares de tau hiperfosforilada são características patológicas da doença de Alzheimer (DA) que acabam por levar ao declínio cognitivo e, consequentemente, à neurodegeneração. Recentemente, foi proposto pelo *National Institute on Aging and Alzheimer's Association* um critério de pesquisa clínica onde imagens [ressonância nuclear magnética estrutural (RM) e tomografia por emissão de pósitrons (PET)] e medidas baseadas no líquido cefalorraquidiano (LCR) são utilizadas para classificar o paciente no sistema A, T e (N), que indica respectivamente positividade para amiloide, tau e neurodegeneração. A imagem PET pode ser usada para identificar e quantificar os agregados de Aβ e tau, enquanto a redução dos níveis de $A\beta_{1-42}/A\beta_{1-40}$ e aumento de tau [tanto tau total (t-tau) quanto tau fosforilada (p-tau)] podem ser medidos no LCR. No entanto, se os níveis de Aβ podem predizer características patológicas da DA em indivíduos cognitivamente saudáveis (CU) permanece incerto. Acredita-se que esses biomarcadores sigam uma cascata temporal onde as anormalidades seguem o modelo a seguir: A → T → N. Recentes avanços no campo da neuroinformática, possibilitaram a expansão de estratégias analíticas e computacionais para estudar dados multimodais na DA. A integração de imagens PET e dados ômicos pode fornecer novos *insights* sobre a fisiopatologia da DA. Assim, nesta tese, primeiro investigamos o papel das isoformas solúveis de Aβ na predição de T e (N), usando modelos de aprendizado de máquina (ML). Em segundo lugar, usamos a biologia de sistemas para ajudar a elucidar os fundamentos biológicos e destacar novos biomarcadores potenciais da fisiopatologia da DA usando um método de integração de imagens de PET com fluordeoxiglicose (FDG-PET), um marcador de atividade sináptica, e dados de transcriptômica no sangue. Em resumo, mostramos que as isoformas de Aβ, especialmente as espécies menores, podem predizer T e (N) com alta acurácia em indivíduos CU. Além disso, a integração de imagens mostrou uma forte associação entre um *cluster* relacionado à regulação da atividade da proteína serina/treonina cinase e a unidade reguladora ZNF653 com o sinal do PET-FDG cerebral. Para finalizar, mostramos o potencial das assinaturas gênicas associadas ao metabolismo cerebral como novos biomarcadores de DA e que a combinação de metodologias utilizadas neste trabalho pode ajudar a entender melhor a heterogeneidade da patologia da DA.

RESUMO EM INGLÊS (ABSTRACT)

Brain deposition of beta-amyloid (Aβ) plaques and neurofibrillary tangles of hyperphosphorylated tau are pathological features of Alzheimer's disease (AD) that ultimately lead to cognitive decline and, consequently, to neurodegeneration. Recently, a clinical research criterion was proposed by the National Institute on Aging and Alzheimer's Association where imaging [structural magnetic resonance imaging (MRI) and positron emission tomography (PET)] and measurements based on cerebrospinal fluid (CSF) are used to classify the patient in the A, T and (N) system, which respectively indicate positivity for amyloid, tau and neurodegeneration. PET imaging can be used to identify and quantify Aβ and tau aggregates, while reducing $A\beta_{1-42}/A\beta_{1-40}$ levels and increasing tau [both total tau (t-tau) and phosphorylated tau (p-tau)] can be measured in the CSF. However, whether Aβ levels can predict pathological features of AD in cognitively healthy individuals (CU) remains unclear. These biomarkers are believed to follow a temporal cascade where the abnormalities follow the following pattern: A → T → N. Recent advances in the field of neuroinformatics have enabled the expansion of analytical and computational strategies to study multimodal data in AD. The integration of PET images and omics data may provide new insights into the pathophysiology of AD. Thus, in this thesis, we first investigate the role of soluble Aβ isoforms in the prediction of T and (N), using machine learning (ML) models. Second, we use systems biology to help elucidate the biological underpinnings and highlight potential new biomarkers of AD pathophysiology using a method of integrating PET images with fluorodeoxyglucose (FDG-PET), a marker of synaptic activity, and transcriptomics data in blood. In summary, we show that Aβ isoforms, especially the smaller species, can predict T and (N) with high accuracy in CU individuals. Furthermore, image integration showed a strong association between a cluster related to the regulation of protein serine/threonine kinase activity and the regulatory unit ZNF653 with the brain PET-FDG signal. Finally, we show the potential of gene signatures associated with brain metabolism as new biomarkers of AD and that the combination of methodologies used in this work can help to better understand the heterogeneity of AD pathology.

LISTA DE ABREVIAÇÕES

A - Amiloide

A+ - Positividade de Aβ

APP - Proteína precursora de amiloide

Aβ - Beta-amiloide

BACE - Enzima de clivagem beta-amiloide

DA - Doença de Alzheimer

DP - Doença de Parkinson

ELA - Esclerose Lateral Amiotrófica

FDG - [^{18}F]-fluorodesoxiglicose

GFAP - Proteína glial fibrilar ácida

IP-MS - Imunoprecipitação acoplada à espectrometria de massa

LCR - Líquido Cefalorraquidiano

ML - Aprendizado de Máquina

N - Neurodegeneração

(N)+ - Positividade de neurodegeneração

NFT - Emaranhados neurofibrilares

NIA-AA - *National Institute on Aging-Alzheimer's Association*

NfL - Neurofilamento de cadeia leve

PET - Tomografia por emissão de pósitrons

RM - Ressonância Magnética

SNC - Sistema Nervoso Central

SPECT - Tomografia computadorizada por emissão de fóton único

T - Tau

T+ - Positividade de tau

TC - Tomografia Computadorizada

fMRI - Ressonância magnética funcional

p-tau - Tau fosforilada

p-tau181 - Tau hiperfosforilada em treonina 181

p-tau217 - Tau hiperfosforilada em treonina 217

p-tau231 - Tau hiperfosforilada em treonina 231

t-tau - Tau total

1. INTRODUÇÃO

O crescimento da população mundial tem sido acompanhado por um aumento progressivo do número de idosos. Em países desenvolvidos, a expectativa de vida já atinge valores acima dos 80 anos. Embora as causas de morte predominantes em pessoas idosas ainda sejam as doenças cardiovasculares e diferentes tipo de câncer, a ocorrência de doenças neurodegenerativas está fortemente relacionada com a idade e estão entre as dez principais doenças que ocasionam óbito (G7, 2017, p. 7).

No entanto, as mortes causadas por doenças cardiovasculares e câncer têm decrescido anualmente (ALZHEIMER'S & DEMENTIA, 2019) o que contribuiu ainda mais para o crescimento no número de cidadãos idosos, provocando um aumento expressivo no número de pessoas afetadas por doenças neurodegenerativas (GOOCH; PRACHT; BORENSTEIN, 2017).

Doenças neurodegenerativas são definidas por condições nas quais há disfunção neuronal progressiva e atrofia cerebral. Essas doenças são condições, até o momento, incuráveis e debilitantes que resultam em degeneração progressiva, o que refletem em disfunções motoras e/ou cognitivas. Temos como doenças neurodegenerativas clássicas, em que a neurodegeneração é a principal marca registrada, a doença de Alzheimer (DA), a doença de Parkinson (DP) e a esclerose lateral amiotrófica (ELA) (DUGGER; DICKSON, 2017; GBD 2017 US NEUROLOGICAL DISORDERS COLLABORATORS et al., 2021).

1.1. A Doença de Alzheimer

A DA é a doença neurodegenerativa mais prevalente no mundo (GBD 2017 US NEUROLOGICAL DISORDERS COLLABORATORS et al., 2021). Suas principais características neuropatológicas envolvem a deposição de duas proteínas, beta-amiloide (Aβ) e tau, em agregados insolúveis no cérebro (PERL, 2010; SERRANO-POZO et al., 2011).

A proteína Aβ denota peptídeos de 36 a 43 aminoácidos que são o principal componente das placas amiloides encontradas no cérebro de pessoas com DA. As placas amiloides são depósitos extracelulares da proteína Aβ principalmente na substância cinzenta do cérebro (CRAS et al., 1991; DICKSON, 1997). Os peptídeos de Aβ são produzidos pela clivagem proteolítica da proteína precursora de amiloide (APP) (HAMLEY, 2012). A APP é uma proteína transmembrana e é produzida por muitos tipos de células do corpo, mas é especialmente abundante nos neurônios (HAASS et al., 2012). Para liberação de Aβ, a APP é clivada sequencialmente por duas enzimas: pela beta secretase [ou enzima de clivagem beta-amiloide (BACE)] fora da membrana, e pela gama secretase (γ-secretase), um complexo enzimático dentro da membrana celular (HAASS et al., 2012). São as ações sequenciais dessas secretases que fazem com que fragmentos da proteína Aβ sejam liberados no espaço extracelular (HAASS et al., 2012; SUH; CHECLER, 2002). Esses fragmentos geralmente são compostos por peptídeos de Aβ com 40 ou 42 aminoácidos. Porém, vários fragmentos Aβ de outros tamanhos e menos abundantes também são gerados (DUNYS; VALVERDE; CHECLER, 2018; KUMMER; HENEKA, 2014). O comprimento desses peptídeos e modificações químicas aplicadas a eles podem influenciar tanto sua tendência de agregação quanto sua toxicidade (WALKER,

2020). O segundo componente da patologia da DA são os emaranhados neurofibrilares (NFT), derivados do acúmulo anormal da proteína tau. Neurônios saudáveis, em parte, são sustentados internamente por estruturas chamadas microtúbulos, que ajudam a guiar nutrientes e moléculas do corpo celular para o axônio e os dendritos. Em neurônios saudáveis, normalmente a tau se liga e estabiliza os microtúbulos. Na DA, no entanto, excesso de fosforilação em sítios aceptores de fosfato faz com que a tau se desestabilize e se separe dos microtúbulos, se agregando intracelularmente. Esses emaranhados bloqueiam o sistema de transporte neuronal, o que prejudica a comunicação sináptica entre os neurônios, que mais tarde, acabam sofrendo morte celular (CHUN; JOHNSON, 2007; LAKHAN, 2016).

1.2. O Sistema AT(N)

O modelo teórico de DA mais aceito sugere que o dismetabolismo do Aβ desencadeia uma cascata de eventos patológicos, incluindo a patologia de tau, disfunção sináptica e neurodegeneração, que leva ao declínio cognitivo e, finalmente, à demência. Ou seja, uma cadeia linear que leva à positividade de Aβ (A+) → positividade de tau (T+) → positividade de neurodegeneração [(N)+] → sintomas cognitivos (HARDY; HIGGINS, 1992; SELKOE, 1991). Essa cascata previamente proposta baseada em estudos em cérebros *post mortem,* mais recentemente passou a poder ser identificada in vivo graças aos avanços no área de biomarcadores. Os biomarcadores são medidas objetivas de um processo biológico ou patogênico que podem ser usados para avaliar o risco ou prognóstico da doença, para orientar o diagnóstico clínico ou para monitorar as intervenções terapêuticas (BLENNOW et al., 2010).

A compreensão da progressão longitudinal desses biomarcadores serviram como base para a definição biológica da DA e constituem a base do *National Institute on Aging-Alzheimer's Association* (NIA-AA) *Research Framework* proposto para estudos clínicos, que adotou o sistema AT(N) para biomarcadores amiloide (A), tau (T) e neurodegeneração (N). Em cada categoria, os biomarcadores são dicotomizados para indicar um estado normal (negativo para biomarcadores) ou anormal (positivo para biomarcadores) (JACK et al., 2016). Esse modelo teórico baseia-se em dados derivados de estudos multicêntricos transversais e longitudinais usando vários biomarcadores. Atualmente, os biomarcadores de DA são divididos em duas classes principais: medida em biofluidos [sangue e líquido cefalorraquidiano (LCR)] e medida por neuroimagem [ressonância magnética (RM) e tomografia por emissão de pósitrons (PET)] (BLENNOW; ZETTERBERG, 2018).

1.3. Biomarcadores de imagem

Biomarcadores de neuroimagem têm um papel importante tanto no diagnóstico precoce, bem como no acompanhamento periódico da DA (VARGHESE et al., 2013). Podemos classificar as técnicas de neuroimagem em duas grandes categorias: estruturais e funcionais.

As principais técnicas de imagem estrutural são a tomografia computadorizada (TC) e a RM. A TC permite distinguir estruturas diferentes. A RM, devido à sua alta resolução espacial, pode ser usada para distinguir a diferença entre dois tecidos arbitrariamente semelhantes, mas não idênticos (PERRIN; FAGAN; HOLTZMAN, 2009; WOLZ et al., 2011).

No contexto de técnicas funcionais, temos o PET, tomografia computadorizada por emissão de fóton único (SPECT) e ressonância magnética

funcional (fMRI) (WALHOVD et al., 2010). Embora a técnica de imagem funcional forneça algumas informações estruturais, sua resolução espacial é menor do que a técnica de imagem estrutural. No campo da DA, a RM é uma das técnicas de imagem não invasivas para a análise estrutural de cérebros (JACK et al., 2008), utilizada para a identificação de neurodegeneração, ou seja, para a classificação da positividade de N no sistema AT(N).

1.4. Tomografia por emissão de pósitrons (PET)

O PET, por outro lado, tem sido amplamente utilizado para investigar alterações funcionais do cérebro tanto em indivíduos saudáveis como no contexto patológico. O PET é uma técnica de imagem molecular que permite obter imagens tridimensionais do que está acontecendo no cérebro de um paciente em nível molecular e celular (ELLIS et al., 2011). Estudos do metabolismo cerebral com PET utilizam [^{18}F]-fluorodesoxiglicose (FDG) como marcador metabólico no diagnóstico diferencial da da DA. Com o FDG-PET é possível avaliar o metabolismo da glicose em diferentes regiões cerebrais, o que permite, em última instância, assim como a RM, medir a positividade para a neurodegeneração no sistema AT(N) (YANASE et al., 2005).

No entanto, diferentes radiotraçadores podem ser utilizados com a técnica de imagem por PET. Com isso, é possível visualizar o acúmulo de placa Aβ em um cérebro com DA e monitorar a progressão da doença através de imagens PET de Aβ (HAMEED et al., 2020). Dentre os radiotraçadores de Aβ, os mais conhecidos são Florbetapir, Flutemetamol e Florbetaben. Estes, por sua vez, podem ser utilizados para classificar a categoria A do sistema AT(N).

Também temos diversos estudos utilizando radiotraçadores de tau, possibilitando identificar pacientes com acúmulo de NFT. A imagem por tau PET demonstrou ser sensível e detecta alterações cognitivas precoces (pré-clínica) na DA (BRIER et al., 2016). Atualmente, os radiotraçadores de tau ainda não estão disponíveis para uso clínico. Imagens obtidas por tau PET podem ser utilizados para classificar a categoria T do sistema AT(N)

1.5. Biomarcadores de fluído

Alternativamente aos biomarcadores de imagens, os biomarcadores de fluídos podem ser utilizados como critério diagnóstico de cada categoria de biomarcadores do sistema AT(N). Atualmente, são aceitos, para indicar a positividade de cada categoria, dentre os biomarcadores de fluídos, aqueles obtidos a partir do LCR (JACK et al., 2016).

1.5.1. Líquido cefalorraquidiano (LCR)

O LCR está em contato direto com o espaço extracelular do cérebro e, portanto, as alterações bioquímicas no cérebro são refletidas nele, fazendo com que ele seja uma das fontes ideais para biomarcadores da DA (BLENNOW et al., 2010). Atualmente sabe-se que os sistemas de clearance das proteínas clássicas da patologia da DA, Aβ e tau, envolvem a liberação dessas proteínas para o LCR com posterior absorção para o sistema linfático (TARASOFF-CONWAY et al., 2015). No LCR, podemos medir inúmeros biomarcadores com significado clínico para a DA. Os mais utilizados, mas não limitados a eles, incluem a razão $A\beta_{1-42}/A\beta_{1-40}$, tau hiperfosforilada em treonina 181 (p-tau181) e neurofilamento de cadeia leve (NfL) (BLENNOW; ZETTERBERG; FAGAN, 2012; JACK et al., 2016).

O $A\beta_{1-42}$ e tau demonstraram ser componentes primários de placas amiloides e NFT, respectivamente. Por isso, os níveis dessas proteínas no LCR foram avaliados como potenciais biomarcadores dessas características patológicas (BLENNOW; ZETTERBERG; FAGAN, 2012).

1.5.2. Sangue

No entanto, em busca de exames com menor custo e maior acessibilidade, vem sendo aplicado um grande esforço na descoberta de exames sanguíneos no campo de pesquisa em biomarcadores de fluídos para a DA. A otimização de ferramentas analíticas permitindo uma sensibilidade na magnitude de picogramas na detecção de biomarcadores sanguíneos, incluindo a razão $A\beta_{1-42}/A\beta_{1-40}$, tau fosforilada em diversos sítios aceptores (p-tau) e NfL (CULLEN et al., 2021) trouxe expectativas promissoras para a área.

1.6. Técnicas neurocomputacionais na Doença de Alzheimer

Quando consideramos os avanços obtidos na medicina nas últimas décadas, é inegável que a computação foi uma grande contribuinte para que esses pudessem ser atingidos. Ademais, a computação se mostra uma grande aliada para ajudar no diagnóstico de doenças, uma vez que a Inteligência Artificial (IA) tem sido cada vez mais aplicada na área médica (HAMET; TREMBLAY, 2017).

Além disso, é crescente a preocupação na medicina para obter a maior quantidade possível de dados sobre a saúde ou doença dos pacientes e tomar decisões com base nisso. Antes, os médicos tinham a necessidade de confiar em sua experiência, capacidade de julgamento e habilidade de resolução de problemas enquanto usavam ferramentas rudimentares e recursos limitados. No entanto, nos

dias de hoje, as tecnologias disruptivas começaram a disponibilizar métodos avançados não só para profissionais da medicina, mas também para seus pacientes. Dentre estas técnicas neurocomputacionais, temos a ômica, biotecnologia, sensores portáteis e a IA (MESKO, 2017).

Ao invés de desenvolver tratamentos para populações e tomar as mesmas decisões médicas com base em algumas características físicas semelhantes entre os pacientes, a medicina tem avançado para a prevenção, personalização e precisão, o que fará com que soluções médicas tradicionais *one-fits-all* migrem para tratamentos direcionados, terapias personalizadas e drogas exclusivas. Em outras palavras: medicina de precisão. Nesta mudança e transformação cultural, técnicas neurocomputacionais são uma tecnologia chave que pode trazer esta oportunidade à prática diária (MESKO, 2017).

No aspecto da IA, a sua aplicação na medicina se divide em dois ramos principais: virtual e físico. O ramo físico envolve o uso de robôs enquanto o ramo virtual, representado pelo Aprendizado de Máquina (ML), utiliza algoritmos matemáticos que melhoram a aprendizagem através da experiência (HAMET; TREMBLAY, 2017).

Os algoritmos de ML podem ser classificados em três tipos: (i) supervisionados, (ii) não supervisionados e (iii) aprendizagem de reforço (HAMET; TREMBLAY, 2017). Dentre esses tipos, o mais comum e utilizado é o aprendizado supervisionado (LECUN; BENGIO; HINTON, 2015). Os algoritmos de aprendizado supervisionado constroem modelos a partir de um conjunto de dados que contém tanto as entradas quantos as saídas desejadas (RUSSELL; NORVIG; DAVIS, 2010).

Dentre as principais abordagens de ML supervisionada podemos citar as árvores de decisão, regressão logística e redes neurais artificiais (RNA).

1.7. Biologia de Sistemas

A natureza multifacetada da DA exige a incorporação de paradigmas complexos para estudar suas origens, mecanismos, desenvolvimento e possíveis tratamentos. Assim, o uso de métodos de biologia de sistemas se torna crucial na pesquisa da DA (VILLOSLADA; STEINMAN; BARANZINI, 2009; WANG et al., 2019). Uma visão sistêmica da biologia descreve uma abordagem multidisciplinar e holística para entender os fenômenos biológicos, focando nas interações de muitos elementos simultaneamente (KIRSCHNER, 2005; OLTVAI; BARABÁSI, 2002). Nesse contexto, tecnologias ômicas, como a transcriptômica, são os métodos de escolha para avaliar propriedades e dinâmicas de sistemas de forma rápida, ampla e confiável. A transcriptômica é especialmente atraente porque os RNAs representam um nível intermediário entre um contexto genômico estático e a dinâmica espaço-temporal da complexidade proteômica (VERHEIJEN; SLEEGERS, 2018).

1.8. Justificativa

No contexto deste trabalho, podemos considerar que esforços realizados nas pesquisas da área de biomarcadores da DA sejam divididos em dois grandes tipos: i) identificação de biomarcadores em diferentes compartimentos biológicos (cérebro, LCR e sangue) para classificação de cada uma das etapas do atual sistema AT(N) e ii) descoberta de novos de biomarcadores capazes de predizer alterações biológicas na DA. Desta forma, propomos duas estratégias neste trabalho. A primeira, apresentada no Capítulo 1, para a classificação de eventos patológicos da DA

através do uso de técnicas de ML com a utilização de diferentes isoformas de Aβ e a segunda, exposta no Capítulo 2, com o objetivo de descobrir potenciais novos biomarcadores sanguíneos da DA.

2. OBJETIVOS

2.1. Objetivo principal

Aplicar estratégias neurocomputacionais para a identificação de alterações patofisiológicas na Doença de Alzheimer.

2.2. Objetivos específicos

- Revisar a literatura de biomarcadores de fluídos e imagem para definir potenciais biomarcadores de estágios iniciais da DA;
- Investigar se a combinação de isoformas solúveis de Aβ no LCR podem predizer a positividade de patologia de tau e neurodegeneração utilizando aprendizado de máquina;
- Desenvolver um método de integração de tecnologia ômica e imagens PET para descoberta de potenciais novos biomarcadores sanguíneos da DA;

PARTE II

Na Parte II, são apresentados dois capítulos que representam artigos científicos que compõem esta tese de doutorado.

Capítulo 1

Soluble amyloid-beta isoforms predict downstream Alzheimer's disease pathology

No capítulo 1 apresentamos o artigo publicado no periódico *Cell & Bioscience.*

Sabe-se que alterações nos níveis de Aβ solúvel no LCR são detectáveis nos estágios pré-clínicos da DA. No entanto, não se sabe se os níveis de Aβ podem predizer os eventos patológicos seguintes na DA em indivíduos cognitivamente saudáveis. Para isso, propusemos o uso de aprendizado de máquina para criar modelos a partir da combinação de isoformas solúveis de Aβ para predizer T+ e (N)+ nesses indivíduos. Além disso, utilizamos dados de proteômica do LCR para investigar o enriquecimento funcional de processos biológicos alterados em indivíduos T+ e (N)+. Com este trabalho, demonstramos que a combinação de isoformas de Aβ pode prever T+ e (N)+ com alta AUC. A análise proteômica do LCR destacou um grupo promissor de proteínas que podem ser exploradas para melhorar a previsão de T+ e (N)+.

Soluble amyloid-beta isoforms predict downstream Alzheimer's disease pathology

Guilherme Povala[1,2], Bruna Bellaver[1], Marco Antônio De Bastiani[1], Wagner S. Brum[1], Pamela C. L. Ferreira[1,3], Andrei Bieger[1], Tharick A. Pascoal[3], Andrea L. Benedet[4,5], Diogo O. Souza[1,6], Ricardo M. Araujo[2], Bruno Zatt[2], Pedro Rosa-Neto[4,5,7], Eduardo R. Zimmer[1,8,9]* and for the Alzheimer's Disease Neuroimaging Initiative

[1] Graduate Program in Biological Sciences: Biochemistry, Universidade Federal do Rio Grande do Sul (UFRGS), Porto Alegre, Brazil.

[2] Graduate Program in Computing, Universidade Federal de Pelotas (UFPEL), Pelotas, Brazil.

[3] Department of Neurology and Psychiatry, University of Pittsburgh, Pittsburgh, US.

[4] Translational Neuroimaging Laboratory, The McGill University Research Centre for Studies in Aging, 6825 LaSalle Boulevard, Verdun, QC, H4H 1R3, Canada.

[5] Montreal Neurological Institute, 3801 University Street, Montreal, QC, H3A 2B4, Canada.

[6] Department of Biochemistry, Universidade Federal do Rio Grande do Sul (UFRGS), Porto Alegre, Brazil.

[7] Douglas Hospital, McGill University, 6875 La Salle Blvd-FBC room 3149, Montreal, QC, H4H 1R3, Canada.

[8] Department of Pharmacology, Universidade Federal do Rio Grande do Sul (UFRGS), Porto Alegre, Brazil.

[9] Graduate Program in Biological Sciences: Pharmacology and Therapeutics, Universidade Federal do Rio Grande do Sul (UFRGS), Porto Alegre, Brazil.

* Corresponding author. Email: erzimmer@gmail.com

Guilherme Povala: guilhermepovala@gmail.com

Bruna Bellaver: brunabellaver90@gmail.com

Marco Antônio De Bastiani: tyrev@hotmail.com

Wagner S. Brum: wagnersbrum@gmail.com

Pamela C. L. Ferreira: pamlukasewicz@gmail.com

Andrei Bieger: andreibieger@gmail.com

Tharick A. Pascoal: pascoal@pitt.edu

Andrea L. Benedet: andrea.benedet@mail.mcgill.ca

Diogo O. Souza: diogo@ufrgs.br

Ricardo M. Araujo: ricardo.araujo@gmail.com

Bruno Zatt: zatt@inf.ufpel.edu.br

Pedro Rosa-Neto: pedro.rosa@mcgill.ca

Eduardo R. Zimmer: erzimmer@gmail.com

Abstract

Background: Changes in soluble amyloid-beta (Aβ) levels in cerebrospinal fluid (CSF) are detectable at early preclinical stages of Alzheimer's disease (AD). However, whether Aβ levels can predict downstream AD pathological features in cognitively unimpaired (CU) individuals remains unclear. With this in mind, we aimed at investigating whether a combination of soluble Aβ isoforms can predict tau pathology (T+) and neurodegeneration (N+) positivity.

Methods: We used CSF measurements of three soluble Aβ peptides ($Aβ_{1-38}$, $Aβ_{1-40}$ and $Aβ_{1-42}$) in CU individuals (n = 318) as input features in machine learning (ML) models aiming at predicting T+ and N+. Input data was used for building 2046 tuned predictive ML models with a nested cross-validation technique. Additionally, proteomics data was employed to investigate the functional enrichment of biological processes altered in T+ and N+ individuals.

Results: Our findings indicate that Aβ isoforms can predict T+ and N+ with an area under the curve (AUC) of 0.929 and 0.936, respectively. Additionally, proteomics analysis identified 17 differentially expressed proteins (DEPs) in individuals wrongly classified by our ML algorithm. More specifically, enrichment analysis of gene ontology biological processes revealed an upregulation in myelinization and glucose metabolism-related processes in CU individuals wrongly predicted as T+. A significant enrichment of DEPs in pathways including biosynthesis of amino acids, glycolysis/gluconeogenesis, carbon metabolism, cell adhesion molecules and prion disease was also observed.

Conclusions: Our results demonstrate that, by applying a refined ML analysis, a combination of Ab isoforms can predict T+ and N+ with a high AUC. CSF proteomics

analysis highlighted a promising group of proteins that can be further explored for improving T+ and N+ prediction.

Keywords: Alzheimer's disease; amyloid-beta; tau pathology; neurodegeneration; machine learning; proteomics.

Background

Alzheimer's disease (AD) is the most prevalent neurodegenerative disease worldwide (1). Its main neuropathological features involve the deposition of two proteins, amyloid-β (Aβ) and tau, into insoluble aggregates in the brain (2, 3). Indeed, the most accepted AD theoretical model suggests that Aβ dysmetabolism triggers a cascade of downstream pathological events, including tau pathology, synaptic dysfunction, and neurodegeneration, which leads to cognitive decline and, ultimately, to dementia (4, 5).

This theoretical model relies on data derived from cross-sectional and longitudinal multicentric studies using multiple biomarkers. Currently, AD biomarkers are divided into two main classes: biofluid-based [blood and cerebrospinal fluid (CSF)] and neuroimaging [magnetic resonance imaging (MRI) and positron emission tomography (PET)] (6). These biomarkers constitute the basis of the National Institute on Aging-Alzheimer's Association (NIA-AA) Research Framework proposed for clinical studies, which adopted the A/T/(N) system for amyloid, tau, and neurodegeneration biomarkers (7). In each category, biomarkers are dichotomized to indicate a normal or abnormal status (7).

Importantly, this system relies on the amyloid cascade hypothesis, i.e., the linear chain Aβ positivity (A+) à tau positivity (T+) à neurodegeneration positivity (N+) à cognitive symptoms (4, 5). However, around 30% of cognitively unimpaired (CU) individuals are A+ but do not present any other AD pathological features (8-10). Thus, A+, usually indexed by CSF $A\beta_{1-42}$ or PET, does not infer *per se* if an individual presents or will develop tau pathology or neurodegeneration. Therefore, it is clear

that other biological processes are also critical in the progression toward clinical symptoms.

In this study, we asked (i) whether a combination of Aβ isoforms, measured in the CSF, would be capable of predicting downstream pathological biomarkers and (ii) what biological processes are related to an increase in Aβ isoforms' prediction power over downstream AD pathology. To answer these inquiries, we aimed at predicting T+ and N+ using a combination of demographics and Aβ isoforms levels in the CSF ($A\beta_{1-38}$, $A\beta_{1-40}$, and $A\beta_{1-42}$) as input features in machine learning models (ML). We also evaluated whether CSF proteomic analyses could reveal altered biological processes heterogeneity in individuals wrongly classified in ML models.

Methods

ADNI description

Data used in this article are available at the Alzheimer's Disease Neuroimaging Initiative (ADNI) database (adni.loni.usc.edu). ADNI is a longitudinal multicentric study launched in 2004, as a result of a public-private partnership, including the Foundation for the National Institutes of Health and the National Institute on Aging alongside contributors from many other sources. The study is currently in its 4th phase (ADNI1, ADNI GO, ADNI2, and ADNI3) and has recruited over 2300 participants in North America, to develop clinical, imaging, genetic, and biochemical biomarkers for the early detection and tracking of AD. More information on the study design can be found in adni.loni.esc.edu/about/.

Eligibility criteria

In this study, data from 318 CU subjects were collected from ADNI1 and ADNI2 database. Specific criteria for inclusion in this study were the availability of

CSF levels of $A\beta_{1-38}$, $A\beta_{1-40}$, and $A\beta_{1-42}$ proteins measured by 2D-ultra-performance liquid chromatography-tandem mass spectrometry (2D-UPLC-MS/MS). ADNI's inclusion and diagnostic criteria have been described elsewhere (11).

CSF biomarker collection and analysis

CSF $A\beta_{1–38}$, $A\beta_{1–40}$, and $A\beta_{1–42}$ peptide levels were measured using the 2D-UPLC-MS/MS method (Waters® XEVO-TQ-S), which had been previously described (12) and has been recently revalidated. This updated technique has been recognized as an accepted analytical reference by the Joint Committee for Traceability in Laboratory Medicine (JCTLM), in whose database it was published under the JCTLM Identification Number C12RMP1. For defining T+ and N+, p-tau (Thr-181) and t-tau levels used in this study were measured by the Elecsys® immunoassay, with T+ defined as CSF p-tau (181-Thr) > 19.2 pg/mL and N+ defined as CSF t-tau > 242 pg/mL (13). Data for the 2D-UPLC-MS/MS and Elecsys® methods are available, respectively, at the ADNI database under the file names "UPENNMSMSABETA.csv" and "UPENNBIOMK9_04_19_17.csv".

Statistical analysis

All statistical analyses were performed in GraphPad Prism 8. Data are expressed as mean ± standard deviation (SD). Normality was evaluated using histograms and quantile plots. Because samples did not have Gaussian distributions, comparisons between groups were carried out using Mann-Whitney test. P-values of less than 0.05 were reported as statistically significant.

Machine learning framework

We developed a ML framework that combines multiple techniques and models to predict T+ and N+ with the use of CSF Aβ isoform levels, demographic information

and APOE **ε**4 status. The framework was coded in Python (version 3.6.8, https://www.python.org/), using the scikit-learn (version 0.20.2, https://scikit-learn.org/) and xgboost (version 0.81, https://xgboost.readthedocs.io/) libraries. The supervised ML algorithms used in our framework are composed of Logistic Regression, Naive Bayes, k-Nearest Neighbors (kNN), Support Vector Classifier (SVC), Decision Trees, Random Forest, Gradient Boosting, XGBoost, and AdaBoost.

As input features for our framework, we used Aβ peptide levels ($A\beta_{1-38}$, $A\beta_{1-40}$, and $A\beta_{1-42}$), demographic information (age, sex and years of education), and APOE **ε**4 status. For feature selection, we evaluated all possible feature combinations, generating 1023 subsets. For each feature subset, we performed the nested cross-validation (CV) technique. Here, we used the nested CV since we needed to train different ML models together with its hyperparameter optimization. The nested CV has an inner CV loop nested in outer CV. The inner loop is composed of a 2-fold CV, and it is responsible for model selection and hyperparameter tuning, which is similar to a validation set. The outer loop, however, is composed of a 5-fold CV and it is used for error estimation, as a test set. The nested cross-validation uses the area under de curve (AUC) metric to select the best hyperparameters and models. Then, an independent test set is used to test the overall performance of the best model and to generate the AUC result. The hyperparameters evaluated for each ML algorithm used in this work are shown in **Table 1**. After obtaining the AUC results for tuned ML algorithms with the nested cross-validation, only the model that presented the best performance is chosen for each feature subset. Among all these models, we selected the best one and then extracted the AUC for the independent test set.

CSF proteomics analysis

Processed CSF proteomics data were collected from the ADNI database. Samples were measured using the LC/MS-MRM method (12). Proteins and peptides were selected based upon their previous detection in CSF, relevance to AD, and previous results from the Rules Based Medicine (RBM) multiplex immunoassay analysis of ADNI CSF. The final MRM panel consisted of 567 peptides representing 221 proteins. From these 567 peptides, 320 were detectable in > 10% of ADNI samples and are available in the file “CSFMRM.csv”.

From the previously included CU individuals, only 76 presented CSF proteomics data in the ADNI database and were included in further analyses. CSF proteomics analysis was performed comparing T− (n = 55) and T+ (n = 21) individuals and N− (n = 57) and N+ (n = 19). All proteomic analyses were implemented in an R statistical environment. Differentially expressed analysis was computed for T−/T+ and N−/N+ groups independently, using the LIMMA (version 3.46.0) package (14), and considering FDR-adjusted p-value < 0.05 as differentially expressed proteins (DEP) criteria. Finally, functional enrichment analyses of gene ontology (GO) biological processes and KEGG pathways were computed and visualized using the clusterProfiler (version 3.18.1) and Goplot (version 1.0.2) packages (15, 16).

Results

Sample characteristics

For this study, we included 318 CU individuals from ADNI, whose CSF had been analyzed with 2D-UPLC-MS/MS. Characteristics of the ADNI cohort and the different A, T, and N status of samples are provided in **Table 2.** Population

characteristics were compared between positive and negative group status for each of the above-mentioned biomarker categories. A+ and T+ showed significantly more APOE ε4 carriers than Aβ negative (A−) and tau negative (T−) groups. As already observed in previous studies, APOE ε4 carriers are associated with decreased $A\beta_{1-42}$ and elevated CSF p-tau in the CSF (14, 15). T+ and N+ presented elevated age, when compared with T− and neurodegeneration negative (N−) groups, respectively. No significant differences were observed in sex, years of education, Mini-Mental State Examination (MMSE), and Alzheimer's Disease Assessment Scale-Cognitive Subscale (ADAS-Cog) among groups.

Changes in Aβ soluble isoforms in T+ and N+ CU individuals

Fig. 1 compares Aβ isoform levels and their respective ratios between T+ and T- (**Fig. 1a**), and N+ and N- (**Fig. 1b**). When comparing T status, T+ group presented higher levels of $A\beta_{1-38}$ (**Fig. 1c**, T− = 1764 ± 496.1 pg/mL, T+ = 2411 ± 566.95 pg/mL, $p < 0.0001$) and $A\beta_{1-40}$ (**Fig. 1d**, T− = 7617 ± 2052 pg/mL, T+ = 10424 ± 2529 pg/mL, $p < 0.0001$). Additionally, a decrease in $A\beta_{1-42}/A\beta_{1-40}$ (**Fig. 1f**, T− = 0.1749 ± 0.05, T+ = 0.1381 ± 0.06, $p < 0.0001$) and $A\beta_{1-42}/A\beta_{1-38}$ ratios (**Fig. 1g**, T− = 0.7610 ± 0.22, T+ = 0.6014 ± 0.25, $p < 0.0001$) was observed in T+ individuals. However, we did not observe any significant difference in $A\beta_{1-42}$ levels (**Fig. 1e**, T− = 1353 ± 559.4 pg/mL, T+ = 1492 ± 784 pg/mL, $p = 0.41$) and $A\beta_{1-40}/A\beta_{1-38}$ ratio (**Fig. 1h**, T− = 4.354 ± 0.42, T+ = 4.329 ± 0.35, $p = 0.60$) between T+ and T- groups.

For N+ individuals, $A\beta_{1-38}$ (**Fig. 1i**, N− = 1760 ± 469.6 pg/mL, N+ = 2503 ± 567.2 pg/mL, $p < 0.0001$), $A\beta_{1-40}$ (**Fig. 1j**, N− = 7593 ± 1945 pg/mL, N+ = 10838 ± 2503 pg/mL, $p < 0.0001$), and $A\beta_{1-42}$ (**Fig. 1k**, N− = 1328 ± 565.1 pg/mL, N+ = 1575 ± 778.8 pg/mL, $p = 0.03$) measures were significantly elevated when compared to N−,

along with a decrease in $A\beta_{1-42}/A\beta_{1-40}$ ratio (**Fig. 1l**, N− = 0.1720 ± 0.05, N+ = 0.1411 ± 0.05, p < 0.0001) and $A\beta_{1-42}/A\beta_{1-38}$ ratio (**Fig. 1m**, N− = 0.7483 ± 0.23, N+ = 0.6146 ± 0.25, p < 0.0001). By contrast, $A\beta_{1-40}/A\beta_{1-38}$ ratio (**Fig. 1n**, N− = 4.350 ± 0.41, N+ = 4.336 ± 0.35, p = 0.78) does not differ between N+ and N- groups.

To test whether single Aβ isoforms or its ratios can predict downstream AD pathological processes in CU individuals, we used logistic regression models. The AUC results for predicting T+ and N+ individuals are shown in **Table 3**. Among all results, $A\beta_{1–38}$ and $A\beta_{1–40}$ seem to be the most reliable features to predict T+, with an AUC of 0.811 for both Aβ isoforms. For predicting N+, $A\beta_{1-38}$ and $A\beta_{1-40}$ showed similar results, with AUCs of 0.847 and 0.855, respectively. On the other hand, $A\beta_{1-42}$ presented an AUC of 0.580 for predicting N+ and 0.529 for T+.

Machine learning framework

Aiming at better predictive models, we proposed a ML framework, which is presented in **Fig. 2**. Aβ isoforms in the CSF ($A\beta_{1-38}$, $A\beta_{1-40}$, and $A\beta_{1-42}$; measured by 2D-UPLC-MS/MS), APOE **ε**4 carrier status, and demographic information (age, sex, and years of education) were used as input features. Besides, for feature generation, Aβ isoforms were used either alone or combined in ratios (**Fig. 2a**). In the feature subset generation step (**Fig. 2b**), all possible combinations of features were created (1023 different subsets). Then, for each subset, two models were selected using the nested CV technique (**Fig. 2c**): one for T+ prediction and another to predict N+ (**Fig. 2d**).

In our ML framework, to choose the best model for each subset to classify T+ and N+, we evaluated the use of the following ML algorithms: Logistic Regression, Naïve Bayes, kNN, SVC, Decision Trees, Random Forest, Gradient Boosting,

XGBoost, and AdaBoost within the nested CV technique. For each subset, the best model was defined based on the model's AUC obtained from the validation set. The top 1 model among the 1023 models (one for each subset) was evaluated using an independent test set and was defined as the best model to predict T+ or N+.

Tau pathology positivity prediction

From our proposed ML framework, 1023 tuned ML models were generated for predicting T+ (**Additional file 1**). **Fig. 3a** shows the AUC results for predicting T+ horizontally ordered by AUC – SD. In **Fig. 3b**, the best 10 models are ranked. Among the 10 models, all of them presented similar results, ranging from 0.877 to 0.887.

The top 1 model was a logistic regression model using $A\beta_{1-42}$, $A\beta_{1-42}/A\beta_{1-40}$, $A\beta_{1-42}/A\beta_{1-38}$, $A\beta_{1-40}/A\beta_{1-38}$, and years of education as input features. The AUC result obtained for the validation set was 0.881 +/- 0.024. For the independent test set, we achieved an AUC of 0.929 (**Fig. 3c**).

Neurodegeneration positivity prediction

For N+ prediction, we generated another 1023 models using the same method (**Additional file 2**). The AUC results for the N+ predictions are shown in **Fig. 3d** horizontally ordered by AUC – SD. The best 10 models were ranked and plotted on the graph represented in **Fig. 3e**. The best 10 models presented similar results, ranging from 0.909 to 0.915.

A kNN generated the best results, which had $A\beta_{1–42}$, $A\beta_{1-40}$, $A\beta_{1-42}/A\beta_{1-40}$, $A\beta_{1-42}/A\beta_{1-38}$, and $A\beta_{1-40}/A\beta_{1-38}$ as input features. The AUC result for the validation set for this model was 0.915 +/- 0.018. The independent test set achieved an AUC of 0.936 (**Fig. 3f**).

CSF proteomics of T+ and N+ CU individuals

To address T+ and N+ CU individuals' functional changes in biological processes, we performed CSF-based proteomics analyses. A total of 112 DEPs were observed in the CSF of CU T+ compared to T− subjects (**Additional file 3**). The enrichment analysis of GO biological processes in T+ individuals evidenced processes related to myelinization, synapse and neurogenesis regulation, immune response, carbohydrate metabolism, memory and learning, and glial cell differentiation (**Fig. 4a**). **Fig. 4b** depicts top 20 GO terms enriched in T+ subjects compared to T−. To identify the most affected pathways related to changes in proteomics profile of T+, we performed an enrichment analysis using canonical pathways described in the KEGG pathway database (17). This revealed a significant enrichment of 112 DEPs in 4 signaling pathways: "cell adhesion molecules", "biosynthesis of amino acids", "carbon metabolism", and "prion disease" (**Fig. 4c**-**g**). Regarding proteomics analysis of N+, we identified 123 DEPs when compared to N− individuals (**Additional file 4**). Of note, T+ and N+ subjects share 101 DEPs. Functional enrichment analyses revealed an overlap of enriched GO terms in N+ individuals and T+ individuals (**Fig. 5a**). Synapse organization, learning and memory processes, and APP metabolic processes are among the top 20 GO terms enriched in N+ (**Fig. 5b**). Interestingly, the same 4 KEGG pathways enriched for T+ were found enriched for N+ individuals (**Fig. 5c**-**g**).

CSF proteomics analysis for ML wrong predictions

Because Aβ isoforms predicted T+ and N+ outcomes with an AUC of up to 0.936, we next aimed, with a second proteomics analysis, at identifying differences in biological processes occurring in CU individuals that were wrongly classified by our

ML algorithm in the test set. First, we stratified the ML predictions for T+ in false-positive (n = 17), false-negative (n = 23), true-positive (n = 51), and true-negative (n = 147). Proteomic analyses for N+ prediction model was not carried out, since few wrong predictions were generated, leading to a small sample size.

We identified 17 upregulated DEPs between true-positive and false-positive (**Fig. 6a**) and 67 upregulated DEPs between true-negative and false-negatives for T+ individuals (**Fig. 7a**). Interestingly, enrichment analysis of GO biological processes revealed that processes related to myelinization, and glucose metabolism are enriched when comparing false-positive and true-positive predictions for T+ (**Fig. 6a-b**). When considering the false-negative and true-negative predictions for T+, DEPs related to glucose metabolism, synapse transmission, gliogenesis, and axogenesis appeared among the enriched GO terms (**Fig. 7a-b**). Finally, to recognize the most affected pathways related to changes in proteomics profile of individuals that were wrongly predicted, we performed an enrichment analysis using canonical pathways described in the KEGG pathway database. This revealed a significant enrichment of DEPs in pathways including “biosynthesis of amino acids”, “glycolysis/gluconeogenesis”, “carbon metabolism”, “cell adhesion molecules”, and “prion disease” (**Fig. 6c-g** and **7c-l**).

Discussion

In the present study, we demonstrated that ML models using combined Aβ soluble isoforms can predict downstream AD pathological processes, T+ and N+, in CU individuals with better results than Aβ isoforms independently. In the generated models, a higher AUC was achieved for predicting N+ when comparing with the T+. Our proteomics analysis identified several biological processes and signaling

pathways altered at pre-symptomatic phase of AD. These findings are especially relevant when considering that AD pathological processes initiate around 20-30 years before the occurrence of the first clinical symptoms (18-22). Finally, we identified DEPs among individuals wrongly classified as T+ by ML that can be further explored to improve prediction performance of the models.

The notion that Aβ triggers tau hyperphosphorylation and neurodegeneration has been corroborated by multiple experimental studies (23-26). In fact, Höglund and colleagues demonstrated that CU individuals with amyloidosis presented increased levels of p-tau181 and t-tau in the CSF (27). However, the diagnostic value of $A\beta_{1-42}$ has been explored in the literature delivering, though, only modest accuracy for AD prediction (28, 29). Accordingly, here we demonstrated a poor AUC of 0.580 for N+ and 0.529 for T+ prediction modeled using the $A\beta_{1-42}$ isoform by itself, the most used CSF biomarker in the diagnosis of AD. *Per se*, the poorly explored isoform $A\beta_{1-38}$ (AUC of 0.847) along with $A\beta_{1-40}$ (AUC of 0.811) were the most accurate predictors for both T+ and N+, respectively. In clinical studies, the $A\beta_{1-42}/A\beta_{1-38}$ ratio has been capable of significantly discriminating AD from other forms of dementia (30-32) and shown to be negatively correlated with CSF p-tau levels in AD patients (31). Additionally, a slight increase in $A\beta_{1-38}$ levels was found in a disease-specific manner in the CSF of AD subjects (32, 33). Nevertheless, a meta-analysis pointed no significant difference in $A\beta_{1-38}$ levels between AD individuals and control group after comparing eight studies (34). Cullen and colleagues more recently demonstrated that higher CSF $A\beta_{1-38}$ levels are negatively associated with cognitive decline and risk of developing AD (35). In this context, it is evident that the potential of this isoform to add information in the preclinical stage of the disease remains under-explored.

In this work, we showed that a logistic regression model could predict T+ using multiple input features, with an AUC of 0.929. It has been demonstrated that Aβ dysmetabolism is capable of triggering the conversion from a normal to a toxic state of tau-dependent synaptic (23). As well, a synergistic interaction between Aβ and tau pathology is likely to occur in AD, rather than the sum of their independent effects (36-38). Bilgel and colleagues showed that a higher baseline amyloid load in CU individuals was associated with steeper cognitive decline (39). In parallel, we hereby demonstrated that amyloid isoforms levels can predict N+ in CU individuals with an AUC of 0.936 using a kNN model. The combination of Aβ isoforms, especially those including smaller Aβ isoforms, seems to help to deliver the best results to predict N+. Indeed, we only found one *in vivo* study showing significant correlations between $A\beta_{1-42}$ levels in the CSF and neurodegeneration in CU individuals (27). On the other hand, the importance of $A\beta_{1-42}$ isoform as a toxic amyloid specie has been extensively demonstrated (23-26). In the context of isoform production, literature indicates that $A\beta_{1-38}$ is partially formed by cleavage of the $A\beta_{1-42}$ isoform (40). Also, it seems that no further cleavage of $A\beta_{1-38}$ occurs, resulting in a “more stable” isoform of Aβ, easier to detect (40). One could argue that a more prominent amyloid dysmetabolism, with higher rates of cleavage of $A\beta_{1-42}$ into $A\beta_{1-38}$, might be a crucial process that seems to drive tau pathology and neurodegeneration. However, the already described (41) faster turnover of $A\beta_{1-42}$ might be accounting for its poor predictive value in our model. Accordingly, our model shows an important role for less explored Aβ isoforms as indicators of emerging tau pathology and neurodegeneration. In addition to CSF, plasma biomarkers have been gaining attention in the recent years for their valuable contribution to AD diagnosis.

Aβ isoforms used in combination seems key for predicting T+ and N+, but do not completely explain all the aspects of AD downstream events. Thus, it is believed that simultaneous phenomena, that account for AD heterogeneity, are taking place in the brains of these individuals. In this context, CSF proteomics has been increasingly applied in the attempt to discover novel biomarkers for AD. However, it is mainly focused in comparing CU and AD individuals (42, 43). Here, we showed Aβ pathology-dependent changes at protein level occurring in the CSF of CU individuals. Similarly, Whelan and colleagues performed a multiplex proteomics analysis in the CSF of CU A+ and A− patients and found two DEPs significantly altered: Chitinase 3-like protein (YKL-40) and SPARC-related modular calcium binding protein 2 (SMOC2) (44). The great number of DEPs between CU T+ and T− subjects identified in our study allowed the further determination of biological processes and signaling pathways significantly enriched in these individuals. Additionally, significant differences in DEPs and its associated biological processes and signaling pathways were observed when comparing right and wrong ML predictions for T+. Interestingly, DEPs identified in other studies comparing CU and AD were also found in our analysis of ML wrong predictions for T+ (43). In specific, YKL-40, SOD1, PKM, and glucose metabolism related proteins are among the DEPs found in both studies. The degree of similarity between studies seems to highlight a robust pattern of change rather than a cohort-specific effect. These results might shed light to key proteins that can be further explored to improve ML performance for predicting T+ and N+.

Conclusions

Our findings indicate that the use of ML models with Aβ isoforms as input features might help to predict individuals with AD downstream pathology. In addition,

CSF proteomics analysis highlighted a promising group of proteins potentially driving tau pathology, which can be further explored for improving future T+ and N+ prediction. Finally, the combination of methodologies used here - ML and proteomics - may help to further understand AD pathology heterogeneity.

List of abbreviations

2D-UPLC-MS/MS: 2D-ultra-performance liquid chromatography-tandem mass spectrometry; A+: amyloid-beta positivity; A-: Aβ negative; AD: Alzheimer's disease; ADAS-Cog: Alzheimer's Disease Assessment Scale-Cognitive Subscale; ADNI: Alzheimer's Disease Neuroimaging Initiative; AUC: area under the curve; Aβ: amyloid-beta; CSF: cerebrospinal fluid; CU: cognitively unimpaired; DEP: differentially expressed proteins; GO: gene ontology; JCTLM: Joint Committee for Traceability in Laboratory Medicine; ML: machine learning; MMSE: Mini-Mental State Examination; MRI: magnetic resonance imaging; N+: neurodegeneration positivity; N-: neurodegeneration negative; NIA-AA: National Institute on Aging - Alzheimer's Association; p-tau: phosphorylated tau; PET: positron emission tomography; RBM: Rules Based Medicine; SD: standard deviation; SMOC2: SPARC-related modular calcium binding protein 2; T+: tau pathology positivity; T-: tau pathology negative; t-tau: total tau; YKL-40: Chitinase 3-like protein.

Declarations

Ethics approval and consent to participate

ADNI was ethically approved by the institutional review board of all participating sites, subjects provided written informed consent.

Consent for publication

Not applicable.

Availability of data and materials

Data used in preparation of this article were obtained from the Alzheimer's Disease Neuroimaging Initiative (ADNI) database. The dataset supporting the conclusions of this manuscript is available at the ADNI website (http://adni.loni.usc.edu/).

Competing interests

The authors declare that they have no competing interests.

Funding

GP receives financial support from CAPES [88882.345577/2019-01]. BB receives financial support from CAPES [88887.336490/2019-00]. PRN receive grants from CIHR [MOP-11-51-31; FRN, 152985], Alzheimer's Association [NIRG-12-92090; NIRP-12-259245] and FRQS [2020-VICO-279314]. ERZ receives grants from CNPq [435642/2018-9; CNPq 312410/2018-2] Instituto Serrapilheira [Serra-1912-31365], FAPERGS/MS/CNPq/SESRS–PPSUS [30786.434.24734.23112017] and ARD/FAPERGS [54392.632.30451.05032021].

Authors' contributions

Conceptualization: GP, BB, WSB, BZ, EZ.

Methodology: GP, BB, WSB, MADB.

Software: GP.

Investigation: GP.

Visualization: GP, MADB.

Supervision: BB, BZ, RMA, EZ.

Writing—original draft: GP, BB, WSB, PCLF, EZ.

Writing—review & editing: GP, BB, WSB, MADB, PCLF, TAP, ALB, PRN, DOS, BZ, EZ.

All authors read and approved the final manuscript.

Acknowledgements

Data used in preparation of this manuscript were obtained from the ADNI database (adni.loni.usc.edu). The list of ADNI investigators can be found online at: http://adni.loni.usc.edu/wp-content/uploads/how_to_apply/ADNI_Acknowledgement_List.pdf.

References

1. Collaborators GBDD. Global, regional, and national burden of Alzheimer's disease and other dementias, 1990-2016: a systematic analysis for the Global Burden of Disease Study 2016. Lancet Neurol. 2019;18(1):88-106.

2. Serrano-Pozo A, Frosch MP, Masliah E, Hyman BT. Neuropathological alterations in Alzheimer disease. Cold Spring Harb Perspect Med. 2011;1(1):a006189.

3. Perl DP. Neuropathology of Alzheimer's disease. Mt Sinai J Med. 2010;77(1):32-42.

4. Selkoe DJ. The molecular pathology of Alzheimer's disease. Neuron. 1991;6(4):487-98.

5. Hardy JA, Higgins GA. Alzheimer's disease: the amyloid cascade hypothesis. Science. 1992;256(5054):184-5.

6. Blennow K, Zetterberg H. Biomarkers for Alzheimer's disease: current status and prospects for the future. J Intern Med. 2018;284(6):643-63.

7. Jack CR, Jr., Bennett DA, Blennow K, Carrillo MC, Feldman HH, Frisoni GB, et al. A/T/N: An unbiased descriptive classification scheme for Alzheimer disease biomarkers. Neurology. 2016;87(5):539-47.

8. Aizenstein HJ, Nebes RD, Saxton JA, Price JC, Mathis CA, Tsopelas ND, et al. Frequent amyloid deposition without significant cognitive impairment among the elderly. Arch Neurol. 2008;65(11):1509-17.

9. Jack CR, Jr., Lowe VJ, Weigand SD, Wiste HJ, Senjem ML, Knopman DS, et al. Serial PIB and MRI in normal, mild cognitive impairment and Alzheimer's disease: implications for sequence of pathological events in Alzheimer's disease. Brain. 2009;132(Pt 5):1355-65.

10. Pike KE, Savage G, Villemagne VL, Ng S, Moss SA, Maruff P, et al. Beta-amyloid imaging and memory in non-demented individuals: evidence for preclinical Alzheimer's disease. Brain. 2007;130(Pt 11):2837-44.

11. Petersen RC, Aisen PS, Beckett LA, Donohue MC, Gamst AC, Harvey DJ, et al. Alzheimer's Disease Neuroimaging Initiative (ADNI): clinical characterization. Neurology. 2010;74(3):201-9.

12. Korecka M, Waligorska T, Figurski M, Toledo JB, Arnold SE, Grossman M, et al. Qualification of a surrogate matrix-based absolute quantification method for

amyloid-beta(4)(2) in human cerebrospinal fluid using 2D UPLC-tandem mass spectrometry. J Alzheimers Dis. 2014;41(2):441-51.

13. Schindler SE, Gray JD, Gordon BA, Xiong C, Batrla-Utermann R, Quan M, et al. Cerebrospinal fluid biomarkers measured by Elecsys assays compared to amyloid imaging. Alzheimers Dement. 2018;14(11):1460-9.

14. Ritchie ME, Phipson B, Wu D, Hu Y, Law CW, Shi W, et al. limma powers differential expression analyses for RNA-sequencing and microarray studies. Nucleic Acids Res. 2015;43(7):e47.

15. Yu G, Wang LG, Han Y, He QY. clusterProfiler: an R package for comparing biological themes among gene clusters. OMICS. 2012;16(5):284-7.

16. Walter W, Sanchez-Cabo F, Ricote M. GOplot: an R package for visually combining expression data with functional analysis. Bioinformatics. 2015;31(17):2912-4.

17. Kanehisa M, Goto S. KEGG: kyoto encyclopedia of genes and genomes. Nucleic Acids Res. 2000;28(1):27-30.

18. Bateman RJ, Xiong C, Benzinger TL, Fagan AM, Goate A, Fox NC, et al. Clinical and biomarker changes in dominantly inherited Alzheimer's disease. N Engl J Med. 2012;367(9):795-804.

19. Braak H, Braak E. Diagnostic criteria for neuropathologic assessment of Alzheimer's disease. Neurobiol Aging. 1997;18(4 Suppl):S85-8.

20. Fagan AM, Xiong C, Jasielec MS, Bateman RJ, Goate AM, Benzinger TL, et al. Longitudinal change in CSF biomarkers in autosomal-dominant Alzheimer's disease. Sci Transl Med. 2014;6(226):226ra30.

21. Morris JC, Price JL. Pathologic correlates of nondemented aging, mild cognitive impairment, and early-stage Alzheimer's disease. J Mol Neurosci. 2001;17(2):101-18.

22. Villemagne VL, Burnham S, Bourgeat P, Brown B, Ellis KA, Salvado O, et al. Amyloid beta deposition, neurodegeneration, and cognitive decline in sporadic Alzheimer's disease: a prospective cohort study. Lancet Neurol. 2013;12(4):357-67.

23. Bloom GS. Amyloid-beta and tau: the trigger and bullet in Alzheimer disease pathogenesis. JAMA Neurol. 2014;71(4):505-8.

24. Nisbet RM, Polanco JC, Ittner LM, Gotz J. Tau aggregation and its interplay with amyloid-beta. Acta Neuropathol. 2015;129(2):207-20.

25. Jacobs HIL, Hedden T, Schultz AP, Sepulcre J, Perea RD, Amariglio RE, et al. Structural tract alterations predict downstream tau accumulation in amyloid-positive older individuals. Nat Neurosci. 2018;21(3):424-31.

26. Jeong S. Molecular and Cellular Basis of Neurodegeneration in Alzheimer's Disease. Mol Cells. 2017;40(9):613-20.

27. Hoglund K, Kern S, Zettergren A, Borjesson-Hansson A, Zetterberg H, Skoog I, et al. Preclinical amyloid pathology biomarker positivity: effects on tau pathology and neurodegeneration. Transl Psychiatry. 2017;7(1):e995.

28. Hampel H, Toschi N, Baldacci F, Zetterberg H, Blennow K, Kilimann I, et al. Alzheimer's disease biomarker-guided diagnostic workflow using the added value of six combined cerebrospinal fluid candidates: Abeta1-42, total-tau, phosphorylated-tau, NFL, neurogranin, and YKL-40. Alzheimers Dement. 2018;14(4):492-501.

29. Khoonsari PE, Shevchenko G, Herman S, Remnestal J, Giedraitis V, Brundin R, et al. Improved Differential Diagnosis of Alzheimer's Disease by Integrating ELISA and Mass Spectrometry-Based Cerebrospinal Fluid Biomarkers. J Alzheimers Dis. 2019;67(2):639-51.

30. Mulugeta E, Londos E, Ballard C, Alves G, Zetterberg H, Blennow K, et al. CSF amyloid beta38 as a novel diagnostic marker for dementia with Lewy bodies. J Neurol Neurosurg Psychiatry. 2011;82(2):160-4.

31. Welge V, Fiege O, Lewczuk P, Mollenhauer B, Esselmann H, Klafki HW, et al. Combined CSF tau, p-tau181 and amyloid-beta 38/40/42 for diagnosing Alzheimer's disease. J Neural Transm (Vienna). 2009;116(2):203-12.

32. Wiltfang J, Esselmann H, Bibl M, Smirnov A, Otto M, Paul S, et al. Highly conserved and disease-specific patterns of carboxyterminally truncated Abeta peptides 1-37/38/39 in addition to 1-40/42 in Alzheimer's disease and in patients with chronic neuroinflammation. J Neurochem. 2002;81(3):481-96.

33. Bibl M, Mollenhauer B, Lewczuk P, Esselmann H, Wolf S, Trenkwalder C, et al. Validation of amyloid-beta peptides in CSF diagnosis of neurodegenerative dementias. Mol Psychiatry. 2007;12(7):671-80.

34. Olsson B, Lautner R, Andreasson U, Ohrfelt A, Portelius E, Bjerke M, et al. CSF and blood biomarkers for the diagnosis of Alzheimer's disease: a systematic review and meta-analysis. Lancet Neurol. 2016;15(7):673-84.

35. Cullen NC, Janelidze S, Palmqvist S, Stomrud E, Mattsson-Carlgren N, Hansson O. CSF Aβ38 levels are associated with Alzheimer-related decline: implications for γ-secretase modulators. medRxiv. 2021:2021.01.31.21250702.

36. Pascoal TA, Mathotaarachchi S, Mohades S, Benedet AL, Chung CO, Shin M, et al. Amyloid-beta and hyperphosphorylated tau synergy drives metabolic decline in preclinical Alzheimer's disease. Mol Psychiatry. 2017;22(2):306-11.

37. Pascoal TA, Mathotaarachchi S, Shin M, Benedet AL, Mohades S, Wang S, et al. Synergistic interaction between amyloid and tau predicts the progression to dementia. Alzheimers Dement. 2017;13(6):644-53.

38. Busche MA, Hyman BT. Synergy between amyloid-beta and tau in Alzheimer's disease. Nat Neurosci. 2020;23(10):1183-93.

39. Bilgel M, An Y, Helphrey J, Elkins W, Gomez G, Wong DF, et al. Effects of amyloid pathology and neurodegeneration on cognitive change in cognitively normal adults. Brain. 2018;141(8):2475-85.

40. Okochi M, Tagami S, Yanagida K, Takami M, Kodama TS, Mori K, et al. gamma-secretase modulators and presenilin 1 mutants act differently on presenilin/gamma-secretase function to cleave Abeta42 and Abeta43. Cell Rep. 2013;3(1):42-51.

41. Patterson BW, Elbert DL, Mawuenyega KG, Kasten T, Ovod V, Ma S, et al. Age and amyloid effects on human central nervous system amyloid-beta kinetics. Annals of neurology. 2015;78(3):439-53.

42. Sathe G, Na CH, Renuse S, Madugundu AK, Albert M, Moghekar A, et al. Quantitative Proteomic Profiling of Cerebrospinal Fluid to Identify Candidate Biomarkers for Alzheimer's Disease. Proteomics Clin Appl. 2019;13(4):e1800105.

43. Bader JM, Geyer PE, Muller JB, Strauss MT, Koch M, Leypoldt F, et al. Proteome profiling in cerebrospinal fluid reveals novel biomarkers of Alzheimer's disease. Mol Syst Biol. 2020;16(6):e9356.

44. Whelan CD, Mattsson N, Nagle MW, Vijayaraghavan S, Hyde C, Janelidze S, et al. Multiplex proteomics identifies novel CSF and plasma biomarkers of early Alzheimer's disease. Acta Neuropathol Commun. 2019;7(1):169.

Figure legends

Fig. 1. Aβ isoforms levels discriminate tau pathology positivity (T+) and neurodegeneration positivity (N+) in CU individuals. (**A**) T+ indicated by a high level of p-tau in the CSF (p-tau > 19.2 pg/mL). (**B**) N+ indicated by a high level of t-tau in the CSF (t-tau > 242 pg/mL). (**C**) $A\beta_{1-38}$, (**D**) $A\beta_{1-40}$ and (**E**) $A\beta_{1-42}$ levels for T- and T+ individuals. (**F**) $A\beta_{1-42}/A\beta_{1-40}$, (**G**) $A\beta_{1-42}/A\beta_{1-38}$ and (**H**) $A\beta_{1-40}/A\beta_{1-38}$ ratios for T- and T+ individuals. (**I**) $A\beta_{1-38}$, (**J**) $A\beta_{1-40}$ and (**K**) $A\beta_{1-42}$ levels for N- and N+ individuals. (**L**) $A\beta_{1-42}/A\beta_{1-40}$, (**M**) $A\beta_{1-42}/A\beta_{1-38}$ and (**N**) $A\beta_{1-40}/A\beta_{1-38}$ ratios for N- and N+ individuals. Boxplots are displayed as median (center line) and extend from the 25th to 75th percentiles. The whiskers go down to the smallest value and up to the largest. Statistical differences were tested using Mann-Whitney test ($^{*}p \leq 0.05$, $^{***}p \leq 0.001$, $^{****}p \leq 0.0001$).

Fig. 2. Machine learning framework delivers models that predict tau pathology and neurodegeneration. (**A**) cognitively unimpaired (CU) individual's cerebrospinal fluid (CSF) levels of $A\beta_{1–38}$, $A\beta_{1–40}$ and $A\beta_{1–42}$, demographics data and APOE ε4 status were used for feature generation. (**B**) All possible combinations of features were generated using the feature set. (**C**) The subsets were used for generating tuned machine learning models validated with nested cross-validation aiming to (**D**) identify tau pathology (T+) and neurodegeneration (N+) positivity.

Fig. 3. Results for predicting tau pathology (T) and neurodegeneration (N) status. (**A**) Area under the ROC curve (AUC) results (vertical axis) for all 1023 subsets to predict T status ordered by AUC – standard deviation (SD). (**B**) AUC results (horizontal axis) for the top 10 models (vertical axis) to predict T status. (**C**) ROC curve for the best model to predict T status using the independent test set. (**D**)

AUC results (vertical axis) for all 1023 subsets to predict N status ordered by AUC – SD. (**E**) AUC results (horizontal axis) for the top 10 models (vertical axis) to predict N status. (**F**) ROC curve for the best model to predict N status using the independent test set.

Fig. 4. **Proteome analyses results of cerebrospinal fluid (CSF) cells between T- and T+ cognitively unimpaired (CU) patients.** (**A**) Gene ontology (GO) network of enriched terms were constructed from differentially expressed proteins mapping the node sizes to GO term significance and edge width to shared protein proportions (Jaccard coefficient). (**B**) Radial plot of top 20 enriched GO terms. (**C**) Enriched pathways obtained from functional enrichment of KEGG terms. (**D-G**) Pie charts of enriched KEGG pathways showing the proportion of proteins upregulated in T+ vs T- comparison.

Fig. 5. **Proteome analyses results of cerebrospinal fluid (CSF) cells between N- and N+ cognitively unimpaired (CU) patients.** (**A**) Gene ontology (GO) network of enriched terms were constructed from differentially expressed proteins mapping the node sizes to GO term significance and edge width to shared protein proportions (Jaccard coefficient). (**B**) Radial plot of top 20 enriched GO terms. (**C**) Enriched pathways obtained from functional enrichment of KEGG terms. (**D-G**) Pie charts of enriched KEGG pathways showing the proportion of proteins upregulated in N+ vs N- comparison.

Fig. 6. Proteome analyses results of cerebrospinal fluid (CSF) cells between true positive (TP) and false positive (FP) predictions for tau pathology positivity (T+) in cognitively unimpaired (CU) individuals. (**A**) Gene ontology (GO) network of enriched terms were constructed from differentially expressed

proteins mapping the node sizes to GO term significance and edge width to shared protein proportions (Jaccard coefficient). (**B**) Radial plot of top 15 enriched GO terms. (**C**) Enriched pathways obtained from functional enrichment of KEGG terms. (**D-G**) Pie charts of enriched KEGG pathways showing the proportion of proteins upregulated in TP vs FP comparison.

Fig. 7. **Proteome analyses results of cerebrospinal fluid (CSF) cells between true negative (TN) and false negative (FN) predictions for tau pathology positivity (T+) in cognitively unimpaired (CU) individuals.** (**A**) Gene ontology (GO) network of enriched terms were constructed from differentially expressed proteins mapping the node sizes to GO term significance and edge width to shared protein proportions (Jaccard coefficient). (**B**) Radial plot of top 15 enriched GO terms. (**C**) Enriched pathways obtained from functional enrichment of KEGG terms. (**D-L**) Pie charts of enriched KEGG pathways showing the proportion of proteins upregulated in TN vs FN comparison.

Additional files

Additional file 1

File format: .docx

Title of data: Machine learning results for predicting tau pathology positivity (T+).

Description of data: Table containing features, AUC and standard deviation results for all 1023 models for predicting tau pathology positivity.

Additional file 2

File format: .docx

Title of data: Machine learning results for predicting neurodegeneration positivity (N+).

Description of data: Table containing features, AUC and standard deviation results for all 1023 models for predicting neurodegeneration positivity.

Additional file 3

File format: .docx

Title of data: Differentially expressed proteins (DEPs) in the cerebrospinal fluid (CSF) of cognitively unimpaired (CU) tau pathology positive (T+) compared to negative (T−) subjects.

Description of data: Table containing Protein ID, p-value, adjusted p-value, t-value and logFC for differentially expressed proteins in the cerebrospinal fluid of cognitively unimpaired tau pathology positive compared to negative subjects.

Additional file 4

File format: .docx

Title of data: Differentially expressed proteins (DEPs) in the cerebrospinal fluid (CSF) of cognitively unimpaired (CU) neurodegeneration positive (N+) compared to negative (N−) subjects.

Description of data: Table containing Protein ID, p-value, adjusted p-value, t-value and logFC for differentially expressed proteins in the cerebrospinal fluid of cognitively unimpaired neurodegeneration positive compared to negative subjects.

Figure 1

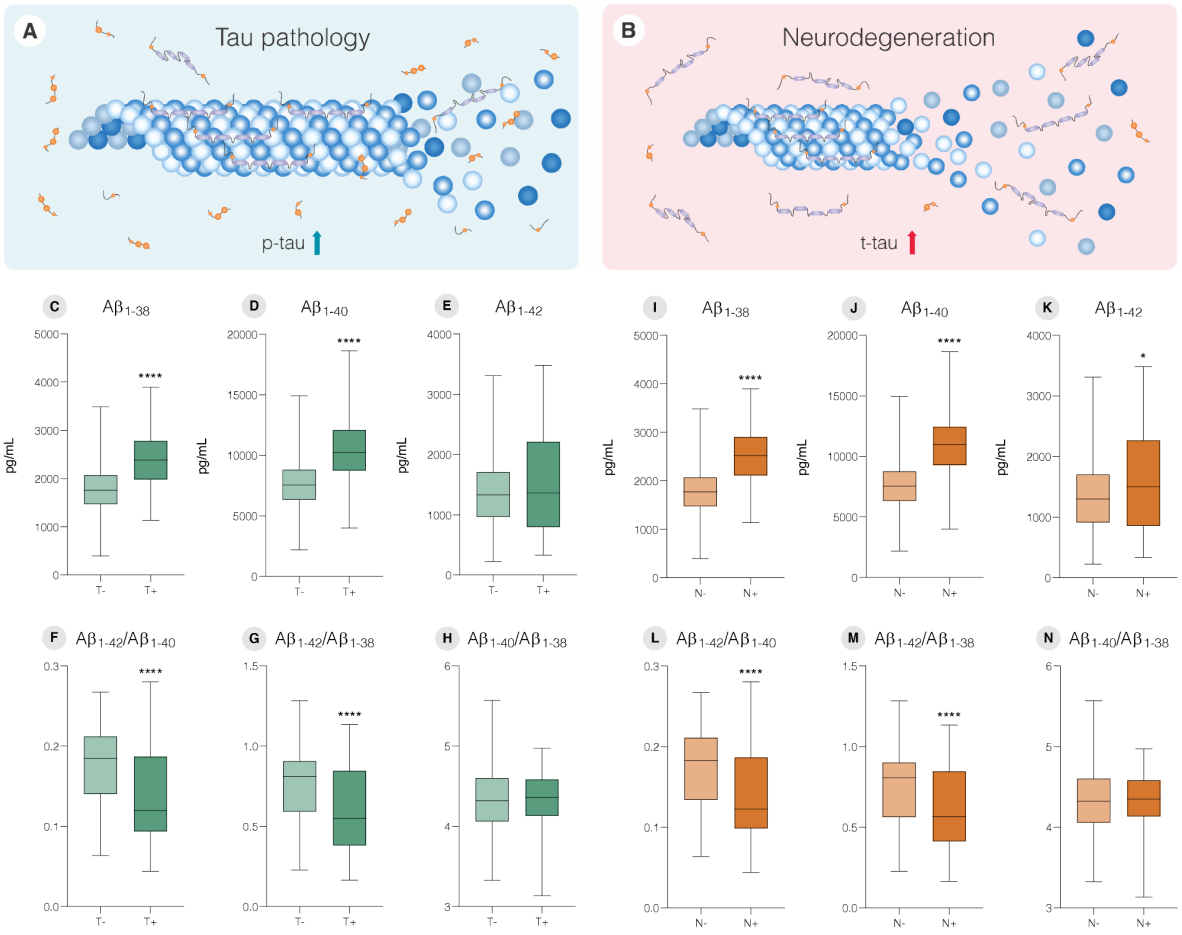
A
Tau pathology
p-tau
B
Neurodegeneration
t-tau
C Aβ1-38
D Aβ1-40
E Aβ1-42
I Aβ1-38
J Aβ1-40
K Aβ1-42
pg/mL
T-
T+
N-
N+
****
*
F Aβ1-42/Aβ1-40
G Aβ1-42/Aβ1-38
H Aβ1-40/Aβ1-38
L Aβ1-42/Aβ1-40
M Aβ1-42/Aβ1-38
N Aβ1-40/Aβ1-38

Figure 2

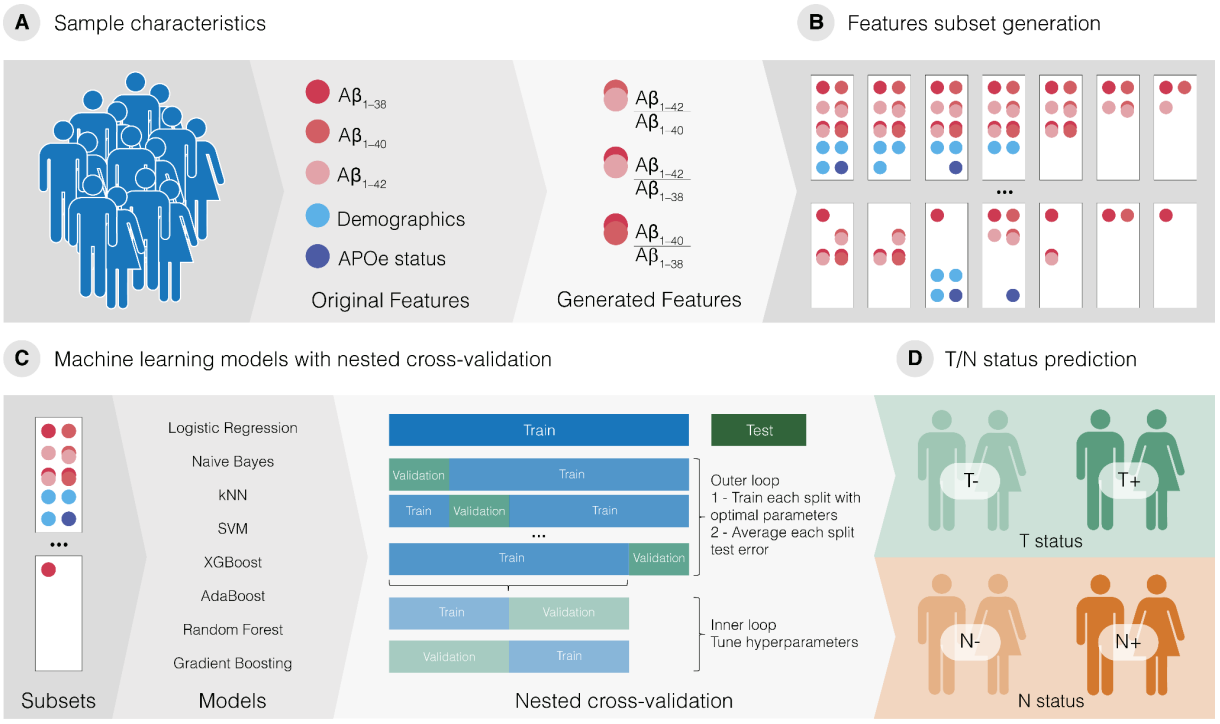
A Sample characteristics
B Features subset generation
Aβ1–38
Aβ1–40
Aβ1–42
Demographics
APOe status
Original Features
Aβ1–42 / Aβ1–40
Aβ1–42 / Aβ1–38
Aβ1–40 / Aβ1–38
Generated Features
C Machine learning models with nested cross-validation
D T/N status prediction
Logistic Regression
Naive Bayes
kNN
SVM
XGBoost
AdaBoost
Random Forest
Gradient Boosting
Subsets
Models
Train
Test
Validation
Outer loop
1 - Train each split with optimal parameters
2 - Average each split test error
Inner loop
Tune hyperparameters
Nested cross-validation
T-
T+
T status
N-
N+
N status

Figure 3

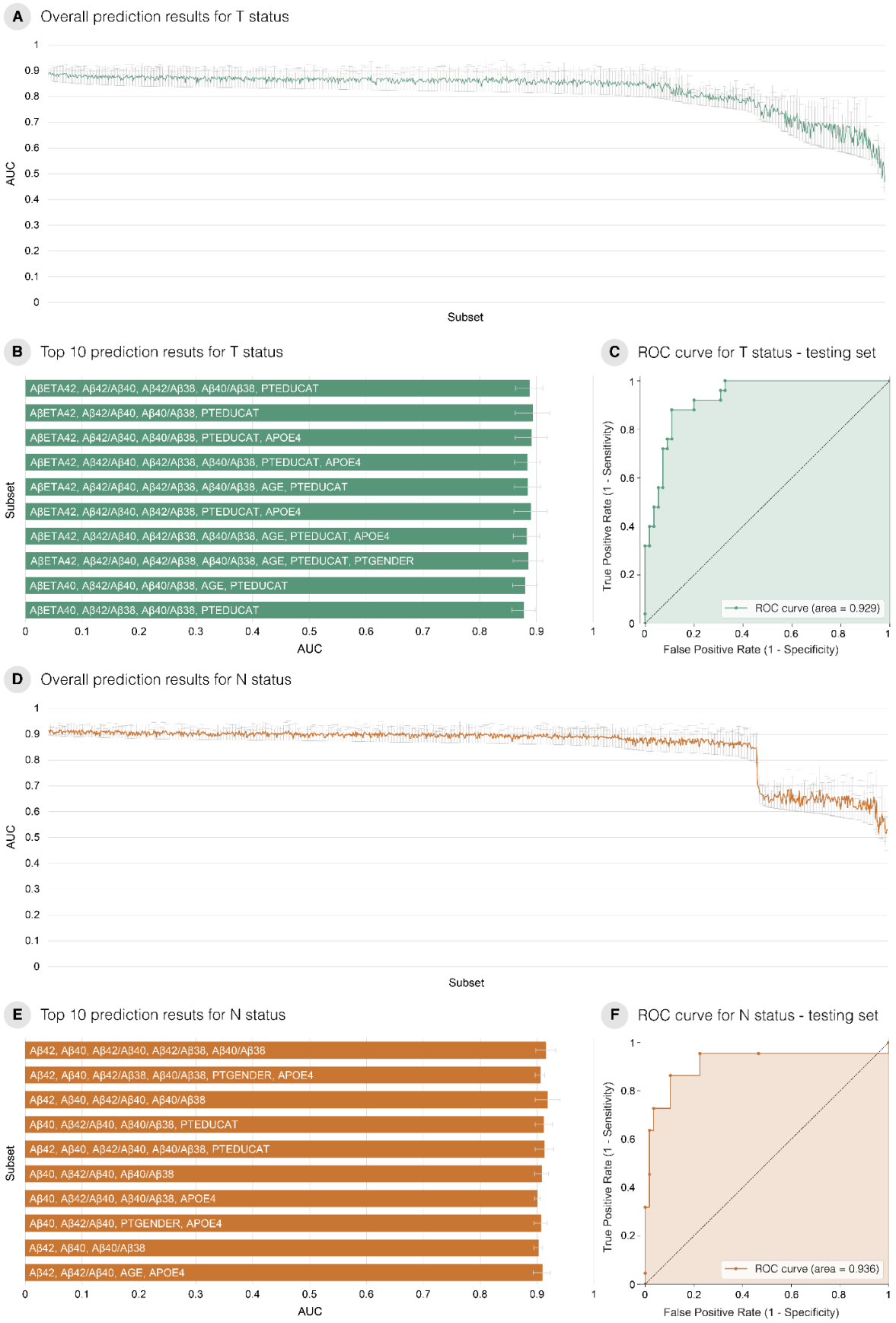
A Overall prediction results for T status
AUC
Subset
B Top 10 prediction resuts for T status
AβETA42, Aβ42/Aβ40, Aβ42/Aβ38, Aβ40/Aβ38, PTEDUCAT
AβETA42, Aβ42/Aβ40, Aβ40/Aβ38, PTEDUCAT
AβETA42, Aβ42/Aβ40, Aβ40/Aβ38, PTEDUCAT, APOE4
AβETA42, Aβ42/Aβ40, Aβ42/Aβ38, Aβ40/Aβ38, PTEDUCAT, APOE4
AβETA42, Aβ42/Aβ40, Aβ42/Aβ38, Aβ40/Aβ38, AGE, PTEDUCAT
AβETA42, Aβ42/Aβ40, Aβ42/Aβ38, PTEDUCAT, APOE4
AβETA42, Aβ42/Aβ40, Aβ42/Aβ38, Aβ40/Aβ38, AGE, PTEDUCAT, APOE4
AβETA42, Aβ42/Aβ40, Aβ42/Aβ38, Aβ40/Aβ38, AGE, PTEDUCAT, PTGENDER
AβETA40, Aβ42/Aβ40, Aβ40/Aβ38, AGE, PTEDUCAT
AβETA40, Aβ42/Aβ38, Aβ40/Aβ38, PTEDUCAT
Subset
AUC
C ROC curve for T status - testing set
True Positive Rate (1 - Sensitivity)
False Positive Rate (1 - Specificity)
ROC curve (area = 0.929)
D Overall prediction results for N status
AUC
Subset
E Top 10 prediction resuts for N status
Aβ42, Aβ40, Aβ42/Aβ40, Aβ42/Aβ38, Aβ40/Aβ38
Aβ42, Aβ40, Aβ42/Aβ38, Aβ40/Aβ38, PTGENDER, APOE4
Aβ42, Aβ40, Aβ42/Aβ40, Aβ40/Aβ38
Aβ40, Aβ42/Aβ40, Aβ40/Aβ38, PTEDUCAT
Aβ42, Aβ40, Aβ42/Aβ40, Aβ40/Aβ38, PTEDUCAT
Aβ40, Aβ42/Aβ40, Aβ40/Aβ38
Aβ40, Aβ42/Aβ40, Aβ40/Aβ38, APOE4
Aβ40, Aβ42/Aβ40, PTGENDER, APOE4
Aβ42, Aβ40, Aβ40/Aβ38
Aβ42, Aβ42/Aβ40, AGE, APOE4
Subset
AUC
F ROC curve for N status - testing set
True Positive Rate (1 - Sensitivity)
False Positive Rate (1 - Specificity)
ROC curve (area = 0.936)

Figure 4

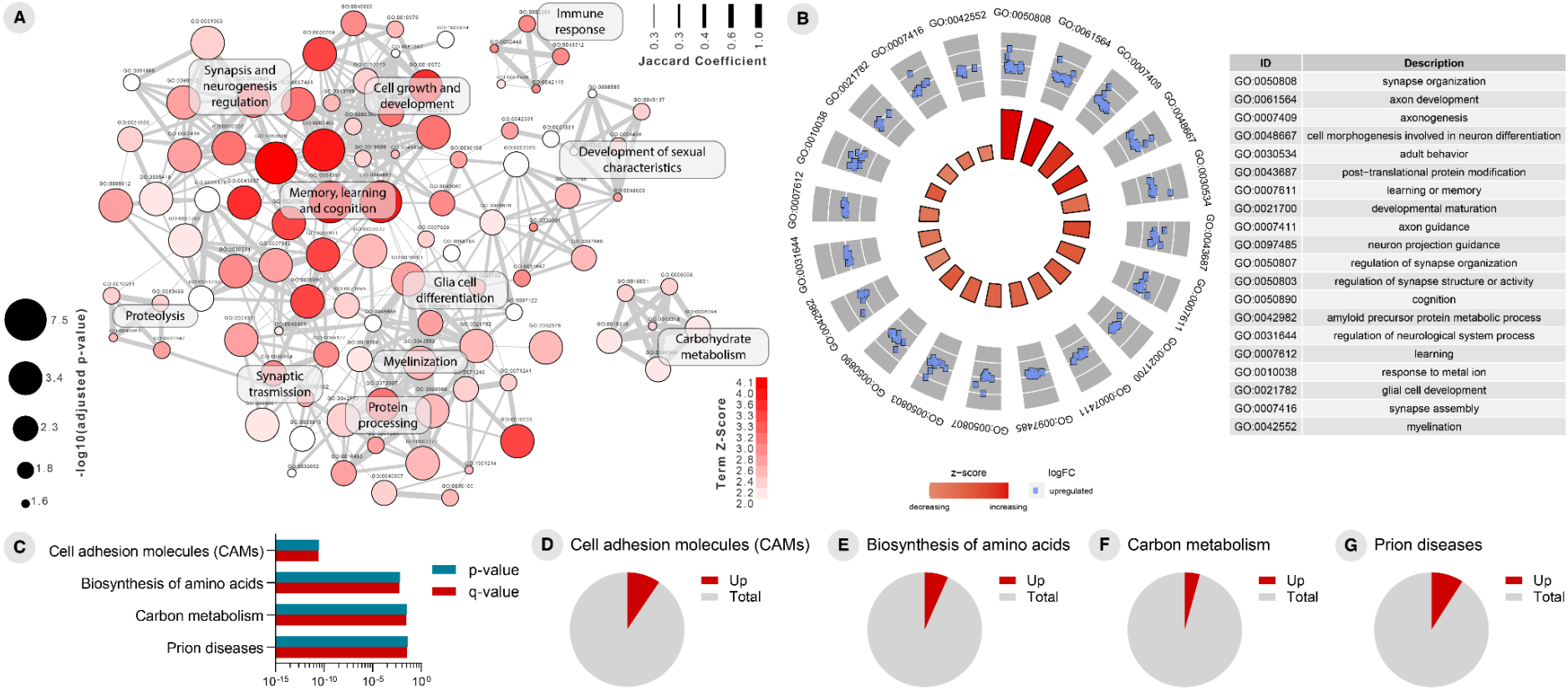

ID	Description
GO:0050808	synapse organization
GO:0061564	axon development
GO:0007409	axonogenesis
GO:0048667	cell morphogenesis involved in neuron differentiation
GO:0030534	adult behavior
GO:0043687	post−translational protein modification
GO:0007611	learning or memory
GO:0021700	developmental maturation
GO:0007411	axon guidance
GO:0097485	neuron projection guidance
GO:0050807	regulation of synapse organization
GO:0050803	regulation of synapse structure or activity
GO:0050890	cognition
GO:0042982	amyloid precursor protein metabolic process
GO:0031644	regulation of neurological system process
GO:0007612	learning
GO:0010038	response to metal ion
GO:0021782	glial cell development
GO:0007416	synapse assembly
GO:0042552	myelination

Figure 5

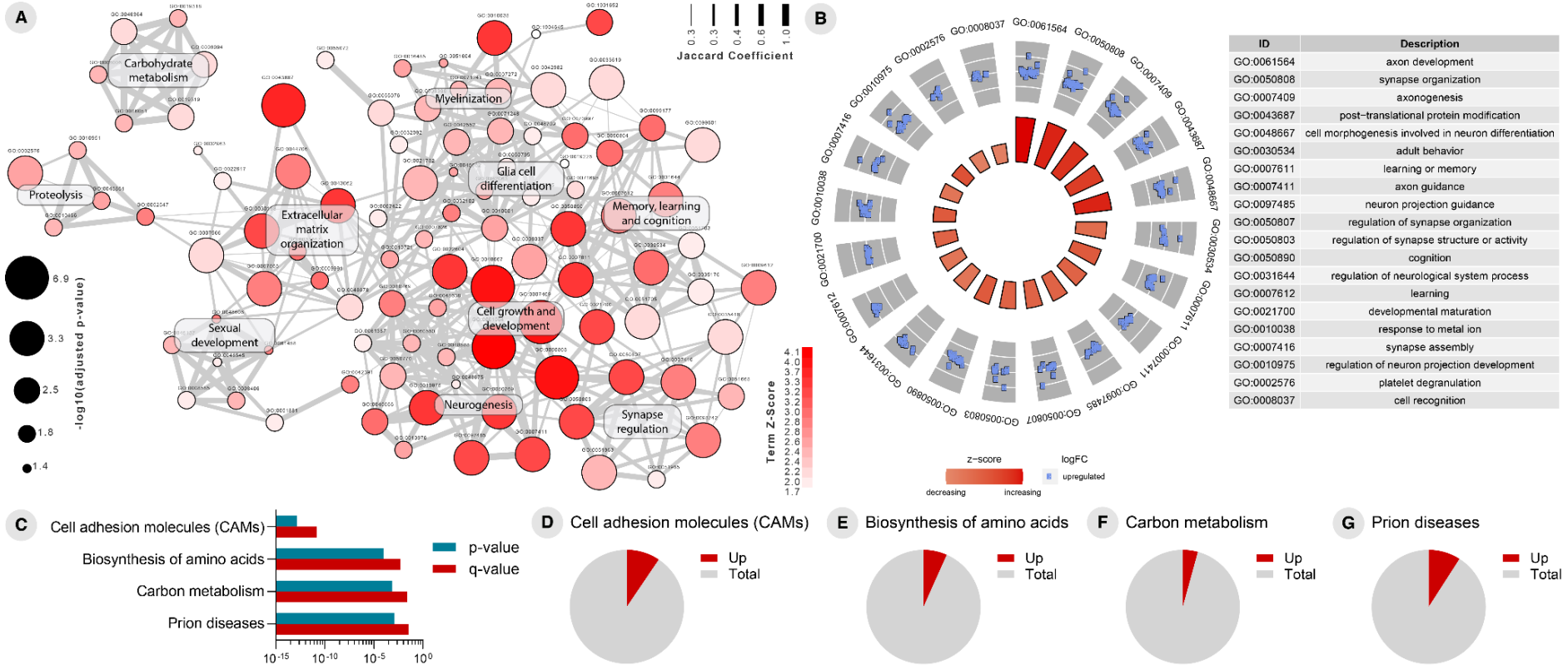

ID	Description
GO:0061564	axon development
GO:0050808	synapse organization
GO:0007409	axonogenesis
GO:0043687	post−translational protein modification
GO:0048667	cell morphogenesis involved in neuron differentiation
GO:0030534	adult behavior
GO:0007611	learning or memory
GO:0007411	axon guidance
GO:0097485	neuron projection guidance
GO:0050807	regulation of synapse organization
GO:0050803	regulation of synapse structure or activity
GO:0050890	cognition
GO:0031644	regulation of neurological system process
GO:0007612	learning
GO:0021700	developmental maturation
GO:0010038	response to metal ion
GO:0007416	synapse assembly
GO:0010975	regulation of neuron projection development
GO:0002576	platelet degranulation
GO:0008037	cell recognition

Figure 6

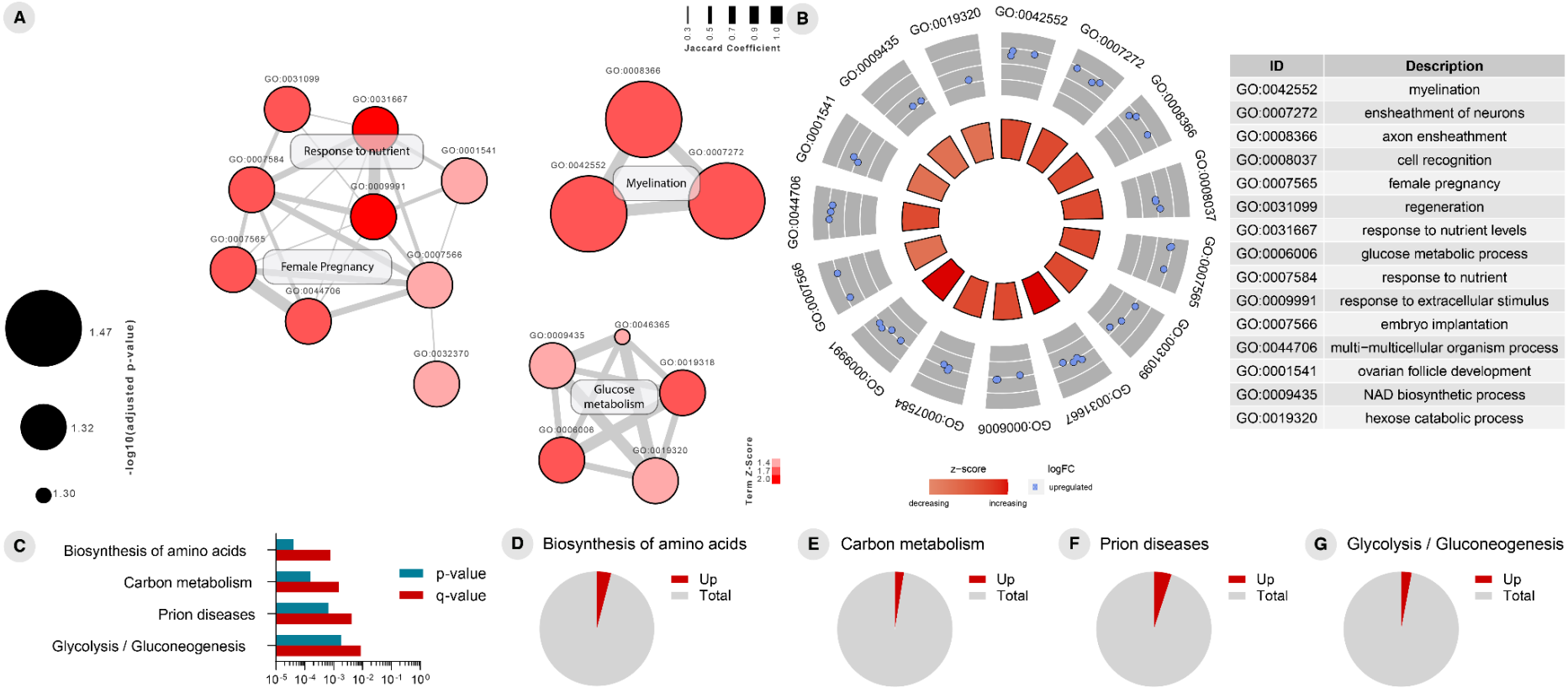

ID	Description
GO:0042552	myelination
GO:0007272	ensheathment of neurons
GO:0008366	axon ensheathment
GO:0008037	cell recognition
GO:0007565	female pregnancy
GO:0031099	regeneration
GO:0031667	response to nutrient levels
GO:0006006	glucose metabolic process
GO:0007584	response to nutrient
GO:0009991	response to extracellular stimulus
GO:0007566	embryo implantation
GO:0044706	multi−multicellular organism process
GO:0001541	ovarian follicle development
GO:0009435	NAD biosynthetic process
GO:0019320	hexose catabolic process

Figure 7

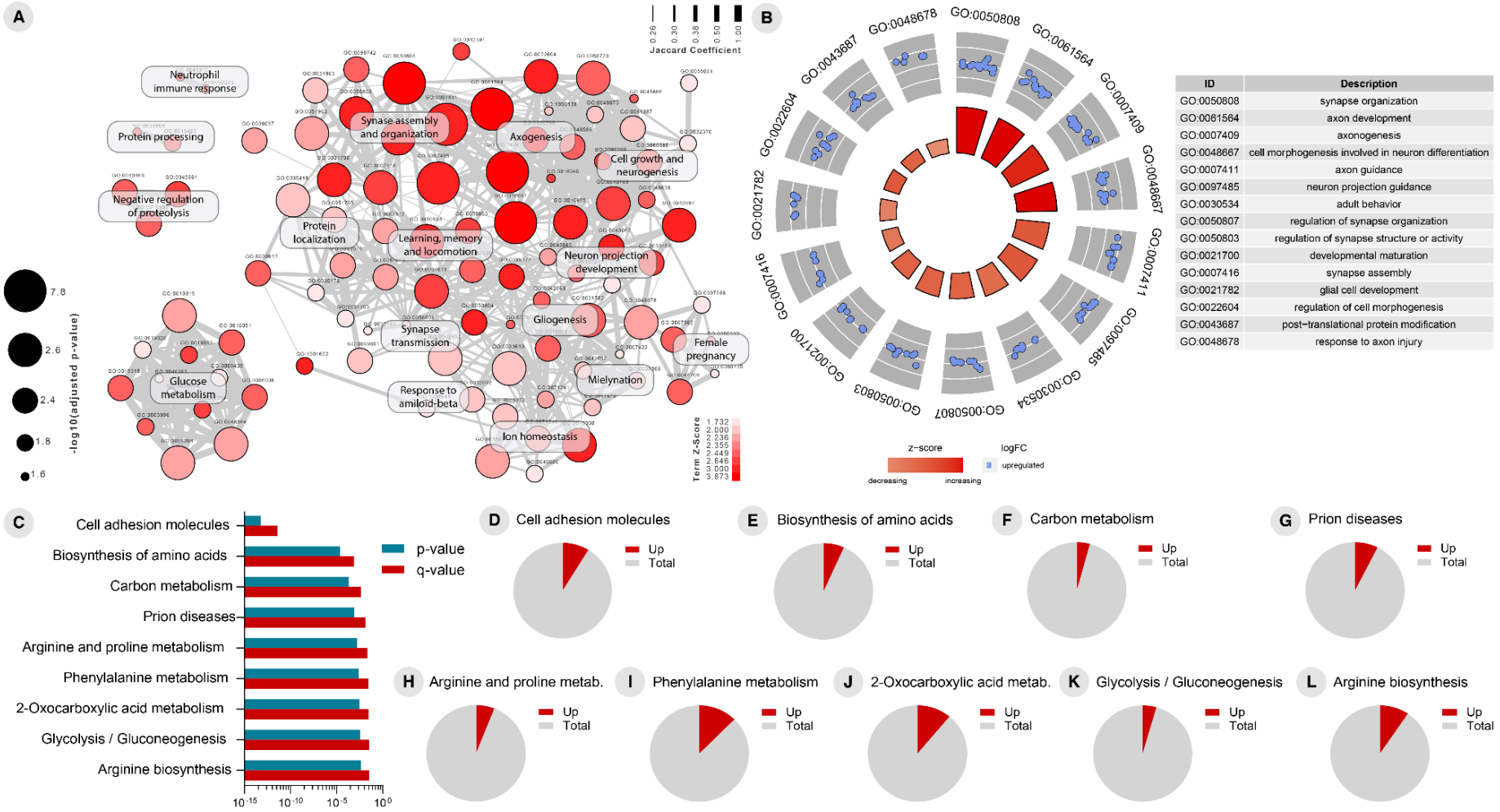

ID	Description
GO:0050808	synapse organization
GO:0061564	axon development
GO:0007409	axonogenesis
GO:0048667	cell morphogenesis involved in neuron differentiation
GO:0007411	axon guidance
GO:0097485	neuron projection guidance
GO:0030534	adult behavior
GO:0050807	regulation of synapse organization
GO:0050803	regulation of synapse structure or activity
GO:0021700	developmental maturation
GO:0007416	synapse assembly
GO:0021782	glial cell development
GO:0022604	regulation of cell morphogenesis
GO:0043687	post−translational protein modification
GO:0048678	response to axon injury

Table 1. Hyperparameters evaluated for the Machine Learning models used in the proposed framework.

Algorithm	Fixed Parameters	Iterated Parameters
Logistic Regression	solver: lbfgs max_iter: 250 penalty: l2	C: [0.0001, 0.001, 0.01, 0.1, 1, 10, 100, 1000]
Naive Bayes	-	-
kNN	algorithm: ball_tree leaf_size: 50	n_neighbors: [1, 2, 3, 4, 5, 6, 7, 8, 9] p: [1, 2]
SVC	-	for kernels: [rbf, poly, sigmoid] C: [-4, -3, -2, -1, 0, 1, 2, 3] for kernel: linear gamma: [0.00001, 0.0001, 0.001, 0.01, 0.1] C: [0.0001, 0.001, 0.01, 0.1, 1, 10, 100, 1000]
Decision Trees	-	max_depth: [1, 2, 3, 4, 5, 6, 7, 8, 9] criterion: [gini, entropy]
Random Forest	-	max_depth: [3, 4, 5, 8, 10] n_estimators: [5, 20, 50, 100, 200, 500, 1000]
Gradient Boosting	-	max_depth: [3, 4, 5, 8, 10] leargning_rate: [0.01, 0.05, 0.1, 0.2] n_estimators: [5, 20, 50, 100, 200, 500, 1000]
XGBoost	-	max_depth: [6, 7, 8] leargning_rate: [0.01, 0.025, 0.05, 0.075, 0.1] n_estimators: [5, 20, 50, 100, 200, 500, 1000]
AdaBoost	-	learning_rate: [0.25, 0.5, 1.0, 1.25, 1.5] n_estimators: [20, 50, 100, 150, 200]

kNN: k-Nearest Neighbors; SVC: Support Vector Classifier

Table 2. Sample characteristics.

Characteristic	CU	A-	A+	T-	T+	N-	N+
# of individuals	318	60	50	52	58	67	43
Sex (% female)	50%	51.67%	48%	50%	50%	50.75%	48.84%
Age (y)	75.66 ± 5.22	75.37 ± 5.67	76.01 ± 4.67	73.87 ± 4.54	77.26 ± 5.32[b***]	74.46 ± 4.66	77.52 ± 5.55[c**]
Education (y)	15.73 ± 2.83	15.42 ± 2.68	16.1 ± 2.99	15.77 ± 2.77	15.69 ± 2.91	15.57 ± 3.1	15.98 ± 2.37
MMSE	29.08 ± 1.03	28.98 ± 1.1	29.2 ± 0.95	29.13 ± 0.93	29.03 ± 1.12	29.01 ± 1.05	29.19 ± 1.01
ADAS-cog11	6.42 ± 2.92	6.09 ± 2.91	6.81 ± 2.92	6.18 ± 2.85	6.64 ± 2.99	6.22 ± 2.69	6.73 ± 3.27
APOE e4 carriers (%)	24.55%	11.67%	40%[a***]	15.38%	32.76% [b*]	19.40%	32.56%

CU: Cognitively Unimpaired; A+: Amyloid-beta positive; A-: Amyloid-beta negative; T+: tau positive; T-: tau negative; N+: neurodegeneration positive; N-: neurodegeneration negative; y: year; MMSE: Mini-Mental State Exam; ADAS-cog: Alzheimer's Disease Assessment Scale-cognitive subscale. Statistical differences for numerical characteristics were tested using t test. Statistical differences for sex and APOE status were tested using Fisher's exact test. ($^{*}p < 0.05$, $^{**}p \leq 0.01$, $^{***}p \leq 0.001$). [a] significantly different from A-, [b] significantly different from T-, [c] significantly different from N-.

Table 3. AUC results for predicting T+ and N+ CU individuals using single Aβ isoforms or its ratios.

Prediction	$A\beta_{1-38}$	$A\beta_{1-40}$	$A\beta_{1-42}$	$A\beta_{1-42}/A\beta_{1-40}$	$A\beta_{1-42}/A\beta_{1-38}$	$A\beta_{1-40}/A\beta_{1-38}$
T+	0.811	0.811	0.529	0.693	0.682	0.484
N+	0.847	0.855	0.580	0.663	0.652	0.479

T+: tau positive; N+: neurodegeneration positive; Aβ: Amyloid-beta.

Additional file 1
Machine learning results for predicting tau pathology positivity (T+).

Additional file 1.docx

Additional file 2
Machine learning results for predicting neurodegeneration positivity (N+).

Additional file 2.docx

Additional file 3
Differentially expressed proteins (DEPs) in the cerebrospinal fluid (CSF) of cognitively unimpaired (CU) tau pathology positive (T+) compared to negative (T−) subjects.

Additional file 3.docx

Additional file 4
Differentially expressed proteins (DEPs) in the cerebrospinal fluid (CSF) of cognitively unimpaired (CU) neurodegeneration positive (N+) compared to negative (T−) subjects.

Additional file 4.docx

Capítulo 2

Serine/threonine kinase activity regulates brain glucose metabolism in Alzheimer's Disease

No capítulo 2 apresentamos o manuscrito a ser submetido ao periódico *eLife*.

O diagnóstico e o monitoramento da DA melhoraram muito devido ao papel fundamental da imagem PET. Desta forma, integrar imagens PET e dados ômicos pode fornecer novos *insights* sobre a fisiopatologia da DA. Para isso, neste trabalho utilizamos genes diferencialmente expressos (DEGs) para implementar uma abordagem de redução de dimensão baseada em Gene Ontology (GO) e engenharia reversa de redes transcricionais centradas em fatores de transcrição (TF). A partir disso, selecionamos *clusters* de GOs e unidades reguladoras de TF para serem integrados com imagens de FDG-PET utilizando modelos de regressão linear a nível de *voxel*. A partir deste trabalho, identificamos processos biológicos periféricos associados ao metabolismo de FDG-PET no cérebro de indivíduos em todo o espectro clínico da DA. Além disso, destacamos o potencial das assinaturas gênicas como novos biomarcadores da DA.

Serine/threonine kinase activity regulates brain glucose metabolism in Alzheimer's Disease

Guilherme Povala[1,2,3,†], Marco Antônio De Bastiani[1,†], Bruna Bellaver[1,3], Pamela C. L. Ferreira[3], João Pedro Ferrari-Souza[1], Firoza Z. Lussier[3,5], Diogo O. Souza[1,4], Pedro Rosa-Neto[5,6,7], Bruno Zatt[2], Tharick A. Pascoal[3], Eduardo R. Zimmer[1,8,9*] and for the Alzheimer's Disease Neuroimaging Initiative

[1] Graduate Program in Biological Sciences: Biochemistry, Universidade Federal do Rio Grande do Sul,(UFRGS), Porto Alegre, Brazil.

[2] Graduate Program in Computing, Universidade Federal de Pelotas (UFPEL), Pelotas, Brazil.

[3] Department of Neurology and Psychiatry, University of Pittsburgh, Pittsburgh, US.

[4] Department of Biochemistry, Universidade Federal do Rio Grande do Sul (UFRGS), Porto Alegre, Brazil.

[5] Translational Neuroimaging Laboratory, The McGill University Research Centre for Studies in Aging, 6825 LaSalle Boulevard, Verdun, QC, H4H 1R3, Canada.

[6] Montreal Neurological Institute, 3801 University Street, Montreal, QC, H3A 2B4, Canada.

[7] Douglas Hospital, McGill University, 6875 La Salle Blvd-FBC room 3149, Montreal, QC, H4H 1R3, Canada.

[8] Department of Pharmacology, Universidade Federal do Rio Grande do Sul (UFRGS), Porto Alegre, Brazil.

[9] Graduate Program in Biological Sciences: Pharmacology and Therapeutics, Universidade Federal do Rio Grande do Sul (UFRGS), Porto Alegre, Brazil.

† These authors contributed equally to this work

* Corresponding author. Email: erzimmer@gmail.com

Guilherme Povala: guilhermepovala@gmail.com

Marco Antônio De Bastiani: tyrev@hotmail.com

Bruna Bellaver: brb253@pitt.edu

Pamela C. L. Ferreira: pamlukasewicz@gmail.com

João Pedro Ferrari-Souza: joaopedroferrarisouza@gmail.com

Firoza Z. Lussier: lussierfz@upmc.edu

Diogo O. Souza: diogo@ufrgs.br

Pedro Rosa-Neto: pedro.rosa@mcgill.ca

Bruno Zatt: zatt@inf.ufpel.edu.br

Tharick A. Pascoal: pascoal@pitt.edu

Eduardo R. Zimmer: erzimmer@gmail.com

ABSTRACT

Background

Positron emission tomography (PET) imaging has greatly improved the diagnosis and monitoring of Alzheimer's disease (AD). Now, the recently developed neuroinformatic field is expanding analytical and computational strategies to study multimodal neuroscience data. One such strategy is integrating PET imaging and omics data to provide new insights into AD pathophysiology.

Methods

Hippocampal and blood transcriptomic data of cognitively unimpaired (CU) and cognitively impaired (CI) individuals were obtained from Gene Expression Omnibus (GEO) databases and the Alzheimer's Disease Neuroimaging Initiative (ADNI). We used the differentially expressed genes (DEGs) from these datasets to implement a modular dimension reduction approach based on Gene Ontology (GO) and reverse engineering of transcriptional networks centered on transcription factors (TF). GO clusters and regulatory units of TF were selected to undergo integration with ADNI [^{18}F]Fluorodeoxyglucose ([^{18}F]FDG)-PET images using voxel-wise linear regression models adjusted for age, gender, years of education, and *APOE* ε4 status.

Results

The GO semantic similarity resulted in 16 GO clusters enriched with overlapping DEGs present in blood and the brain. Voxel-wise analysis revealed a strong association between the cluster related to the regulation of protein serine/threonine kinase activity and the [^{18}F]FDG-PET signal in the brain. The master regulator

analysis showed 61 regulatory units of TF significantly enriched with DEGs. The voxel-wise analysis of these regulons showed that zinc-finger-related regulatory units had the closest association with brain glucose metabolism.

Conclusion

We identified multiple biological processes and regulatory units of TF associated with [^{18}F]FDG-PET metabolism in the brain of individuals across the aging and AD clinical spectrum. Furthermore, the prominent enrichment of protein serine/threonine kinase activity-related GO cluster and the zinc-finger-related regulatory units highlight the potential of the gene signatures associated with AD pathology.

Keywords

Alzheimer's disease; transcriptomics; PET imaging; regulatory unit; gene ontology.

INTRODUCTION

Alzheimer's disease (AD) is in the spotlight among neurodegenerative diseases affecting the elderly (1). In recent decades, a vital concept shift has led to AD being recognized as a clinical-biological entity. High-resolution magnetic resonance imaging (MRI) and positron emission tomography (PET) currently allow for the visualization of AD pathological changes in living individuals and have enormously contributed to an improved understanding of AD (2). Indeed, these technologies boosted a new era of enormous imaging data collection in multiple centers worldwide and collaborative initiatives.

The multifaceted nature of AD requires the incorporation of complex paradigms to study its origins, mechanisms, development, and possible treatments. In this context, systems biology methods can be extremely useful to unravel disease complexity and better understand AD etiology and progression (3,4). A systems view of biology describes a multidisciplinary and holistic approach to understanding biological phenomena, focusing on the interactions of many elements simultaneously (5,6). Among many possibilities, omics technologies, such as transcriptomics, are the methods of choice to quickly, broadly, and reliably evaluate systems properties and dynamics. Transcriptomics is especially attractive because RNAs represent an intermediate level between a static genomics context and the spatio-temporal dynamic of proteomics complexity (7).

There has been an ever-increasing call for data integration in recent years. The systems biology field culminated in current trends toward multi-omics approaches to generate models of hierarchical biological networks and changes in the system as it moves from a normal to a pathological condition (8–11). In

neurosciences, these concepts and ideas resulted in the neuroinformatic subfield devoted to developing analytical and computational models for sharing, integrating, and analyzing multimodal neuroscience data. In this context, strategies to integrate neuroimaging data with transcriptomics started to emerge at the gene level (12–14). However, genes rarely dictate phenotypes alone, acting in concert to modulate phenotypic transitions.

In the present study, we sought to implement two modular, systems-based strategies to integrate the transcriptomics information of groups of genes with PET neuroimaging data in AD. In the first, clusters of Gene Ontology (GO) terms grouped by semantic similarity were associated with [^{18}F]FDG-PET images, highlighting a GO cluster significantly associated with AD. The second strategy used reverse engineering of transcriptional networks to integrate regulatory units of transcription factors with [^{18}F]FDG-PET images.

METHODS

Blood Expression Data Acquisition

Blood microarray data of 743 individuals were obtained from the Alzheimer's Disease Neuroimaging Initiative (ADNI) (http://adni.loni.usc.edu/). Samples with RNA integrity (RIN) scores above seven were included in the study. After RIN and quality control filters, the resulting ADNI dataset retained 317 samples [218 cognitively impaired (CI) and 99 cognitively unimpaired (CU) individuals]. Additional processed blood microarray datasets were obtained from Gene Expression Omnibus (GEO) repository (https://www.ncbi.nlm.nih.gov/geo/). GSE63063 (15) contains 433 CI and 223 CU samples from AddneuroMed Cohort, and GSE97760 (16) includes 8 CI and

7 CU controls (**Figure 1A**). Metadata from these datasets are shown in **Supplemental Table 1**.

Healthy human blood samples from two large microarray datasets were obtained from the GEO repository [GSE48348 (17) and GSE99039 (18)], downloaded using the *GEOquery* package (v2.56.0) (19), and combined under common gene symbol annotations using the *virtualArray* package (v1.8.0) (20). The resulting dataset retained 967 healthy blood samples used for transcriptional network inference.

Brain Expression Data Acquisition

Human AD hippocampal microarray data of six studies were obtained from GEO repository [GSE5281 (21), GSE28146 (22), GSE29378 (23), GSE36980 (24), GSE48350 (25) and GSE84422 (26)], downloaded using the *GEOquery* package (v2.56.0) (19) and combined under common gene symbol annotations using the *virtualArray* package (v1.8.0) (20) (**Figure 1A**). Raw CEL data was processed using the *affy* package (v1.70.0) (27), and RMA was corrected using the *vsn* package (v3.60.0) (28). Afterward, a batch correction was implemented using the *sva* package (v3.40.0) (29). The combined dataset contained 90 CI and 116 CU individuals (**Supplemental Table 1**). Sample demographics can be found in **Supplemental Table 2**.

Differential Expression Analyses

Differential expression analyses were computed on microarray data using the *limma* package (v3.48.3) (30) *lmFit* function to fit multiple linear models by generalized least squares. In addition, *eBayes* function was used to compute

moderated t-statistics, moderated F-statistics, and log-odds of differential expression by empirical Bayes moderation of the standard errors towards a common value (**Figure 1B**).

We reasoned that brain expression would be more sensitive to alterations than blood expression in AD. Thus, genes with an unadjusted p-value < 0.05 in at least ⅔ of the tested datasets were considered differentially expressed genes (DEGs) for blood samples. While, for brain samples, genes with FDR adjusted p-value < 0.01 from the merged dataset were considered DEGs. The final list of genes used for further analyses was obtained from the intersection between blood and brain DEGs. Venn diagrams were constructed using the *VennDiagram* package (v1.6.20) (31). Details about differentially expressed genes from datasets are shown in **Supplemental Tables 3 and 4**.

Functional Enrichment Analyses and Gene Ontology Semantic Similarity

DEGs intersecting blood between brain datasets were submitted to Gene Ontology (GO) enrichment analysis using the *clusterProfiler* package (v4.0.5) (32) *enrichGO* function. The GO biological process terms were clustered by semantic similarity using the *mgoSim* function from the *GOSemSim* (v2.18.1) package (33) (arguments measure = "Wang" and combine = NULL). Semantic comparisons of Gene Ontology (GO) annotations provide quantitative ways to compute similarities between genes and gene groups. The resulting similarity matrices were represented as GO networks using the *RedeR* (v1.40.0) package (34) for interactive visualization and manipulation of nested networks. We retained only similarity scores above the 80th percentile of score distribution for building the network. Clusters of GO terms

obtained from the GOSemSim algorithm were manually named for their biological interpretation (**Figure 1C**).

Reverse Engineering of Transcriptional Network and Master Regulator Analysis

The transcriptional network (TN) centered on transcription factors (TF), and their predicted target genes were inferred using a large cohort of healthy blood samples and merged as described in **Blood Expression Data Acquisition**. Herein, the terms “regulatory unit” or “regulon” are used to describe the groups of inferred genes and their associated TFs. *RTN* (v2.16.1) package was used to reconstruct and analyze TNs based on the mutual information (MI) using the Algorithm for the Reconstruction of Accurate Cellular Networks (ARACNe) method (35–37). In summary, the regulatory structure of the network is derived by mapping significant associations between known TFs and all potential targets. A curated list of genes obtained from (38) was used to annotate TF eligibility for TN inference input. To create a consensus bootstrap network, the interactions below a minimum MI threshold were eliminated by a permutation step, and unstable interactions were additionally removed by bootstrap. Finally, the data processing inequality algorithm is applied with null tolerance to eliminate interactions likely to be mediated by a third TF. The reference blood TN was built using the package’s default number of 5000 permutations and 100 bootstraps (p-value < 0.001).

We conducted the master regulator analysis (MRA) described by Carro and colleagues (39) on the regulatory units with more than 100 targets using the RTN package. For each regulatory unit in the blood TN, the algorithm computes the statistical overrepresentation (calculated by Fisher's exact test) of genes obtained from differential expression analyses (unadjusted p-value < 0.05). Master regulator

candidates altered in at least ⅔ of the three case-control studies (ADNI, GSE63063, and GSE99039) were selected for gene set variation analysis and neuroimaging integration (**Figure 1D**).

Gene Set Variation Analysis

The enrichment scores (ES) obtained from the gene set variation analysis (GSVA) method were used to collapse the activity of groups of genes into a single value for each sample. This gene set enrichment method estimates group gene activity variation over a sample population in an unsupervised manner. Briefly, genes contained in the clusters of GO terms obtained from GOSemSim or in the regulatory units obtained from master regulator analysis were submitted to the *gsva* function (kcdf="Gaussian") of the *GSVA* package in R (40). The resulting ES was used for further association with neuroimaging data and correlation analyses.

Imaging pre-processing and integration

Imaging data were acquired from ADNI (**Figure 1A**). [^{18}F]FDG-PET images were downloaded in the "*Co-reg, avg, std img and vox size, uniform resolution*" pre-processed format. MPRAGE MRI images were downloaded with "*gradwarp, B1 non-uniformity, and N3 image*" pre-processing correction steps. [^{18}F]FDG-PET images were linearly registered to the T1-weighted image space. T1-weighted images were linearly and nonlinearly registered to the MNI template space. Subsequently, an [^{18}F]FDG-PET nonlinear registration was performed using the linear and nonlinear transformations from the T1-weighted image to the MNI space and the [^{18}F]FDG-PET to T1-weighted image registration. These transformations were performed using the scripts *antsRegistrationSyNQuick* and *antsApplyTransforms*

from advanced normalization tools (ANTs) (41). The [^{18}F]FDG-PET images were spatially smoothed to achieve a final resolution of 8mm full width at half maximum using *mincblur* from MINC Tools (http://bic-mni.github.io/).

The [^{18}F]FDG-PET standardized uptake ratio (SUVr) maps were generated using the cerebellum as a reference region. GO clusters and regulons obtained in the previous step were selected to undergo integration with [^{18}F]FDG-PET images using voxel-wise linear regression models adjusted for age, gender, and years of education (RMINC package) (https://github.com/Mouse-Imaging-Centre/RMINC) (**Figure 1E**). The voxel-wise correlations resulted in t-statistical maps. Afterwards, only statistically significant correlated voxels (| t-value | > 2.6 [p-value of 0.01]) were retained.

RESULTS

The dimension reduction strategy proposed in this work is represented by the Sankey flow diagram in **Figure 2**. Specifically, the union between blood and hippocampus transcriptomic data resulted in 16972 unique genes. When comparing CU and CI individuals from the 16126 blood genes, the differential expression analysis showed 2875 DEGs (unadjusted p-value < 0.05 present in at least ⅔ of datasets). From the 10845 hippocampus genes, 1979 DEGs were found (FDR adjusted p-value < 0.01 from the merged dataset) in the comparison between CU and CI individuals. Considering the DEGs from blood and hippocampus, 428 were consistently altered between tissues. FEA of Gene Ontology using these genes revealed 89 terms significantly enriched with altered elements (**Supplemental Tables 5 and 6**). These results showed consistent modifications in functional terms associated with oxidative phosphorylation in mitochondria and cell cycle and response to stress.

Next, we used semantic similarity to group GO biological process terms into clusters of similar functional relevance. This dimension reduction strategy resulted in 16 clusters (**Figure 2**). **Figure 3A** shows these clusters in a network mapping node sizes to cluster size (number of terms in the cluster) and edge width to the similarity score returned by the GOSemSim algorithm (see *Methods*; network average degree [sd] = 3 [2.07]). We observed that the clusters associated with *'regulation of serine/threonine kinase activity'* and *'DNA repair and metabolism'* had the highest connectivity metric (degree = 6) and degree/size ratio (degree/size = 2). Thus, albeit containing fewer terms than other clusters, these two clusters had the largest influence over the network. **Figure 3B** shows the heatmap of the semantic similarity matrix based on the GO terms and the resulting clusters of terms obtained from GOSemSim. Details about the clusters are reported in **Supplementary Table 7**. For the blood datasets, we also used reverse engineering of transcriptional networks to infer groups of regulatory units under the control of transcription factors. Similar to GO functional enrichment analysis and semantic similarity, the aim was to collapse groups of altered genes into biological modules. The MRA accomplishes this by identifying the regulatory units of transcription factors most enriched with DEGs. We observed 34, 92, and 41 regulatory units statistically altered in ADNI, GSE63063, and GSE97760 blood datasets, respectively (**Supplementary Table 8**). Sixty-one regulatory units were significantly enriched with DEGs in at least ⅔ of the datasets explored, and 12 were altered in all three. **Figure 4A** shows gene set enrichment analyses indicating the phenotypic associations (CI versus CU) of the top 10 regulons altered in brain imaging. We also evaluated the GO functional enrichment of each top 10 regulons and mapped the results in **Figure 4B** as a network. This result showed that the genes inferred for most regulons are associated with biological

processes. However, the regulatory units of GATA1 and ZNF358, for example, had mixed terms and were mainly related to cellular component terms. Interestingly, the ZNF653 regulatory unit is more connected with GOs related to energetic metabolism and protein kinase activity. Finally, we did not observe significant enrichment of GO terms for the ZZZ3 regulatory unit.

With the 16 GO clusters obtained from semantic similarity analysis, we performed voxel-wise correlations testing the topographical associations between [^{18}F]FDG-PET and each GO cluster enrichment score. Out of the 16 t-statistical maps obtained, one showed significant associations (t-value > 2.6, peak-t = 4.86, p-value = 0.01]) between the GO cluster enrichment score and cerebral glucose metabolism measured with [^{18}F]FDG-PET (**Figure 5A**). Interestingly, this cluster showed a positive correlation, indicating that the alterations of the investigated GO cluster are related to brain glucose hypermetabolism. This GO cluster is involved in the regulation of protein serine/threonine kinase activity, and the increase in the brain [^{18}F]FDG-PET signal was more prominent in the precuneus' gray matter (59.25% left, 68.63% right), medial frontal gyrus (52.76% left, 14.01% right), medial frontal-orbital gyrus (51.39% left, 11.58% right) and cingulate region (46.60% left, 18.46% right) (**Figure 5B**).

Similarly, we also performed voxel-wise linear regressions to investigate the spatial association between [^{18}F]FDG-PET and the regulatory units enriched with DEGs. Among the 61 regulatory units, we analyzed the regulatory unit most closely associated with brain glucose metabolism (t-value > 2.6, peak-t = 3.90, p-value = 0.01]) (**Figure 6A**). In general, the association of regulatory unit ZNF653 with [^{18}F]FDG-PET signal was most observed in the precuneus' gray matter (24.24% left,

39.51% right), medial frontal gyrus (17.26% left), medial frontal-orbital gyrus (12.50% left) and precentral gyrus (9.08% left, 8.28% right) (**Figure 6B**).

DISCUSSION

Modularity is a recurrent theme in biology, permitting the development of emergent properties and hierarchical functions (52–54). In the present study, we developed a pipeline composed of two modules that integrates omics data with PET imaging. This method has a straightforward use in identifying altered peripheral biological pathways and novel biomarker candidates representative of specific biological abnormalities in AD. The first module involves omics analysis, composed of dimension reduction through the differential expression analysis, followed by functional enrichment analysis using the GO semantic similarity, or transcriptional network analysis, responsible for altered regulatory unit selection. The second module is imaging integration, where PET imaging is associated with statistically altered GO clusters and regulatory units. Aiming to validate the proposed method, we integrated blood transcriptomic data with [^{18}F]FDG-PET imaging.

Semantic similarity analysis of the GO biological processes revealed clusters of terms altered in the blood that are significantly associated with [^{18}F]FDG-PET. Finally, applying a reverse engineering strategy, we identified ten transcription factors and their regulatory units potentially acting as master regulators in our analysis and significantly associated with cerebral glucose metabolism. [^{18}F]FDG-PET is an essential modality for detecting functional changes in AD, clinically useful for identifying changes in early AD and differentiating AD from other causes of dementia. The [^{18}F]FDG-PET signal has been claimed to be derived from neurons, astrocytes, and, more recently, microglia (42–44). This newly proposed integration method can

help in the biological interpretation of imaging biomarkers such as the [^{18}F]FDG-PET, providing important insights into understanding AD pathology.

Our newly proposed integration method revealed that the GO cluster representing serine/threonine protein kinase activity was the most closely associated with [^{18}F]FDG-PET hypermetabolism. By adding phosphate groups quickly and dynamically, kinases can coordinate and control complex cellular functions, such as energy production, cell growth, and survival. Our brain is composed of hundreds of protein kinases, with a few already shown to lead to the spread of aberrant signaling in AD (45–47). In this sense, kinases such as Akt, extracellular signal-regulated kinase 1 and 2 (ERK1/2), cAMP-dependent protein kinase (PKA), glycogen synthase kinase-3β (GSK-3β), p70S6 kinase, and cyclin-dependent protein kinases 5 (Cdk5) were found with increased expression or activity in the AD brain. The hyperactivation of these kinases can lead to abnormal tau phosphorylation, amyloid production, apoptosis, and neuroinflammation. For instance, an increase in GSK-3β activity was observed in individuals with familial AD mutation of amyloid precursor protein (Swedish751) (46).

Our findings showed glucose hypermetabolism correlating [^{18}F]FDG-PET imaging and TF related to zinc-finger proteins. Specifically, among the top 10 regulatory units with the most association with [^{18}F]FDG-PET, seven of them are from the zinc-finger family. The zinc-finger units regulate gene expression at the transcriptional and translational levels and are highly expressed in the brain (48). It has already been demonstrated that zinc-finger genes are associated with pathological changes in AD and regulate the expression of AD-related genes that are upstream in the production of hyperphosphorylated tau (49). Altogether, this could

explain the positive association when integrating [^{18}F]FDG-PET and zinc-finger-related regulatory units enriched with DEGs.

When comparing the cluster representing serine/threonine protein kinase activity with the top 10 enriched regulatory units, we did not find any shared GO between them. However, the brain regions that showed significant correlations with zinc-finger genes are included in the regions that correlate with the serine/threonine protein kinase activity cluster. Even without sharing the same GO terms, this overlap could be interpreted as the presence of more than one altered function related to glucose hypermetabolism. Interestingly, the zinc-finger ZNF653 has 52 phosphorylation sites, 9 of which are confirmed in humans, and 5 of them are serine/threonine. This way, one could argue that the serine/threonine kinase may be modulating the activity of these TFs.

A biological definition of AD has recently been proposed solely based on AD biomarkers (50). Although it reflects fundamental advances in the development of neuroimaging and fluid biomarkers in AD research, a significant limitation of implementing this framework in clinical practices is the low predictive accuracy of this system (51). For instance, many Aβ and tau-positive CU individuals remain cognitively stable for their entire lifetime (51), suggesting that pathophysiological processes beyond Aβ and tau pathologies must be considered. Here, we detected abnormalities in critical peripheral biological pathways in AD patients, which has the potential to provide insights for developing novel biomarkers. Additionally, here we presented the integration of blood transcriptomic data and brain imaging as a novel tool that can be applied using multiple PET imaging tracers (*e.g.*, Aβ PET, tau PET,

TSPO PET), as well as adapted and used in the context of different neurological diseases and different omics modalities.

CONCLUSION

We developed a strategy to integrate modular structures obtained from transcriptomic data, e.g., clusters of GO biological processes terms and regulatory units of TF, with [^{18}F]FDG-PET imaging. Our results identified associations between protein serine/threonine kinase activity-related GO cluster and zinc-finger-related regulatory units with [^{18}F]FDG-PET brain metabolism in AD. Finally, given the multifactorial nature of AD, additional studies are required to further validate these findings.

REFERENCES

1. Alzheimer's Disease International. World Alzheimer Report 2018: The state of the art of dementia research: New frontiers [Internet]. Alzheimer's Disease International. 2018. Available from: https://www.alz.co.uk/research/WorldAlzheimerReport2018.pdf
2. Hane FT, Robinson M, Lee BY, Bai O, Leonenko Z, Albert MS. Recent Progress in Alzheimer's Disease Research, Part 3: Diagnosis and Treatment. J Alzheimers Dis. 2017;57(3):645–65.
3. Villoslada P, Steinman L, Baranzini SE. Systems biology and its application to the understanding of neurological diseases. Ann Neurol. 2009 Feb;65(2):124–39.
4. Wang ZTT, Tan CCC, Tan L, Yu JTT. Systems biology and gene networks in Alzheimer's disease. Neurosci Biobehav Rev. 2019 Jan;96:31–44.
5. Oltvai ZN, Barabási AL. Systems biology. Life's complexity pyramid. Science. 2002 Oct;298(5594):763–4.
6. Kirschner MW. The meaning of systems biology. Cell. 2005 May;121(4):503–4.
7. Verheijen J, Sleegers K. Understanding Alzheimer Disease at the Interface between Genetics and Transcriptomics. Trends Genet TIG. 2018;34(6):434–47.
8. Hasin Y, Seldin M, Lusis A. Multi-omics approaches to disease. Genome Biol. 2017;18(1):83–83.
9. Yang X. Multitissue Multiomics Systems Biology to Dissect Complex Diseases. Trends Mol Med. 2020 Aug;26(8):718–28.
10. Hampel H, Lista S, Neri C, Vergallo A. Time for the systems-level integration of aging: Resilience enhancing strategies to prevent Alzheimer's disease. Prog Neurobiol. 2019 Oct;181:101662.
11. the Alzheimer Precision Medicine Initiative (APMI), Hampel H, Vergallo A, Perry G, Lista S. The Alzheimer Precision Medicine Initiative. Ghidoni R, Moreira P, editors. J Alzheimers Dis. 2019 Mar 12;68(1):1–24.
12. Gaiteri C, Dawe R, Mostafavi S, Blizinsky KD, Tasaki S, Komashko V, et al. Gene expression and DNA methylation are extensively coordinated with MRI-based brain microstructural characteristics. Brain Imaging Behav. 2019 Aug;13(4):963–72.
13. Iturria-Medina Y, Carbonell F, Assadi A, Adewale Q, Khan AF, Baumeister TR, et al. Integrating molecular, histopathological, neuroimaging and clinical neuroscience data with NeuroPM-box. Commun Biol. 2021 Dec;4(1):614.
14. Zeiler FA, Iturria-Medina Y, Thelin EP, Gomez A, Shankar JJ, Ko JH, et al. Integrative Neuroinformatics for Precision Prognostication and Personalized Therapeutics in Moderate and Severe Traumatic Brain Injury. Front Neurol. 2021 Sep 7;12:729184.
15. Sood S, Gallagher IJ, Lunnon K, Rullman E, Keohane A, Crossland H, et al. A novel multi-tissue RNA diagnostic of healthy ageing relates to cognitive health status. Genome Biol. 2015 Sep 7;16:185.
16. Naughton BJ, Duncan FJ, Murrey DA, Meadows AS, Newsom DE, Stoicea N, et al. Blood genome-wide transcriptional profiles reflect broad molecular impairments and strong blood-brain links in Alzheimer's disease. J Alzheimers Dis JAD. 2015;43(1):93–108.
17. Westra HJ, Peters MJ, Esko T, Yaghootkar H, Schurmann C, Kettunen J, et al.

Systematic identification of trans eQTLs as putative drivers of known disease associations. Nat Genet. 2013 Oct;45(10):1238–43.
18. Shamir R, Klein C, Amar D, Vollstedt EJ, Bonin M, Usenovic M, et al. Analysis of blood-based gene expression in idiopathic Parkinson disease. Neurology. 2017 Oct 17;89(16):1676–83.
19. Davis S, Meltzer PS. GEOquery: a bridge between the Gene Expression Omnibus (GEO) and BioConductor. Bioinforma Oxf Engl. 2007 Jul;23(14):1846–7.
20. Heider A, Alt R. virtualArray: a R/bioconductor package to merge raw data from different microarray platforms. BMC Bioinformatics. 2013 Mar;14:75–75.
21. Liang WS, Dunckley T, Beach TG, Grover A, Mastroeni D, Walker DG, et al. Gene expression profiles in anatomically and functionally distinct regions of the normal aged human brain. Physiol Genomics. 2007 Feb 12;28(3):311–22.
22. Blalock EM, Buechel HM, Popovic J, Geddes JW, Landfield PW. Microarray analyses of laser-captured hippocampus reveal distinct gray and white matter signatures associated with incipient Alzheimer's disease. J Chem Neuroanat. 2011 Oct;42(2):118–26.
23. Miller JA, Woltjer RL, Goodenbour JM, Horvath S, Geschwind DH. Genes and pathways underlying regional and cell type changes in Alzheimer's disease. Genome Med. 2013;5(5):48.
24. Hokama M, Oka S, Leon J, Ninomiya T, Honda H, Sasaki K, et al. Altered expression of diabetes-related genes in Alzheimer's disease brains: the Hisayama study. Cereb Cortex N Y N 1991. 2014 Sep;24(9):2476–88.
25. Berchtold NC, Cribbs DH, Coleman PD, Rogers J, Head E, Kim R, et al. Gene expression changes in the course of normal brain aging are sexually dimorphic. Proc Natl Acad Sci U S A. 2008 Oct 7;105(40):15605–10.
26. Wang M, Roussos P, McKenzie A, Zhou X, Kajiwara Y, Brennand KJ, et al. Integrative network analysis of nineteen brain regions identifies molecular signatures and networks underlying selective regional vulnerability to Alzheimer's disease. Genome Med. 2016 Nov 1;8(1):104.
27. Gautier L, Cope L, Bolstad BM, Irizarry RA. affy--analysis of Affymetrix GeneChip data at the probe level. Bioinforma Oxf Engl. 2004 Feb 12;20(3):307–15.
28. Huber W, von Heydebreck A, Sültmann H, Poustka A, Vingron M. Variance stabilization applied to microarray data calibration and to the quantification of differential expression. Bioinforma Oxf Engl. 2002;18 Suppl 1:S96-104.
29. Leek JT, Johnson WE, Parker HS, Jaffe AE, Storey JD. The sva package for removing batch effects and other unwanted variation in high-throughput experiments. Bioinforma Oxf Engl. 2012 Mar;28(6):882–3.
30. Ritchie ME, Phipson B, Wu D, Hu Y, Law CW, Shi W, et al. Limma powers differential expression analyses for RNA-sequencing and microarray studies. Nucleic Acids Res. 2015;43(7):e47–e47.
31. Chen H, Boutros PC. VennDiagram: a package for the generation of highly-customizable Venn and Euler diagrams in R. BMC Bioinformatics. 2011 Dec;12(1):35–35.
32. Yu G, Wang LG, Han Y, He QY. clusterProfiler: an R Package for Comparing Biological Themes Among Gene Clusters. Available from: http://bioconductor.org/packages/release/bioc/html/clusterProfiler.html
33. Yu G, Li F, Qin Y, Bo X, Wu Y, Wang S. GOSemSim: an R package for

measuring semantic similarity among GO terms and gene products. Bioinforma Oxf Engl. 2010 Apr;26(7):976–8.
34. Castro MAA, Wang X, Fletcher MNC, Meyer KB, Markowetz F. RedeR: R/Bioconductor package for representing modular structures, nested networks and multiple levels of hierarchical associations. Genome Biol. 2012 Apr 24;13(4):R29.
35. Fletcher MNC, Castro MAA, Wang X, De Santiago I, O'Reilly M, Chin SF, et al. Master regulators of FGFR2 signalling and breast cancer risk. Nat Commun. 2013;4(May):1–12.
36. Margolin AA, Nemenman I, Basso K, Wiggins C, Stolovitzky G, Favera RD, et al. ARACNE: An algorithm for the reconstruction of gene regulatory networks in a mammalian cellular context. BMC Bioinformatics. 2006;7(SUPPL.1):1–15.
37. Margolin AA, Wang K, Lim WK, Kustagi M, Nemenman I, Califano A. Reverse engineering cellular networks. Nat Protoc. 2006;1(2):662–71.
38. Lambert SA, Jolma A, Campitelli LF, Das PK, Yin Y, Albu M, et al. The Human Transcription Factors. Cell. 2018;172(4):650–65.
39. Carro MS, Lim WK, Alvarez MJ, Bollo RJ, Zhao X, Snyder EY, et al. The transcriptional network for mesenchymal transformation of brain tumours. Nature. 2010 Jan;463(7279):318–25.
40. Hanzelmann S, Castelo R, Guinney J. GSVA: gene set variation analysis for microarray and RNA-Seq data. BMC Bioinformatics. 2013;14(1):7–7.
41. Avants BB, Tustison NJ, Stauffer M, Song G, Wu B, Gee JC. The Insight ToolKit image registration framework. Front Neuroinformatics [Internet]. 2014 Apr 28 [cited 2022 Apr 25];8. Available from: http://journal.frontiersin.org/article/10.3389/fninf.2014.00044/abstract
42. Xiang X, Wind K, Wiedemann T, Blume T, Shi Y, Briel N, et al. Microglial activation states drive glucose uptake and FDG-PET alterations in neurodegenerative diseases. Sci Transl Med. 2021 Oct 13;13(615):eabe5640.
43. Zimmer ER, Parent MJ, Souza DG, Leuzy A, Lecrux C, Kim HI, et al. [18F]FDG PET signal is driven by astroglial glutamate transport. Nat Neurosci. 2017 Mar;20(3):393–5.
44. Mosconi L, Tsui WH, Herholz K, Pupi A, Drzezga A, Lucignani G, et al. Multicenter standardized 18F-FDG PET diagnosis of mild cognitive impairment, Alzheimer's disease, and other dementias. J Nucl Med Off Publ Soc Nucl Med. 2008 Mar;49(3):390–8.
45. Perluigi M, Barone E, Di Domenico F, Butterfield DA. Aberrant protein phosphorylation in Alzheimer disease brain disturbs pro-survival and cell death pathways. Biochim Biophys Acta BBA - Mol Basis Dis. 2016 Oct;1862(10):1871–82.
46. Ryder J, Su Y, Ni B. Akt/GSK3β serine/threonine kinases: evidence for a signalling pathway mediated by familial Alzheimer's disease mutations. Cell Signal. 2004 Feb;16(2):187–200.
47. Rosenberger AFN, Hilhorst R, Coart E, García Barrado L, Naji F, Rozemuller AJM, et al. Protein Kinase Activity Decreases with Higher Braak Stages of Alzheimer's Disease Pathology. J Alzheimers Dis. 2015 Oct 27;49(4):927–43.
48. ZNF653 zinc finger protein 653 [Homo sapiens (human)] - Gene - NCBI [Internet]. [cited 2022 Apr 25]. Available from: https://www.ncbi.nlm.nih.gov/gene?Db=gene&Cmd=DetailsSearch&Term=115950#gene-expression

49. Bu S, Lv Y, Liu Y, Qiao S, Wang H. Zinc Finger Proteins in Neuro-Related Diseases Progression. Front Neurosci. 2021;15:760567.
50. Jack CR, Bennett DA, Blennow K, Carrillo MC, Dunn B, Haeberlein SB, et al. NIA‐AA Research Framework: Toward a biological definition of Alzheimer's disease. Alzheimers Dement. 2018 Apr;14(4):535–62.
51. Dubois B, Villain N, Frisoni GB, Rabinovici GD, Sabbagh M, Cappa S, et al. Clinical diagnosis of Alzheimer's disease: recommendations of the International Working Group. Lancet Neurol. 2021 Jun;20(6):484–96.
52. Lorenz DM, Jeng A, Deem MW. The emergence of modularity in biological systems. Phys Life Rev. 2011 Jun;8(2):129–60.
53. Alcalá-Corona SA, Sandoval-Motta S, Espinal-Enríquez J, Hernández-Lemus E. Modularity in Biological Networks. Front Genet. 2021;12:701331.
54. Melo D, Porto A, Cheverud JM, Marroig G. Modularity: genes, development and evolution. Annu Rev Ecol Evol Syst. 2016;47:463–86.

Figure legends

Figure 1. Omics-imaging integration pipeline. (A) Data collection of blood and hippocampus samples and imaging data from multiple datasets. (B) Transcriptomics dimension reduction using differential expression analysis. (C) Functional enrichment analysis using the Gene Ontology (GO) semantic similarity. (D) Transcriptional network analysis, responsible for selecting altered regulatory units. (E) Imaging integration using voxel-wise generalized linear regression between PET images and statistically altered GO clusters and regulatory units.

Figure 2. Sankey Flow Diagram representing the Dimension Reduction Strategy. (A) Blood and hippocampus transcriptomic data were obtained from the available cohorts. For each tissue, the Differential Expression Analysis (DEA) was performed comparing Cognitively Unimpaired (CU) and Cognitively Impaired (CI) individuals to generate Differentially Expressed Genes (DEGs). Considering the DEGs from blood and hippocampus, the ones that were consistently altered between tissues were selected (overlapping DEGs). The Gene Ontology (GO) Biological Processes were generated through the Functional Enrichment Analysis (FEA) of GOs using overlapping DEGs between blood and hippocampus. The semantic similarity method was used to group GO biological process terms into clusters of similar functional relevance (GO clusters). Regulatory Units of transcriptional factors (regulons) were generated using the same overlapping DEGs. (B) The Sunburst plot of Regulatory Units shows the number of genes for 12 regulons selected considering the tail-end quartiles (10% and 90%) of the enrichment score. (C) Given that the GO clusters are composed of multiple GOs, each segment in the Sunburst plot of GO clusters shows the number of genes for each GO that comprise the specific cluster.

Figure 3. Functional Enrichment of Gene Ontology Biological Processes. (A) Gene Ontology (GO) semantic similarity network. GO biological process (GOBP) terms were clustered by semantic similarity and networked mapping cluster sizes to nodes and cluster similarity coefficients to edges. (B) Semantic similarity matrix heatmap of GOBP terms.

Figure 4. Enrichment of Regulatory Units of Transcription Factors. (A) Gene set enrichment analysis of top 10 regulatory units associated with brain imaging alterations. For each regulon, the gene set association was evaluated against Cognitively Impaired (CI) versus Cognitively Unimpaired (CU) phenotypes. (B) Gene Ontology (GO) functional enrichment of the top 10 regulons associated with brain modification. Each altered regulon was evaluated for GO enrichment and networked mapping of the nodes to different edges to the gene overlap between GO terms (Jaccard Coefficient). TF = transcription factors; MF = molecular function; CC = cellular component; BP = biological process.

Figure 5. Voxel-wise correlation between the enrichment score of the Gene Ontology cluster related to the regulation of protein serine/threonine kinase activity and [^{18}F]FDG-PET. (A) T-statistical map from the generalized linear regression model and (B) the top 20 brain regions with more statistically correlated voxels in the gray matter. t-value=2.0, DF=220, p-value=0.05; * tvalue=2.6, DF=220, p-value=0.01.

Figure 6. Voxel-wise correlation between the enrichment score of the regulatory unit ZNF653 and [^{18}F]FDG-PET. (A) T-statistical map from the generalized linear regression model and (B) the top 20 brain regions with more statistically correlated voxels in the gray matter. t-value=2.0, DF=220, p-value=0.05; * tvalue=2.6, DF=220, p-value=0.01.

Figure 1

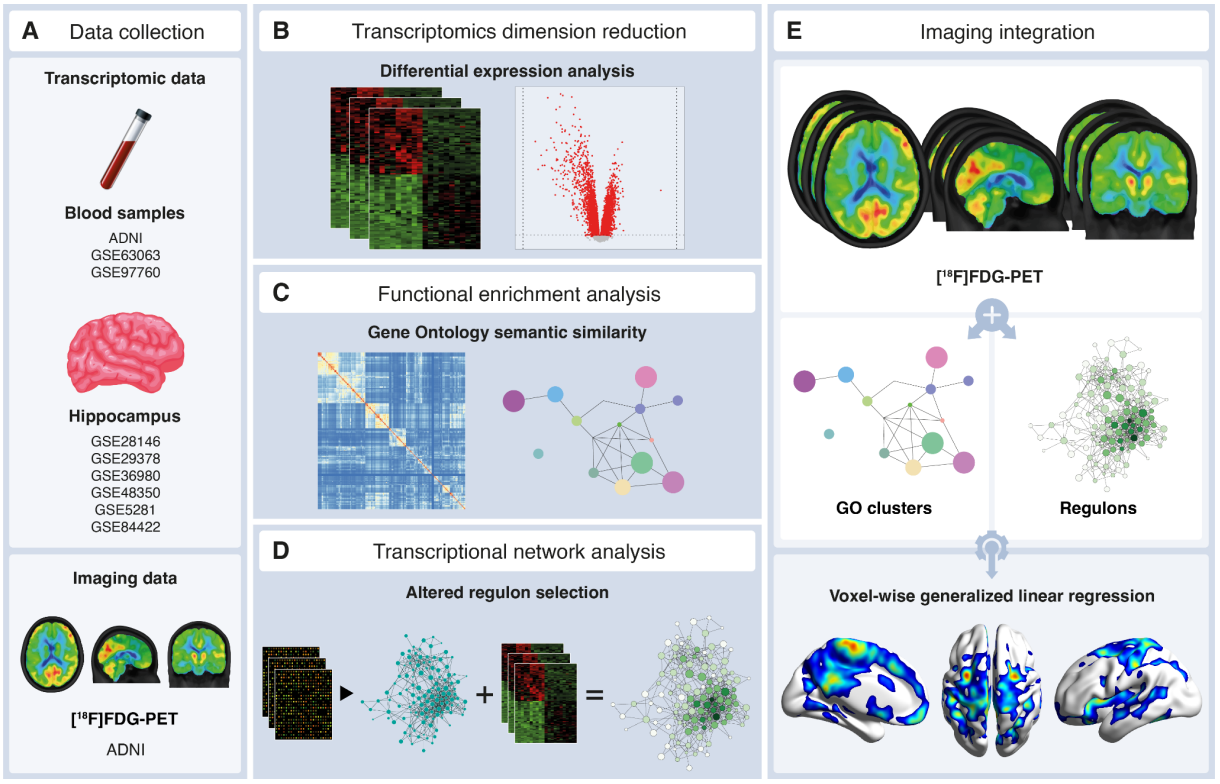
A Data collection
Transcriptomic data
Blood samples
ADNI
GSE63063
GSE97760
Hippocampus
GSE28146
GSE29378
GSE36980
GSE48350
GSE5281
GSE84422
Imaging data
[18F]FDG-PET
ADNI
B Transcriptomics dimension reduction
Differential expression analysis
C Functional enrichment analysis
Gene Ontology semantic similarity
D Transcriptional network analysis
Altered regulon selection
E Imaging integration
[18F]FDG-PET
GO clusters
Regulons
Voxel-wise generalized linear regression

Figure 2

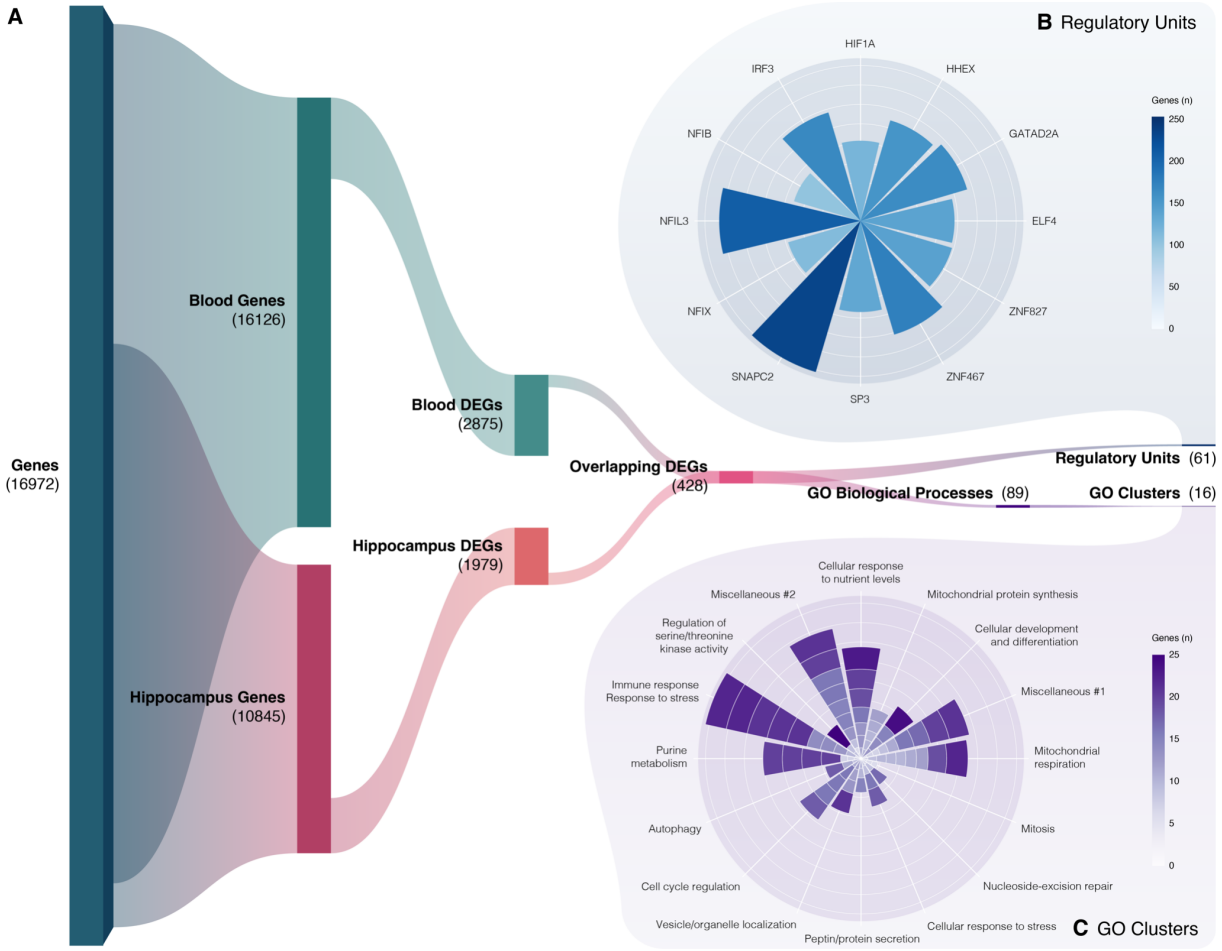
A
Genes
(16972)
Blood Genes
(16126)
Hippocampus Genes
(10845)
Blood DEGs
(2875)
Hippocampus DEGs
(1979)
Overlapping DEGs
(428)
GO Biological Processes (89)
Regulatory Units (61)
GO Clusters (16)
B Regulatory Units
HIF1A
HHEX
GATAD2A
ELF4
ZNF827
ZNF467
SP3
SNAPC2
NFIX
NFIL3
NFIB
IRF3
Genes (n)
250
200
150
100
50
0
C GO Clusters
Cellular response to nutrient levels
Mitochondrial protein synthesis
Cellular development and differentiation
Miscellaneous #1
Mitochondrial respiration
Mitosis
Nucleoside-excision repair
Cellular response to stress
Peptin/protein secretion
Vesicle/organelle localization
Cell cycle regulation
Autophagy
Purine metabolism
Immune response Response to stress
Regulation of serine/threonine kinase activity
Miscellaneous #2
Genes (n)
25
20
15
10
5
0

Figure 3

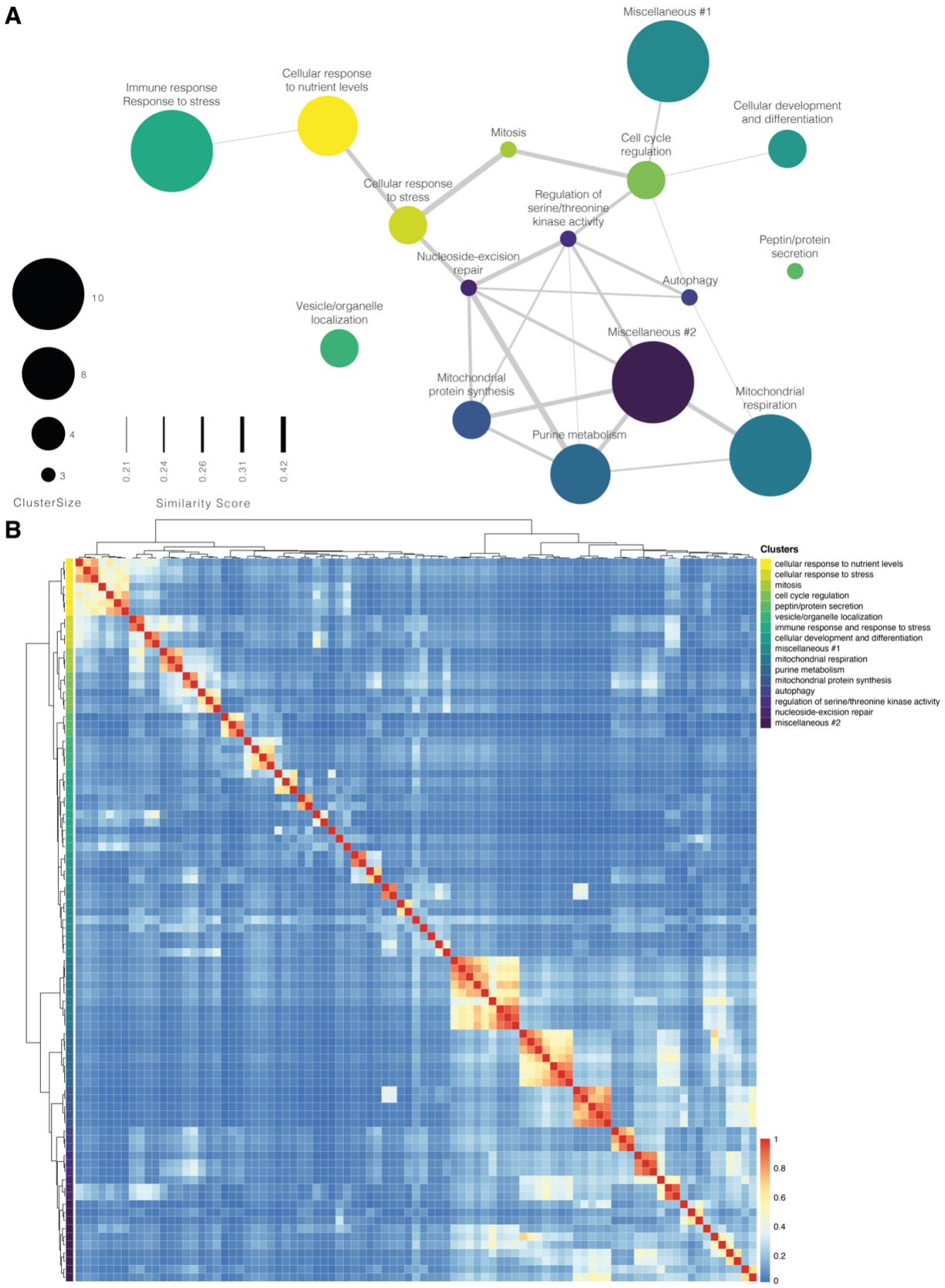
A
Miscellaneous #1
Immune response
Response to stress
Cellular response
to nutrient levels
Cellular development
and differentiation
Mitosis
Cell cycle
regulation
Cellular response
to stress
Regulation of
serine/threonine
kinase activity
Peptin/protein
secretion
Nucleoside-excision
repair
Autophagy
Vesicle/organelle
localization
Miscellaneous #2
Mitochondrial
protein synthesis
Mitochondrial
respiration
Purine metabolism
10
8
4
3
ClusterSize
0.21
0.24
0.26
0.31
0.42
Similarity Score
B
Clusters
cellular response to nutrient levels
cellular response to stress
mitosis
cell cycle regulation
peptin/protein secretion
vesicle/organelle localization
immune response and response to stress
cellular development and differentiation
miscellaneous #1
mitochondrial respiration
purine metabolism
mitochondrial protein synthesis
autophagy
regulation of serine/threonine kinase activity
nucleoside-excision repair
miscellaneous #2
1
0.8
0.6
0.4
0.2
0

Figure 4

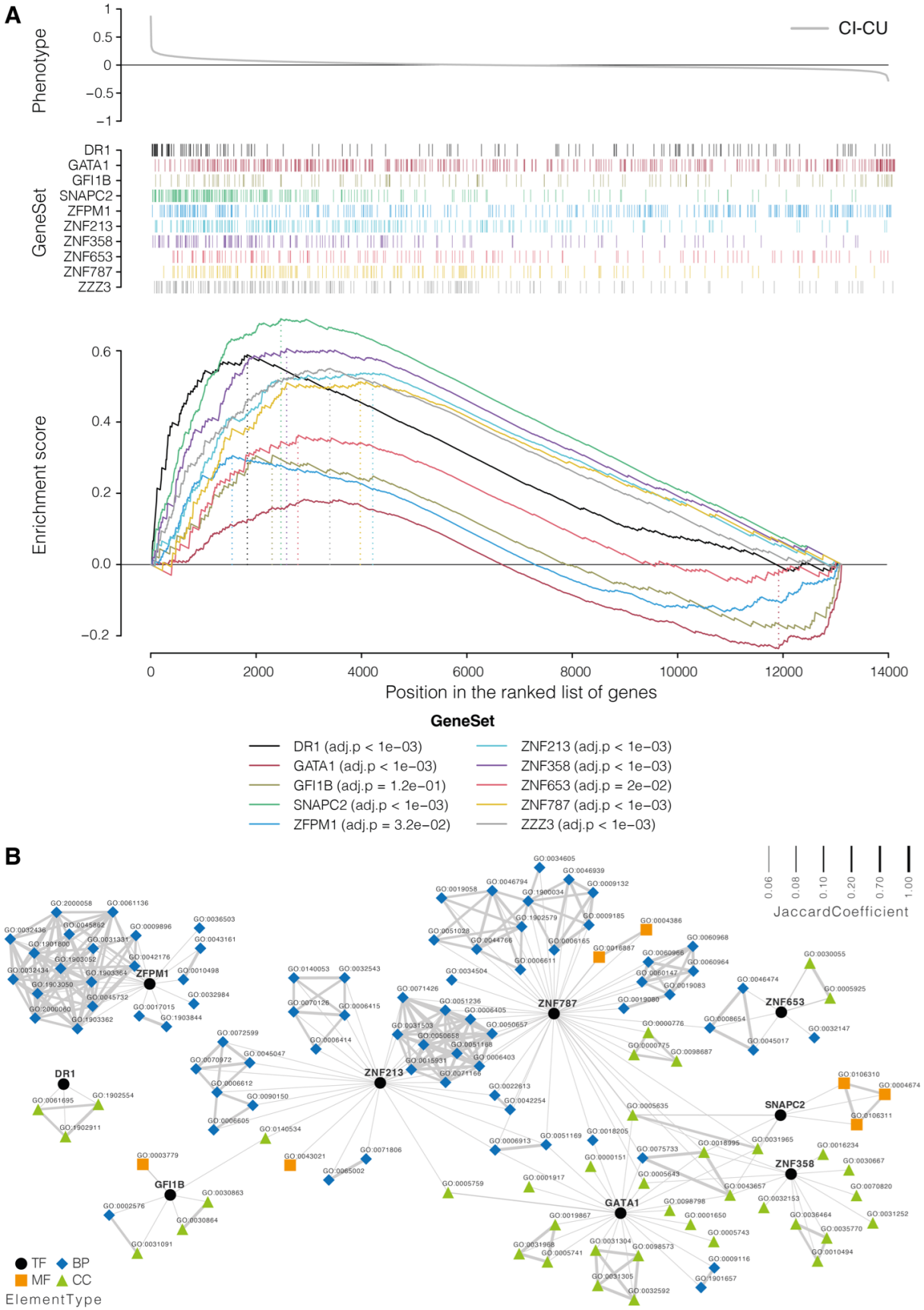
A
Phenotype
CI-CU
GeneSet
DR1
GATA1
GFI1B
SNAPC2
ZFPM1
ZNF213
ZNF358
ZNF653
ZNF787
ZZZ3
Enrichment score
Position in the ranked list of genes
GeneSet
DR1 (adj.p < 1e−03)
GATA1 (adj.p < 1e−03)
GFI1B (adj.p = 1.2e−01)
SNAPC2 (adj.p < 1e−03)
ZFPM1 (adj.p = 3.2e−02)
ZNF213 (adj.p < 1e−03)
ZNF358 (adj.p < 1e−03)
ZNF653 (adj.p = 2e−02)
ZNF787 (adj.p < 1e−03)
ZZZ3 (adj.p < 1e−03)
B
JaccardCoefficient
TF
BP
MF
CC
ElementType

Figura 5

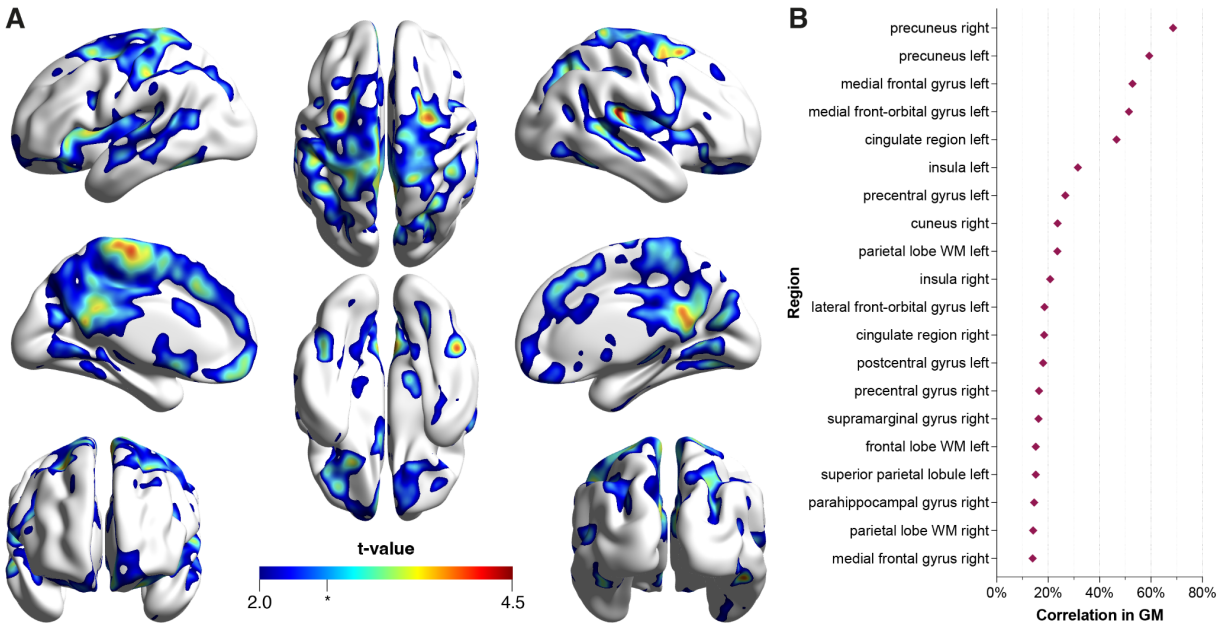

Figure 6

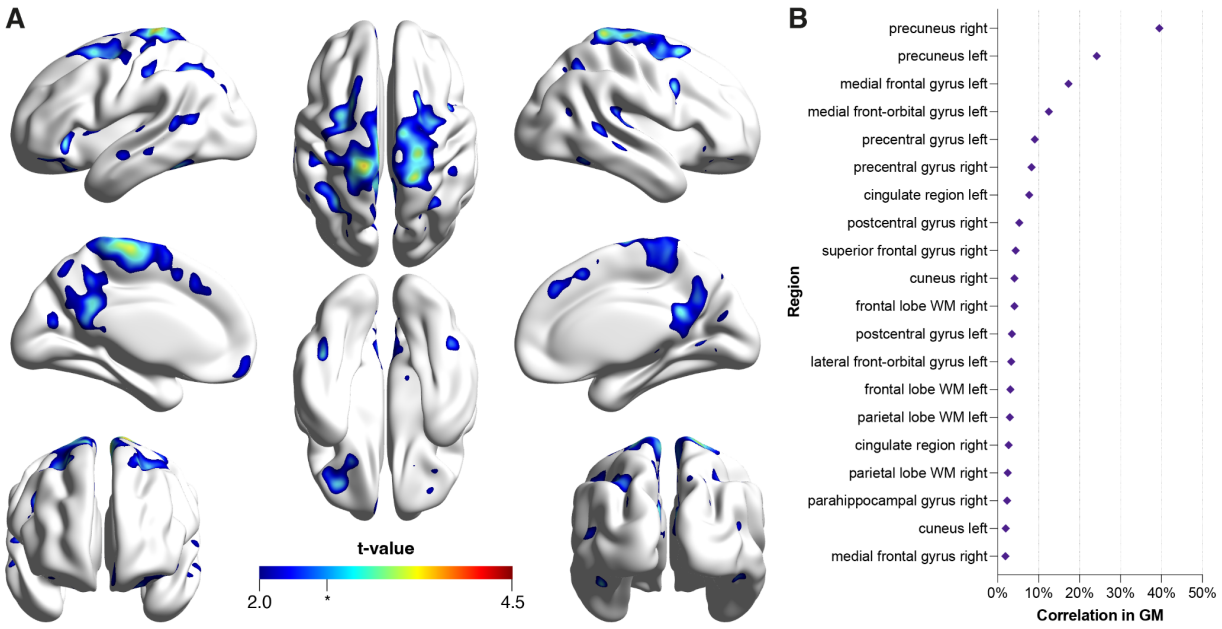

Supplemental Table 1. Dataset information and characteristics

Tissue	Database	Identifier	Samples Used	Usage
Blood	ADNI	ADNI	218 CI and 99 CU samples	Dimension Reduction, Functional Enrichment, Transcription Network and Master Regulator analysis, Neuroimaging Integration
Blood	GEO	GSE63063	433 CI and 223 CU samples from AddneuroMed Cohort	Dimension Reduction, Functional Enrichment, Transcription Network and Master Regulator analysis
Blood	GEO	GSE97760	8 CI and 7 CU samples	Dimension Reduction, Functional Enrichment, Transcription Network and Master Regulator analysis
Blood	GEO	GSE48348	734 whole-blood RNA samples from healthy individuals	Transcription Network and Master Regulator analysis
Blood	GEO	GSE99039	Whole blood samples of 233 healthy individuals	Transcription Network and Master Regulator analysis
Hippocampus	GEO	GSE28146	6 CI and 7 CU samples	Dimension Reduction, Functional Enrichment
Hippocampus	GEO	GSE29378	31 CI and 32 CU samples	Dimension Reduction, Functional Enrichment
Hippocampus	GEO	GSE36980	7 CI and 10 CU individuals	Dimension Reduction, Functional Enrichment
Hippocampus	GEO	GSE48350	19 CI and 43 CU samples	Dimension Reduction, Functional Enrichment
Hippocampus	GEO	GSE5281	9 CI and 13 CU samples	Dimension Reduction, Functional Enrichment
Hippocampus	GEO	GSE84422	18 CI and 11 CU samples	Dimension Reduction, Functional Enrichment

Supplemental Table 2. Datasets Demographics

Tissue	Database	Identifier	Samples Used	Age - mean(sd)	Sex (F/M)	Notes
Blood	ADNI	ADNI	218 CI / 99 CU	72.4(6.95)	145/172	
Blood	GEO	GSE63063	433 CI / 223 CU	75.77(6.85)	399/257	
Blood	GEO	GSE97760	8 CI / 7 CU	NA	15/0	
Blood	GEO	GSE48348	734 healthy individuals	NA	NA	
Blood	GEO	GSE99039	233 healthy individuals	NA	142/70*	*21 NA
Hippocampus	GEO	GSE28146	6 CI / 7 CU	85.4(8.87)	6/7	
Hippocampus	GEO	GSE29378	31 CI / 32 CU	79.12(8.26)	25/38	
Hippocampus	GEO	GSE36980	7 CI / 10 CU	83.52(11.13)	9/8	
Hippocampus	GEO	GSE48350	19 CI / 43 CU	68.8(23.59)	30/32	
Hippocampus	GEO	GSE5281	9 CI / 13 CU	79.13(7.94)	7/15	
Hippocampus	GEO	GSE84422	18 CI / 11 CU	84.62(9.8)	16/13	

Supplemental Table 3. Differentially expressed genes from blood datasets

SupplementalTable03_BloodDEA.xlsx

Supplemental Table 4. Differentially expressed genes from hippocampus datasets

SupplementalTable04_BrainDEA.xlsx

Supplemental Table 5. Functional enrichment analysis of Gene Ontology terms using DEGs intersecting blood and hippocampus

SupplementalTable05_FEAGO.xlsx

Supplemental Table 6. Functional enrichment analysis of KEGG terms using DEGs intersecting blood and hippocampus

SupplementalTable06_FEAKEGG.xlsx

Supplemental Table 7. Master Retulator Analysis (MRA) using DEGs (unadjusted pvalue < 0.05)

SupplementalTable07.xlsx

PARTE III

Na Parte III, são apresentadas a discussão e as conclusões finais desta tese. Além disso, são descritas as referências utilizadas no corpo principal do texto.

3. DISCUSSÃO

A DA é uma doença neurodegenerativa progressiva que não possui cura. A primeira alteração patológica detectável por biomarcadores é a diminuição dos níveis da proteína $A\beta_{1-42}$ no compartimento liquórico, indicativo de seu acúmulo em placas extracelulares no cérebro, que ocorre décadas antes da fase clínica da doença (DETURE; DICKSON, 2019). Estudos sugerem que o acúmulo de Aβ é seguido por disfunção sináptica e o aumento da fosforilação e secreção de tau, uma proteína axonal que estabiliza os microtúbulos (PALMQVIST et al., 2019). Consequentemente, desenvolvem-se os NFTs intracelulares que são compostos de proteínas tau hiperfosforiladas (JACK; HOLTZMAN, 2013). Esta descrição define a hipotese da cascata amiloide (HARDY; HIGGINS, 1992), que é o modelo mais aceito da cascata fisiopatológica na DA.

A deposição extracelular de Aβ, gerada através da clivagem da APP por BACE1 e γ-secretase, em placas é a principal característica patológica da DA, e tem sido proposto como um dos principais eventos patogênicos da doença (SELKOE; HARDY, 2016). Atualmente, podemos medir a patologia Aβ *in vivo* por meio de biomarcadores no LCR e de imagem PET. No entanto, os biomarcadores de amiloide, geralmente indexados pelo $A\beta_{1-42}$, não inferem *per se* se um indivíduo apresenta ou desenvolverá patologia de tau ou neurodegeneração. Tanto é que cerca de 30% dos indivíduos considerados positivos para amiloide não apresentam essas outras características patológicas da DA (AIZENSTEIN et al., 2008; JACK et al., 2009; PIKE et al., 2007).

A agregação da proteína tau hiperfosforilada é outra característica patológica chave na DA. Os marcadores tau total (t-tau) e p-tau foram propostos, juntamente

com a razão $A\beta_{1-42}/A\beta_{1-40}$ no LCR, como biomarcadores para definir biologicamente a DA (JACK et al., 2018). As concentrações de t-tau e p-tau no LCR refletem a neurodegeneração e patologia de tau na DA (ITOH et al., 2001; SKILLBÄCK et al., 2015).

A RM e níveis de t-tau no LCR têm sido comumente utilizados como biomarcadores para neurodegeneração relacionada à DA (FRISONI et al., 2010; JACK et al., 2018). A medida de t-tau no LCR foi proposta como um biomarcador de neurodegeneração, e pode ser utilizada como um marcador de intensidade da doença na DA, indicando que quanto mais alta sua concentração, mais rápida a progressão clínica do indivíduo na doença (ZETTERBERG, 2017).

Uma consequência esperada da hipótese da cascata amiloide é que a modulação da produção de níveis de Aβ no cérebro deve prevenir os efeitos subsequentes na DA, retardando o curso da doença (CULLEN et al., 2022). No entanto, apesar das evidências que falam do papel do amiloide como condutor da doença, terapias anti amiloides são altamente questionáveis e dividem a comunidade científica, fato elucidado pela aprovação controversa do anticorpo monoclonal Aducanumab. Associados, esses fatores fazem com que o papel do amiloide na cadeia de eventos que culmina na DA se torne uma questão ainda sem resposta (CULLEN et al., 2022). Uma das possíveis explicações para isso, é que grande parte das pesquisas envolvendo amiloide utilizam apenas a isoforma $A\beta_{1–42}$. Cada vez mais temos evidências que mostram que diferentes isoformas de Aβ, especialmente aquelas com cadeias mais curtas que o $A\beta_{1–42}$, podem desempenhar um papel mais decisivo na patogênese da DA do que inicialmente se pensava (DUNYS; VALVERDE; CHECLER, 2018; WIRTHS; ZAMPAR, 2019). Nesse contexto,

mutações na presenilina podem perturbar a relação entre $A\beta_{1-42}$ e espécies mais curtas de Aβ ao invés de afetarem apenas os níveis de $A\beta_{1-42}$ no cérebro (KELLEHER; SHEN, 2010; KUMAR-SINGH et al., 2006, p. 40; XIA et al., 2015, p.). Assim, fica evidente que atacar o processo amiloidogênico apenas na produção de $A\beta_{1-42}$ - ou a isoforma $A\beta_{1-42}$ diretamente - não é suficiente para interromper a trajetória da DA. É por conta disso que estudos mais recentes têm investigado a associação entre peptídeos de Aβ de cadeia mais curta e as alterações relacionadas à DA, tentando entender o acúmulo de amiloide, particularmente no que se refere a terapias que alteram o curso da doença (CULLEN et al., 2022).

Desta forma, considerando que a deposição de placas de Aβ seja o primeiro evento patológico da DA, ao invés de utilizarmos apenas o $A\beta_{1-42}$, propusemos que a combinação de isoformas de Aβ com cadeias mais curtas (38, 40 e 42 aminoácidos), medidas no LCR, seriam capazes de predizer os eventos subsequentes na DA. De fato, em nosso estudo, demonstramos que utilizando modelos de ML com a combinação de isoformas solúveis de Aβ podemos prever a positividade de tau e neurodegeneração em indivíduos cognitivamente saudáveis. Ao considerarmos as isoformas isoladamente, o valor diagnóstico da $A\beta_{1–42}$ apresentou o menor poder preditivo. Já as isoformas com tamanho menor, apresentaram um desempenho consideravelmente superior. Interessantemente, a isoforma $A\beta_{1–38}$ foi a que teve a melhor performance para predizer a positividade de tau e neurodegeneração.

Evidências recentes sugerem que níveis mais baixos de peptídeos Aβ mais curtos ou uma proporção mais baixa de peptídeos Aβ mais curtos para mais longos podem ser um fator importante na toxicidade de Aβ (BLAIN et al., 2016; DUNYS; VALVERDE; CHECLER, 2018; MOORE et al., 2018). Em nosso estudo, mostramos

que pacientes cognitivamente saudáveis apresentam níveis de $A\beta_{1–42}/A\beta_{1–40}$ diminuídos no LCR (esperado para indivíduos no *continuum* biológico da DA) quando positivos para tau e neurodegeneração. Por outro lado, os níveis de $A\beta_{1–40}$ e $A\beta_{1–38}$ estão aumentados nesses indivíduos. No trabalho de Cullen, foi demonstrado que níveis mais elevados de $A\beta_{1-38}$ no LCR de indivíduos no *continuum* da DA estão negativamente associados ao declínio cognitivo e ao risco de desenvolver a DA (CULLEN et al., 2022). Desta forma, nossos resultados podem levar à interpretação de que, se níveis mais altos de $A\beta_{1-38}$ são neuroprotetores, e os indivíduos cognitivamente saudáveis, mas considerados positivos para tau e neurodegeneração indexados por p-tau e t-tau, apresentam valores maiores de $A\beta_{1-38}$ no LCR, taxas mais altas da clivagem de $A\beta_{1–42}$ em $A\beta_{1–38}$ (OKOCHI et al., 2013, p. 43), podem indicar um processo crucial que parece conduzir a patologia da tau e a neurodegeneração. Alternativamente, podemos hipotetizar a presença de um mecanismo de autodefesa do organismo que esteja tentando processar a isoforma $A\beta_{1–42}$ na tentativa de retardar os efeitos causados pela toxicidade já conhecida da formação de placas de Aβ. Nesse contexto, fica evidente que o potencial dessa isoforma para agregar informações na fase pré-clínica da doença permanece pouco explorado. De qualquer forma, não está claro se os níveis de $A\beta_{1-38}$ modulam, de fato, o desenvolvimento da patologia de tau em indivíduos que já atingiram os limiares para a positividade da patologia de Aβ (CULLEN et al., 2022).

Em meio a tantos questionamentos relacionados à hipótese amiloide, cada vez fica mais evidente que outros processos biológicos também são críticos na progressão em direção aos sintomas clínicos da DA. Portanto, técnicas ômicas, como a proteômica, pode ser uma das escolhas para avaliar de forma rápida, extensiva e confiável as propriedades e a dinâmica do sistema. Neste contexto,

avaliamos quais processos biológicos poderiam estar relacionados a um aumento no poder de predição das isoformas de Aβ sobre os eventos patológicos da DA através de análises proteômicas do LCR. Com a análise proteômica, encontramos muitas proteínas diferencialmente expressas entre os indivíduos T+ ou (N)+, o que permitiu a determinação de processos biológicos e vias de sinalização significativamente enriquecidas nesses indivíduos. Com isso, em um estudo futuro, podemos utilizar essas proteínas diferencialmente expressas para melhorar o poder preditivo dos modelos de ML na detecção da positividade de tau e neurodegeneração.

Neste âmbito, identificamos a partir da rede de ontologia genética de termos enriquecidos construídos a partir de proteínas diferencialmente expressas de indivíduos cognitivamente saudáveis, que aqueles que são T+ apresentam um *cluster* de termos superregulados relacionados à resposta imune. Isso se torna ainda mais interessante uma vez que espécies patológicas de tau hiperfosforiladas podem ser secretadas extracelularmente, levando a disseminação progressiva da tauopatia. Esse evento é capaz de promover tanto uma ativação microglial quanto promover a reatividade astrocitária. Essas células gliais, por sua vez, liberam citocinas e/ou moderadores inflamatórios neurotóxicos, incluindo IL1β ou TNFα. Além disso, por uma modulação das cinases de tau, a ativação microglial pode levar a uma exacerbação da patologia de tau. Por fim, ainda temos o envolvimento da microglia na propagação de tau pela liberação de tau exosomal uma vez que a tau é fagocitada por essas células (LAURENT; BUÉE; BLUM, 2018).

Ainda no contexto da resposta imune, além das patologias amiloide e tau, outra característica histológica da DA é a presença de astrócitos reativos e microglia ativada na proximidade das placas de amiloide. No cérebro saudável, os astrócitos

fornecem energia aos neurônios, participam da função sináptica (como parte da sinapse tripartite), induzem a poda sináptica e a liberação de fatores neurotróficos, dentre outras funções que em conjunto garantem a homeostase do sistema nervoso central (SNC) (LIDDELOW; BARRES, 2015; PELLERIN et al., 1998; STOBART; ANDERSON, 2013). Durante condições neuroinflamatórias, fatores inflamatórios liberados pela microglia ativada, parecem favorecer a formação de um subconjunto neurotóxico de astrócitos reativos que perdem suas funções normais e sua capacidade de promover a formação de sinapses, causando a morte neuronal através da secreção de fatores prejudiciais (LIDDELOW et al., 2017; LIDDELOW; BARRES, 2017). Atualmente acredita-se que os astrócitos possam desenvolver diversos fenótipos de acordo com o microambiente ao qual eles estão inseridos, portanto, a presença de um ou outro evento patológico da DA (tau, amiloide e/ou neurodegeneração) pode ativar diferentes aspectos da resposta astrocitária (DE BASTIANI et al., 2022; ESCARTIN et al., 2021; FERRARI-SOUZA et al., 2022). No que diz respeito às tauopatias, o mal dobramento neuronal da tau é suficiente para induzir alterações morfológicas nos astrócitos impactando seu papel fisiológico. Essas células mudam para um perfil pró-inflamatório, conforme indicado pela regulação positiva da proteína glial fibrilar ácida (GFAP) acompanhado pela secreção de fatores pró-inflamatórios, que contribuem para a patogênese da DA (LAURENT et al., 2017; RODRÍGUEZ-ARELLANO et al., 2016). Desta forma, um ponto chave que pode ser explorado para melhorar o poder de modelos para predição da positividade de tau é a utilização de biomarcadores relacionados com neuroinflamação, como a GFAP, que está, inclusive, dentre as proteínas diferencialmente expressas que encontramos em nosso estudo.

Por outro lado, a rede de ontologia genética para indivíduos (N)+ em comparação com os (N)- não mostrou alteração em termos relacionados à resposta imune. De forma interessante, termos relacionados com a memória, aprendizagem e cognição apresentaram-se suprarregulados tanto em indivíduos T+ e (N)+, ainda que todos sejam cognitivamente saudáveis. Isso demonstra que, conforme esperado, alterações biológicas importantes - e mensuráveis - já estão em ação no cérebro antes da fase clínica da DA. Inclusive, os termos mais enriquecidos estão relacionados com organização sináptica, desenvolvimento axonal e axonogênese, o que significa que tanto a tau quanto a neurodegeneração acabam levando a alterações da função cerebral, o fenômeno mais típico da DA. Esses achados demonstram a importância da definição biológica da DA quando se visa o desenvolvimento de estratégias terapêuticas que previnam o processo de neurodegeneração e consequente perda cognitiva.

De fato, muitas doenças neurodegenerativas, dentre elas a DA, produzem alterações significativas na função cerebral, mesmo quando exames de imagem estrutural como TC ou RM não revelam anormalidades específicas (SILVERMAN, 2004). Neste sentido, uma ferramenta de neuroimagem promissora no diagnóstico da DA é o FDG-PET, pois com ele, é possível observar o consumo cerebral de glicose em estado de repouso ou durante uma tarefa. Essa medida vem sendo utilizada como um indicador da atividade sináptica e vários estudos têm demonstrado que as alterações metabólicas cerebrais precedem a manifestação clínica dos sintomas da DA (MARCUS; MENA; SUBRAMANIAM, 2014). Estudos utilizando FDG-PET fornecem não apenas evidências do processo de demência, mas também permitem a diferenciação dos tipos de transtornos demenciais e seu

estadiamento, uma vez que essas patologias apresentam padrões metabólicos regionais diferentes (BROWN et al., 2014).

De forma geral, a imagem PET permite a quantificação *in vivo* de processos metabólicos, receptores, transportadores e alterações patológicas, de forma não invasiva (ZIMMER et al., 2014). A imagem PET pode ser utilizada para identificar e quantificar placas de Aβ (KLUNK et al., 2004), tau (VILLEMAGNE et al., 2015), e neurodegeneração a partir do hipometabolismo de glicose (BRIER et al., 2016; JACK et al., 2018), enquanto a redução da razão $A\beta_{1-42}/A\beta_{1-40}$ e o aumento dos níveis de t-tau e p-tau podem ser medidos no LCR. Apesar de exames de imagem e as medidas em LCR terem uma maior acurácia e permitirem uma visualização regional (no caso do PET), principalmente no contexto da DA, eles têm um custo relativamente alto e/ou exigem a necessidade de pessoal e instalações especializadas para sua obtenção, o que limita seu uso na prática clínica (WITTENBERG et al., 2019). Assim, há uma necessidade de métodos mais acessíveis e econômicos para identificar com precisão esses processos-chave da DA. Baseado nisso, o campo de biomarcadores nos últimos anos tem voltado os seus esforços para explorar exames sanguíneos como potencial valor para diagnóstico e estadiamento da DA. Com menor custo e maior acessibilidade, os biomarcadores sanguíneos da DA podem contornar as limitações dos exames de imagem e baseados em LCR.

Com base nisso, é de grande interesse encontrar biomarcadores sanguíneos capazes de refletir alterações metabólicas cerebrais. Por esse motivo, propusemos a implementação de duas estratégias baseadas em biologia de sistemas para integrar informações transcriptômicas (genes que estão alterados tanto no cérebro quanto no

sangue de pacientes com a DA) de grupos de genes com dados de neuroimagem. Primeiramente, *clusters* de termos de ontologia gênica agrupados por similaridade semântica foram associados a imagens FDG-PET. Após, utilizamos engenharia reversa de redes transcricionais para integrar unidades reguladoras de fatores de transcrição com imagens FDG-PET. O objetivo dessa nova metodologia de integração é ajudar a elucidar as bases biológicas e destacar novos biomarcadores potenciais da patologia da DA com o uso da biologia de sistemas. De fato, como resultado da aplicação dessa metodologia identificamos uma forte associação entre um *cluster* relacionado à regulação da atividade da proteína serina/treonina cinase e o sinal FDG-PET no cérebro. É importante mencionar que essa técnica de integração oferece informação de topografia, ou seja, indica quais áreas do cérebro temos uma melhor associação entre FDG-PET e os genes identificados. Também, mostramos que a unidade reguladora mais intimamente associada ao metabolismo da glicose no cérebro é a ZNF653.

Neste sentido, essa metodologia é uma nova ferramenta para integrar dados periféricos com imagem, permitindo a identificação de novos biomarcadores sanguíneos que se correlacionam com o metabolismo cerebral. Além disso, a integração de dados transcriptômicos do sangue e imagens cerebrais podem ser aplicadas usando várias modalidades de imagem, bem como adaptadas e usadas no contexto de diferentes doenças neurológicas.

Como mencionado anteriormente, o sistema AT(N) dicotomiza indivíduos usando biomarcadores que mapeiam as principais características fisiopatológicas da DA, ou seja, Aβ, tau e neurodegeneração. Esse sistema é flexível e adaptável e, consequentemente, aberto a evoluir dinamicamente à medida que nosso

conhecimento dos mecanismos fisiopatológicos subjacentes ao *continuum* DA se expande. Por conta disso, conforme evidências emergirem no futuro, novos biomarcadores, que reflitam aspectos complementares da DA, podem ser descobertos e fornecer um componente 'X' para expandir o sistema AT(N) para ATX(N), onde X tem sido proposto como novos biomarcadores para mecanismos fisiopatológicos adicionais (HAMPEL et al., 2021). Levando isso em consideração, nossa metodologia tem o poder de auxiliar na descoberta desses novos componentes, com isso, permitindo detectar anormalidades em vias biológicas críticas em pacientes com DA e que se manifestem também em compartimentos periféricos, o que tem o potencial de fornecer *insights* para o desenvolvimento de novos biomarcadores, inclusive sanguíneos, que quando apropriadamente validados podem ser úteis na prática clínica.

4. CONCLUSÃO

Esta tese destacou a potencial utilização de técnicas neurocomputacionais para a identificação de alterações funcionais na DA. Utilizando aprendizado de máquina, demonstramos que diferentes isoformas de Aβ predizem tanto a positividade para patologia de tau quanto para neurodegeneração em curso em indivíduos cognitivamente saudáveis. Também, mostramos que aqueles indivíduos positivos para patologia de tau apresentaram superregulação de proteínas relacionadas à resposta imune, o que nos levou à discussão sobre resposta neuro-inflamatória e a relação da patologia de tau com a microglia e astrócitos, reforçado pela proteína GFAP que se apresentou diferencialmente expressa no estudo. Subsequentemente, propusemos um método de integração de imagem PET e tecnologias ômicas, em específico, FDG-PET e transcriptômica do sangue. Nesse estudo, usamos genes diferencialmente expressos para implementar uma abordagem de redução de dimensão baseada em Gene Ontology (GO) e engenharia reversa de redes transcricionais centradas em fatores de transcrição (TF). Agrupamentos GO e unidades reguladoras de TF foram selecionados para serem integrados com imagens FDG-PET usando modelos de regressão linear. Com isso, identificamos processos biológicos periféricos associados ao metabolismo de FDG-PET no cérebro de indivíduos em todo o espectro clínico da DA. Por fim, o enriquecimento do cluster relacionado à atividade da proteína serina/treonina quinase e a unidade reguladora sob o TF ZNF653 destacam o potencial das assinaturas gênicas associadas a eles como novos biomarcadores da DA.

5. PERSPECTIVAS

Embora diferentes estudos tenham mostrado uma associação entre os marcadores sanguíneos e a DA até agora, nenhum estudo utilizou ML para determinar qual biomarcador de plasma melhor prevê a positividade de AT(N) em todo o espectro da DA. Desta forma, como proposta para trabalhos futuros, usaremos ML para determinar o desempenho de biomarcadores plasmáticos de Aβ, diferentes isoformas de p-tau, GFAP e NfL para identificar a patologia cerebral de Aβ, tau e neurodegeneração em todo o espectro da DA.

REFERÊNCIAS

AIZENSTEIN, H. J. et al. Frequent amyloid deposition without significant cognitive impairment among the elderly. **Archives of Neurology**, v. 65, n. 11, p. 1509–1517, nov. 2008.

ALZHEIMER'S & DEMENTIA. 2019 Alzheimer's disease facts and figures. **Alzheimer's & Dementia**, v. 15, n. 3, p. 321–387, 1 mar. 2019.

BLAIN, J.-F. et al. Characterization of FRM-36143 as a new γ-secretase modulator for the potential treatment of familial Alzheimer's disease. **Alzheimer's Research & Therapy**, v. 8, p. 34, 30 ago. 2016.

BLENNOW, K. et al. Cerebrospinal fluid and plasma biomarkers in Alzheimer disease. **Nature Reviews Neurology**, v. 6, n. 3, p. 131–144, mar. 2010.

BLENNOW, K.; ZETTERBERG, H. Biomarkers for Alzheimer's disease: current status and prospects for the future. **Journal of Internal Medicine**, v. 284, n. 6, p. 643–663, 2018.

BLENNOW, K.; ZETTERBERG, H.; FAGAN, A. M. Fluid Biomarkers in Alzheimer Disease. **Cold Spring Harbor Perspectives in Medicine**, v. 2, n. 9, set. 2012.

BRIER, M. R. et al. Tau and Aβ imaging, CSF measures, and cognition in Alzheimer's disease. **Science Translational Medicine**, v. 8, n. 338, p. 338ra66, 11 maio 2016.

BROWN, R. K. J. et al. Brain PET in Suspected Dementia: Patterns of Altered FDG Metabolism. **RadioGraphics**, v. 34, n. 3, p. 684–701, maio 2014.

CHUN, W.; JOHNSON, G. V. W. The role of tau phosphorylation and cleavage in neuronal cell death. **Frontiers in Bioscience: A Journal and Virtual Library**, v. 12, p. 733–756, 1 jan. 2007.

CRAS, P. et al. Senile plaque neurites in Alzheimer disease accumulate amyloid precursor protein. **Proceedings of the National Academy of Sciences**, v. 88, n. 17, p. 7552–7556, set. 1991.

CULLEN, N. et al. Association of CSF Aβ38 Levels With Risk of Alzheimer Disease–Related Decline. **Neurology**, v. 98, n. 9, p. e958–e967, 1 mar. 2022.

CULLEN, N. C. et al. Plasma biomarkers of Alzheimer's disease improve prediction of cognitive decline in cognitively unimpaired elderly populations. **Nature Communications**, v. 12, n. 1, p. 3555, 11 jun. 2021.

DE BASTIANI, M. A. et al. **Hippocampal GFAP-positive astrocyte responses to amyloid and tau pathologies**. [s.l.] Neuroscience, 28 fev. 2022. Disponível em: <http://biorxiv.org/lookup/doi/10.1101/2022.02.25.481812>. Acesso em: 29 abr. 2022.

DETURE, M. A.; DICKSON, D. W. The neuropathological diagnosis of Alzheimer's disease. **Molecular Neurodegeneration**, v. 14, n. 1, p. 32, 2 ago. 2019.

DICKSON, D. W. The Pathogenesis of Senile Plaques. **Journal of Neuropathology & Experimental Neurology**, v. 56, n. 4, p. 321–339, 1 abr. 1997.

DUGGER, B. N.; DICKSON, D. W. Pathology of Neurodegenerative Diseases. **Cold Spring Harbor Perspectives in Biology**, v. 9, n. 7, p. a028035, 7 jan. 2017.

DUNYS, J.; VALVERDE, A.; CHECLER, F. Are N- and C-terminally truncated Aβ species key pathological triggers in Alzheimer's disease? **The Journal of Biological Chemistry**, v. 293, n. 40, p. 15419–15428, 5 out. 2018.

ELLIS, K. A. et al. Advances in structural and molecular neuroimaging in Alzheimer's disease. **The Medical Journal of Australia**, v. 194, n. 4, p. S20-23, 21 fev. 2011.

ESCARTIN, C. et al. Reactive astrocyte nomenclature, definitions, and future directions. **Nature Neuroscience**, v. 24, n. 3, p. 312–325, mar. 2021.

FERRARI-SOUZA, J. P. et al. **Astrocyte biomarker signatures of amyloid-β and tau pathologies in Alzheimer's disease**. [s.l.] Neurology, 29 jan. 2022. Disponível em: <http://medrxiv.org/lookup/doi/10.1101/2022.01.25.22269841>. Acesso em: 29 abr. 2022.

FRISONI, G. B. et al. The clinical use of structural MRI in Alzheimer disease. **Nature Reviews. Neurology**, v. 6, n. 2, p. 67–77, fev. 2010.

G7. **The challenge of neurodegenerative diseases in an aging population**. [s.l: s.n.]. Disponível em: <http://www.academie-sciences.fr/en/Advice-Notes-and-Reports/g7-science-academies-statement-2017.html>. Acesso em: 12 dez. 2017.

GBD 2017 US NEUROLOGICAL DISORDERS COLLABORATORS et al. Burden of Neurological Disorders Across the US From 1990-2017: A Global Burden of Disease Study. **JAMA neurology**, v. 78, n. 2, p. 165–176, 1 fev. 2021.

GOOCH, C. L.; PRACHT, E.; BORENSTEIN, A. R. The burden of neurological disease in the United States: A summary report and call to action. **Annals of Neurology**, v. 81, n. 4, p. 479–484, 1 abr. 2017.

HAASS, C. et al. Trafficking and proteolytic processing of APP. **Cold Spring Harbor Perspectives in Medicine**, v. 2, n. 5, p. a006270, maio 2012.

HAMEED, S. et al. Role of Fluid Biomarkers and PET Imaging in Early Diagnosis and its Clinical Implication in the Management of Alzheimer's Disease. **Journal of Alzheimer's Disease Reports**, v. 4, n. 1, p. 21–37, 2020.

HAMET, P.; TREMBLAY, J. Artificial intelligence in medicine. **Metabolism**, Insights Into the Future of Medicine: Technologies, Concepts, and Integration. v. 69, p. S36–S40, 1 abr. 2017.

HAMLEY, I. W. The amyloid beta peptide: a chemist's perspective. Role in Alzheimer's and fibrillization. **Chemical Reviews**, v. 112, n. 10, p. 5147–5192, 10 out. 2012.

HAMPEL, H. et al. Developing the ATX(N) classification for use across the Alzheimer disease continuum. **Nature Reviews. Neurology**, v. 17, n. 9, p. 580–589, set. 2021.

HARDY, J. A.; HIGGINS, G. A. Alzheimer's disease: the amyloid cascade hypothesis. **Science (New York, N.Y.)**, v. 256, n. 5054, p. 184–185, 10 abr. 1992.

ITOH, N. et al. Large-scale, multicenter study of cerebrospinal fluid tau protein phosphorylated at serine 199 for the antemortem diagnosis of Alzheimer's disease. **Annals of Neurology**, v. 50, n. 2, p. 150–156, ago. 2001.

JACK, C. R. et al. The Alzheimer's Disease Neuroimaging Initiative (ADNI): MRI methods. **Journal of magnetic resonance imaging: JMRI**, v. 27, n. 4, p. 685–691,

abr. 2008.

JACK, C. R. et al. Serial PIB and MRI in normal, mild cognitive impairment and Alzheimer's disease: implications for sequence of pathological events in Alzheimer's disease. **Brain: A Journal of Neurology**, v. 132, n. Pt 5, p. 1355–1365, maio 2009.

JACK, C. R. et al. A/T/N: An unbiased descriptive classification scheme for Alzheimer disease biomarkers. **Neurology**, v. 87, n. 5, p. 539–547, 2 ago. 2016.

JACK, C. R. et al. NIA-AA Research Framework: Toward a biological definition of Alzheimer's disease. **Alzheimer's & Dementia: The Journal of the Alzheimer's Association**, v. 14, n. 4, p. 535–562, 2018.

JACK, C. R.; HOLTZMAN, D. M. Biomarker modeling of Alzheimer's disease. **Neuron**, v. 80, n. 6, p. 1347–1358, 18 dez. 2013.

KELLEHER, R. J.; SHEN, J. Genetics. Gamma-secretase and human disease. **Science (New York, N.Y.)**, v. 330, n. 6007, p. 1055–1056, 19 nov. 2010.

KIRSCHNER, M. W. The meaning of systems biology. **Cell**, v. 121, n. 4, p. 503–504, 20 maio 2005.

KLUNK, W. E. et al. Imaging brain amyloid in Alzheimer's disease with Pittsburgh Compound-B. **Annals of Neurology**, v. 55, n. 3, p. 306–319, mar. 2004.

KUMAR-SINGH, S. et al. Mean age-of-onset of familial alzheimer disease caused by presenilin mutations correlates with both increased Abeta42 and decreased Abeta40. **Human Mutation**, v. 27, n. 7, p. 686–695, jul. 2006.

KUMMER, M. P.; HENEKA, M. T. Truncated and modified amyloid-beta species. **Alzheimer's Research & Therapy**, v. 6, n. 3, p. 28, 2014.

LAKHAN, S. E. Alzheimer Disease: Practice Essentials, Background, Anatomy. 5 out. 2016.

LAURENT, C. et al. Hippocampal T cell infiltration promotes neuroinflammation and cognitive decline in a mouse model of tauopathy. **Brain: A Journal of Neurology**, v. 140, n. 1, p. 184–200, jan. 2017.

LAURENT, C.; BUÉE, L.; BLUM, D. Tau and neuroinflammation: What impact for Alzheimer's Disease and Tauopathies? **Biomedical Journal**, v. 41, n. 1, p. 21–33, fev. 2018.

LECUN, Y.; BENGIO, Y.; HINTON, G. Deep learning. **Nature**, v. 521, n. 7553, p. 436–444, 28 maio 2015.

LIDDELOW, S. A. et al. Neurotoxic reactive astrocytes are induced by activated microglia. **Nature**, v. 541, n. 7638, p. 481–487, 26 jan. 2017.

LIDDELOW, S. A.; BARRES, B. A. Reactive Astrocytes: Production, Function, and Therapeutic Potential. **Immunity**, v. 46, n. 6, p. 957–967, 20 jun. 2017.

LIDDELOW, S.; BARRES, B. SnapShot: Astrocytes in Health and Disease. **Cell**, v. 162, n. 5, p. 1170- 1170.e1, 27 ago. 2015.

MARCUS, C.; MENA, E.; SUBRAMANIAM, R. M. Brain PET in the Diagnosis of Alzheimer's Disease. **Clinical nuclear medicine**, v. 39, n. 10, p. e413–e426, out. 2014.

MESKO, B. The role of artificial intelligence in precision medicine. **Expert Review of Precision Medicine and Drug Development**, v. 2, n. 5, p. 239–241, 3 set. 2017.

MOORE, B. D. et al. Short Aβ peptides attenuate Aβ42 toxicity in vivo. **The Journal of Experimental Medicine**, v. 215, n. 1, p. 283–301, 2 jan. 2018.

OKOCHI, M. et al. γ-secretase modulators and presenilin 1 mutants act differently on presenilin/γ-secretase function to cleave Aβ42 and Aβ43. **Cell Reports**, v. 3, n. 1, p. 42–51, 31 jan. 2013.

OLTVAI, Z. N.; BARABÁSI, A.-L. Systems biology. Life's complexity pyramid. **Science (New York, N.Y.)**, v. 298, n. 5594, p. 763–764, 25 out. 2002.

PALMQVIST, S. et al. Cerebrospinal fluid and plasma biomarker trajectories with increasing amyloid deposition in Alzheimer's disease. **EMBO molecular medicine**, v. 11, n. 12, p. e11170, dez. 2019.

PELLERIN, L. et al. Evidence supporting the existence of an activity-dependent astrocyte-neuron lactate shuttle. **Developmental Neuroscience**, v. 20, n. 4–5, p. 291–299, 1998.

PERL, D. P. Neuropathology of Alzheimer's Disease. **The Mount Sinai Journal of Medicine, New York**, v. 77, n. 1, p. 32–42, 2010.

PERRIN, R. J.; FAGAN, A. M.; HOLTZMAN, D. M. Multimodal techniques for diagnosis and prognosis of Alzheimer's disease. **Nature**, v. 461, n. 7266, p. 916–922, 15 out. 2009.

PIKE, K. E. et al. Beta-amyloid imaging and memory in non-demented individuals: evidence for preclinical Alzheimer's disease. **Brain: A Journal of Neurology**, v. 130, n. Pt 11, p. 2837–2844, nov. 2007.

RODRÍGUEZ-ARELLANO, J. J. et al. Astrocytes in physiological aging and Alzheimer's disease. **Neuroscience**, v. 323, p. 170–182, 26 maio 2016.

RUSSELL, S. J.; NORVIG, P.; DAVIS, E. **Artificial intelligence: a modern approach**. 3rd ed ed. Upper Saddle River: Prentice Hall, 2010.

SELKOE, D. J. The molecular pathology of Alzheimer's disease. **Neuron**, v. 6, n. 4, p. 487–498, abr. 1991.

SELKOE, D. J.; HARDY, J. The amyloid hypothesis of Alzheimer's disease at 25 years. **EMBO molecular medicine**, v. 8, n. 6, p. 595–608, jun. 2016.

SERRANO-POZO, A. et al. Neuropathological alterations in Alzheimer disease. **Cold Spring Harbor Perspectives in Medicine**, v. 1, n. 1, p. a006189, set. 2011.

SILVERMAN, D. H. S. Brain 18F-FDG PET in the diagnosis of neurodegenerative dementias: comparison with perfusion SPECT and with clinical evaluations lacking nuclear imaging. **Journal of Nuclear Medicine: Official Publication, Society of Nuclear Medicine**, v. 45, n. 4, p. 594–607, abr. 2004.

SKILLBÄCK, T. et al. Cerebrospinal fluid tau and amyloid-β1-42 in patients with dementia. **Brain: A Journal of Neurology**, v. 138, n. Pt 9, p. 2716–2731, set. 2015.

STOBART, J. L.; ANDERSON, C. M. Multifunctional role of astrocytes as gatekeepers of neuronal energy supply. **Frontiers in Cellular Neuroscience**, v. 7, p. 38, 2013.

SUH, Y.-H.; CHECLER, F. Amyloid precursor protein, presenilins, and alpha-synuclein: molecular pathogenesis and pharmacological applications in Alzheimer's disease. **Pharmacological Reviews**, v. 54, n. 3, p. 469–525, set. 2002.

TARASOFF-CONWAY, J. M. et al. Clearance systems in the brain-implications for Alzheimer disease. **Nature Reviews. Neurology**, v. 11, n. 8, p. 457–470, ago. 2015.

VARGHESE, T. et al. A review of neuroimaging biomarkers of Alzheimer's disease. **Neurology Asia**, v. 18, n. 3, p. 239–248, 2013.

VERHEIJEN, J.; SLEEGERS, K. Understanding Alzheimer Disease at the Interface between Genetics and Transcriptomics. **Trends in genetics: TIG**, v. 34, n. 6, p. 434–447, jun. 2018.

VILLEMAGNE, V. L. et al. Tau imaging: early progress and future directions. **The Lancet. Neurology**, v. 14, n. 1, p. 114–124, jan. 2015.

VILLOSLADA, P.; STEINMAN, L.; BARANZINI, S. E. Systems biology and its application to the understanding of neurological diseases. **Annals of Neurology**, v. 65, n. 2, p. 124–139, fev. 2009.

WALHOVD, K. B. et al. Combining MR imaging, positron-emission tomography, and CSF biomarkers in the diagnosis and prognosis of Alzheimer disease. **AJNR. American journal of neuroradiology**, v. 31, n. 2, p. 347–354, fev. 2010.

WALKER, L. C. Aβ Plaques. **Free Neuropathology**, v. 1, p. 31, 2020.

WANG, Z.-T. et al. Systems biology and gene networks in Alzheimer's disease. **Neuroscience and Biobehavioral Reviews**, v. 96, p. 31–44, jan. 2019.

WIRTHS, O.; ZAMPAR, S. Emerging roles of N- and C-terminally truncated Aβ species in Alzheimer's disease. **Expert Opinion on Therapeutic Targets**, v. 23, n. 12, p. 991–1004, dez. 2019.

WITTENBERG, R. et al. Economic impacts of introducing diagnostics for mild cognitive impairment Alzheimer's disease patients. **Alzheimer's & Dementia: Translational Research & Clinical Interventions**, v. 5, p. 382–387, 1 jan. 2019.

WOLZ, R. et al. Multi-method analysis of MRI images in early diagnostics of Alzheimer's disease. **PloS One**, v. 6, n. 10, p. e25446, 2011.

XIA, D. et al. Presenilin-1 knockin mice reveal loss-of-function mechanism for familial Alzheimer's disease. **Neuron**, v. 85, n. 5, p. 967–981, 4 mar. 2015.

YANASE, D. et al. Brain FDG PET study of normal aging in Japanese: effect of atrophy correction. **European Journal of Nuclear Medicine and Molecular Imaging**, v. 32, n. 7, p. 794–805, jul. 2005.

ZETTERBERG, H. Review: Tau in biofluids – relation to pathology, imaging and clinical features. **Neuropathology and Applied Neurobiology**, v. 43, n. 3, p. 194–199, 2017.

ZIMMER, E. R. et al. MicroPET imaging and transgenic models: a blueprint for Alzheimer's disease clinical research. **Trends in Neurosciences**, v. 37, n. 11, p. 629–641, nov. 2014.